UNIVERSITY OF EXETER

The role of non-structural carbohydrates in predictions of ecosystem carbon fluxes
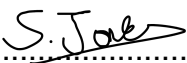
Submitted by

Simon Jones

to the University of Exeter as a thesis for the degree of

Doctor of Philosophy in Mathematics,

June 2021

I certify that all material in this thesis which is not my own work has been identified and that any material that has previously been submitted and approved for the award of a degree by this or any other University has been acknowledged.

Signed: ....

Abstract

Land surface models (LSM) represent a significant source of uncertainty in predictions of future climate. Many LSMs are unable to account for differences between plant carbon assimilation through photosynthesis, and plant carbon expenditure through autotrophic respiration and growth, as they do not comprehensively represent labile non-structural carbohydrate (NSC) stores that allow asynchrony between assimilation and expenditure to occur. This limits the ability of LSMs to accurately capture seasonal and inter-annual variation of ecosystem carbon fluxes in particular during periods of environmental stress.

This thesis discusses the current empirical understanding of NSC, and examines previous representations of NSC storage and utilisation within LSMs. A simple model of NSC designed to decouple plant carbon assimilation and expenditure in LSMs and improve predictions of ecosystem carbon fluxes, is presented. The model is tested at three scales and under varying climatic conditions. First, in simulations across the Amazon rainforest, the model decouples respiration and growth from photosynthesis, resulting in shifts in the seasonal cycle of total carbon expenditure. Then at a tropical drought experiment in Caxiuanã, Brazil, the model allows more accurate predictions of carbon fluxes relative to a LSM that does not represent NSC. Finally, at a global scale, the model is used to highlight the potential importance of NSC in predictions of global terrestrial carbon uptake. The thesis concludes by outlining possible developments for future work.

Contents

List of Figures

List of Tables

Associated Papers

Jones, S., Rowland, L., Cox, P., Hemming, D., Wiltshire, A., Williams, K., Parazoo, N. C., Liu, J., da Costa, A. C. L., Meir, P., Mencuccini, M., and Harper, A. B. (2020). The impact of a simple representation of non-structural carbohydrates on the simulated response of tropical forests to drought. *Biogeosciences*, 17(13):3589–3612

Code availability

A model example of the SUGAR model for a single site and set-up to run at Caxiuanã using output from JULES is available at https://doi.org/10.5281/zenodo.3547613

Acknowledgements

I have been lucky to receive a huge amount of support throughout my PhD. I would first like to thank my supervisor Dr Anna Harper for her guidance over the past four years. Anna's knowledge and expertise have helped direct my research and her enthusiasm and patience have kept me focused and motivated. I would also like to acknowledge my extended supervisor team, Professor Peter Cox, Dr Lucy Rowland and Dr Debbie Hemming, who between them have provided a great deal of support and advice. I also wish to thank Dr Andy Wiltshire and Dr Karina Williams from the Met Office for all of their help, in particular on 'everything JULES'. Thanks goes to everybody from 901 for helping to un-stick me whenever I've gotten stuck. My code is cleaner and my understanding greater, thanks to you all. In particular I'd like to thank Arthur Argles. Discovering the joys of using FORTRAN, presenting at conferences and writing a thesis alongside Arthur has made my PhD significantly more enjoyable.

To everyone I've shared an office with - Becky, Arthur, Femke, Rebecca, Sarah, Paul, Joe and Mark, thank you for creating such a friendly environment to work in. You all made the long walk up to the 9th floor each morning seem all the more worth it. Thank you to all my family for the encouragement they've given me throughout my PhD. In particular, thank you to Becky who has carried me through a difficult final year and been a source of smiles in a time when the world went a bit mad. I would also like to thank Andrew, David, Oli and Tiago for putting up with living with me at different points over the last four years. Finally, I'd like to thank Tim for teaching me that when the going gets tough, a walk in the park is always a good remedy.

Chapter 1

Introduction

1.1 The terrestrial carbon cycle

Forests cover nearly 4000 Mha (UN Food and Agriculture Organization Rome, 2015) of the worlds land surface and represent a significant sink of carbon from the atmosphere. Between 1990 and 2007, forests sequestered an estimated 2.4 ± 0.4 PgC each year (Pan et al., 2011), and since the start of the industrial era in 1750 have absorbed roughly 25% of total anthropogenic carbon emissions (IPCC, 2013). However, despite this uptake, and a similar sink into the oceans, atmospheric CO_2 concentrations have seen an approximately 40% increase since the start of the industrial era (Stocker et al., 2013). Together with changes in the concentrations of other green house gases such as methane (CH_4) and nitrous oxide (N_2O), this change in atmospheric composition has resulted in significant and observable shifts in the global climate. These shifts may have severe and irreversible impacts on human society that will present significant challenges and require long term adaptation from the human population (Stocker et al., 2013). Understanding how the climate will continue to change in the future, and how the most extreme impacts can be mitigated against is therefore crucial. The role that forests play in the climate system is integral to this, and both an understanding of their behaviour and accurate representations of their interactions with the atmosphere in global climate models (GCMs) are required.

The observed uptake of carbon by terrestrial ecosystems over the industrial period is attributed to a stimulation of photosynthesis by increasing atmospheric CO_2 (Kimball et al., 1993; Friedlingstein et al., 1995; Amthor, 1995) and a lengthening of the growing season in northern latitudes associated with changes in temperature (Reichstein et al., 2013). However, whether this sink will continue in the future is not clear. It has been suggested that CO_2 fertilisation of photosynthesis may saturate as CO_2 levels rise further (Cao and Woodward, 1998; Körner, 2006). Changes in temperature and precipitation patterns, as well as an increase in the

frequency and severity of extreme disturbance events including droughts, fires, wind storms and pest outbreaks, all associated with climate change, may also reduce carbon uptake and increase forest mortality. This may outweigh the effects of CO_2 fertilisation, even before it saturates, and result in an overall decrease, or even a reversal of terrestrial carbon uptake in the future. Such a decline would result in a significant increase in atmospheric CO_2 concentrations and an acceleration of climate change.

The impact of climate change on forests in the future, and the extent to which forests will continue to absorb carbon from the atmosphere is uncertain. GCMs disagree not only on the magnitude of future terrestrial carbon uptake but also the sign (Cox et al., 2000; Sitch et al., 2008; Hewitt et al., 2016; Arora et al., 2013). Lovenduski and Bonan (2017) reported a standard deviation of 163PgC in predictions of the total accumulation (or loss) of carbon in the terrestrial biosphere by the year 2100 amongst models from the 5th Coupled Model Inter-comparison Project (CMIP5). For context, this is comparable to the total amount of carbon estimated to have been absorbed into the land surface (165 ± 70PgC) between the years 1750 and 2014 (Le Quéré et al., 2015). While some of this uncertainty stems from the spread of projections that occurs under varying future emission scenarios, the majority ($\sim$80%) has been attributed to differences in the structure of the land surface model (LSM) component of GCMs (Lovenduski and Bonan, 2017), which are exacerbated by non-linearity and feedback loops that exist within the climate system (Friedlingstein et al., 2001). For example, climate induced losses of forest carbon in the Amazon rainforest, from increased temperatures and drought stress, may result in significant increases in atmospheric CO_2 concentrations (Cox et al., 2004). This could accelerate the effects of climate change, causing further drying and warming across the Amazon and creating a positive feedback loop that could see large and rapid losses of forest cover and cause drastic changes to the global climate (Cox et al., 2000; Huntingford et al., 2004). However, the nature and likelihood of this feedback, referred to as 'Amazon dieback', is uncertain. Small differences in the sensitivity of the Amazon rainforest to climate change amongst models can be the difference between the continued absorption of CO_2 and this severe die-back scenario. Hence, even small structural differences in the representation of plant behaviour in LSMs result in large uncertainty in terrestrial carbon uptake. This uncertainty greatly limits the accuracy of future climate predictions (Huntingford et al., 2009) and so it is critical that realistic and mechanistic representations of plant responses to climate change are developed and incorporated into LSMs.

Carbon uptake by forests is controlled by the balance between plant photosyn-

thesis and autotrophic respiration. Like most biochemical reactions, both fluxes depend on temperature and are typically stimulated by warming. However, differences in the responses of the two fluxes to temperature may have a significant impact on the net carbon balance of forests. Sharper increases in respiratory demands relative to the stimulation of photosynthesis in response to increasing temperature (Ryan, 1991) may mean that the net carbon uptake by plants is reduced if temperature increases with climate change. This mechanism was partly responsible for the early predictions of Amazon die-back, as it contributed to a reduction in net carbon uptake below the level required to balance losses from litter-fall and disturbance (Cox et al., 2004). However, our understanding of these processes stems largely from observations over the short-term and the behaviour of photosynthesis and respiration in many GCMs is based upon these instantaneous responses to changes in temperature. Observations over the long-term suggest that significant increases in plant respiration relative to photosynthesis are not sustainable over long time-scales (Gifford, 1995; Saxe et al., 2001), and there is an apparent consistency in the ratio of the two fluxes (Waring et al., 1998). Short term responses of both photosynthesis and respiration are also dependent on long-term temperature exposure, suggesting that plants have some ability to acclimate to their environment (Atkin and Tjoelker, 2003; Berry and Bjorkman, 1980). However, the strength of this acclimation capability, in particular with respect to respiration, is unclear and so the resilience of plants to rising temperatures is uncertain. This represents a significant uncertainty within predictions of terrestrial carbon uptake and makes the likelihood of climate-induced tipping points such as Amazon die-back difficult to determine (Lombardozzi et al., 2015).

A further source of uncertainty is the response of forests to a reduction in water availability. Observations show that intense dry periods can reduce vegetation productivity and increase plant mortality, particularly in the tropics, over both short-term (Phillips et al., 2009; Bastos et al., 2018; Luo et al., 2018; Gloor et al., 2018) and multi-annual time-scales (Rowland et al., 2015; Meir et al., 2018; Fisher et al., 2007; da Costa et al., 2010; Nepstad et al., 2007). When combined with the effects of wildfires, insect infestations, and land-use change, drought can cause tropical regions such as the Amazon basin to shift from a net sink to a net source of carbon to the atmosphere (Gatti et al., 2014; Liu et al., 2017; Phillips et al., 2009). What is less clear, however, is how forests will respond to increasing drought length, severity and frequency. Large scale experimental drought studies (e.g. Meir et al., 2018) show that the responses of vegetation to drought are not linear, meaning that our understanding of short-term responses cannot necessarily be extrapolated to long-term ones (Rowland et al., 2018; Metcalfe et al., 2010). Similarly, the response of forests to individual droughts may change if they

are subjected to multiple droughts in quick succession (Anderegg et al., 2013, 2015, 2020). Both the frequency and severity of droughts are predicted to increase across large parts of the globe as a result of climate change (Marengo et al., 2018; Hartmann et al., 2013), but many large scale vegetation models are currently unable to capture these types of responses correctly (Powell et al., 2013). It is, therefore, vitally important that the response of forests to drought in these models is improved, in particular across tropical regions where terrestrial carbon storage is large (Pan et al., 2011).

1.2 Non-structural carbohydrates: An empirical perspective

1.2.1 Buffering supply and demand

Most LSMs assume that the sum of plant growth and respiration is equal to instantaneous photosynthesis (Fatichi et al., 2014). Consequently at any given time, the total rate of carbon utilisation by respiration and growth, referred to as plant carbon expenditure (PCE), is equal to the gross rate of carbon accumulation by photosynthesis, referred to as Gross Primary Productivity (GPP). However, in reality growth and respiration are not so strictly coupled to photosynthesis and plants regularly experience periods when the supply of carbon from photosynthesis does not equal the demands of growth and respiration (Körner, 2003; Muller et al., 2011). This asynchrony between supply and demand is facilitated by reserve pools of labile carbon known collectively as non-structural carbohydrates (NSC) (Fig. 1.1). The NSC pool within a plant accumulates when photosynthesis exceeds carbon demand and is drawn upon to sustain growth and respiration when they are not supported by instantaneous photosynthetic assimilation (Hartmann and Trumbore, 2016; Dietze et al., 2014). NSCs therefore act as a buffer against changes in productivity, allowing key functional processes to be maintained, even when photosynthetic accumulation is low. Deciduous trees, for example, experience a much larger demand for carbon than can be supplied through photosynthesis at the start of leaf flush when a new canopy must be grown. The capacity of a NSC pool to buffer the impacts of reduced photosynthesis is also particularly important during periods of environmental stress, which can lead to reduced GPP over seasonal to multi-annual time-scales. During prolonged periods of stress, carbon utilisation rates can diverge significantly from photosynthesis (Metcalfe et al., 2010; Doughty et al., 2015a,b) implying that plants rely heavily on their NSC reserves during these periods. Without simulating NSC storage LSMs remain unable to capture this asynchrony between GPP and PCE

and so fail to correctly simulate forest level respiration and growth fluxes.
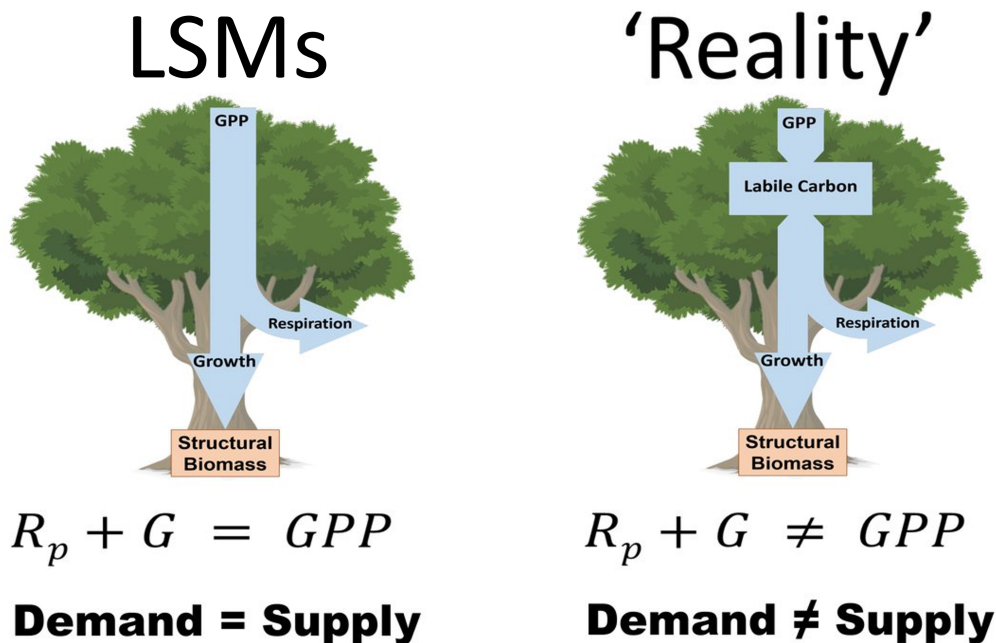
Figure 1.1: Carbon allocation in most land surface models (LSM) vs. a more realistic system. Most LSMs use all assimilated carbon in a single timestep so rate of utilisation (demand) is always equal to rate of photosynthesis (supply). In reality, plants store labile carbon that allows instantaneous carbon utilisation to diverge from instantaneous carbon assimilation.

1.2.2 NSC in drought

The ability to sustain respiration and growth when productivity is reduced has an important role during periods of drought (Doughty et al., 2015b). Under low water availability the transport of water from roots to other organs can be restricted by both temporary stomatal closure and/or longer term damage to the xylem through embolism (Martínez-Vilalta et al., 2014; Sperry and Love, 2015; Tyree and Sperry, 1989). Xylem damage can lead to a drop in hydraulic conductance, resulting in damage to plant tissue and increased risk of mortality (Rowland et al., 2015; Anderegg and Anderegg, 2013; McDowell et al., 2008). Plants combat this threat through control over the aperture of their stomata. Closing the stomata reduces water loss through transpiration and lowers the risk of xylem damage and hydraulic failure. The trade-off to this strategy, however, is a reduction in productivity caused by a decrease in CO_2 diffusion into the leaves. There is evidence that plant growth may decline much earlier than photosynthesis in response to drought, as cell turgor needed for cell expansion depends on water availability

(Muller et al., 2011; Hsiao, 1973; Boyer, 1970). This decrease in carbon demand from growth may actually result in an accumulation of NSC reserves during the early stages of drought (Muller et al., 2011). However, as drought length and water stress increase, the demand for carbon from respiratory processes may exceed photosynthesis and NSC stores will be drawn upon (Hartmann and Trumbore, 2016). The ability of a plant to close its stomata and reduce the risk of hydraulic failure is therefore reliant on its ability to store and utilise NSC.

In theory, if carbon demand exceeds supply over long periods of drought, NSC reserves may become exhausted, causing essential elements of plant function to fail, a process termed 'carbon starvation'. Exactly what happens to a plant at this point is not yet clear, and it is still debated whether NSC stores can actually be fully depleted. It has been suggested, however, that carbon starvation may accelerate the effects of hydraulic failure and in some cases, itself lead directly to mortality (Galiano et al., 2011; Adams et al., 2013). McDowell et al. (2008) proposed a theoretical framework that links drought length and severity to carbon starvation and hydraulic failure. It was hypothesised that the likelihood of death by hydraulic failure increases with the intensity (quantified as the relative decrease in water availability) of drought. In contrast the likelihood that carbon starvation would lead to mortality was assumed to increase with drought duration, provided that the intensity of drought is not sufficient to induce hydraulic failure (Fig. 1.2). This framework has been criticised because of a lack of direct evidence of plants dying due to exhausted NSC stores (Sala et al., 2010). Trees that die after being subject to drought over even decadal time-scales have been found to still have significant stores of NSC after death (Rowland et al., 2015). However, NSC utilisation and hydraulic failure are tightly linked processes (Mitchell et al., 2013; Adams et al., 2017; McDowell, 2011), not only because of their shared dependence on stomatal conductance, but also due to the role that carbohydrates have in processes such as osmoregulation (Morgan, 1984), phloem transport (Ryan and Asao, 2014) and potentially in refilling of embolised xylem (Sevanto et al., 2014). The demand for NSC by these non-metabolic processes may allow carbon starvation to occur before reserves are completely exhausted (McDowell, 2011). Partial declines in NSC may also exacerbate the risk of hydraulic failure as plants rely on concentration gradients of NSC and other compounds to maintain water flow (Signori-Müller et al., 2021). A reduction in the ability to recover and repair damaged xylem associated with depleted (but non-zero) NSC stores, may also increase the likelihood of mortality by hydraulic failure and explain the observed NSC stores in many deceased trees (McDowell, 2011; Mitchell et al., 2013). The relationship between carbon starvation and hydraulic failure during drought is clearly complex, and the role of NSC during drought likely extends beyond a simple buffering of carbon

supply and demand. Recent developments in modelling plant hydraulics (Mencuccini et al., 2019; Eller et al., 2018, 2020; Sperry et al., 2017; Baker et al., 2008) provide more accurate predictions of stomatal behaviour during drought, however, these developments must also be accompanied by models of carbon storage in order to effectively simulate the trade-off between hydraulic damage and productivity loss. Until such developments are made, predictions of plant mortality and recovery in response to climate extremes such as drought will remain uncertain.
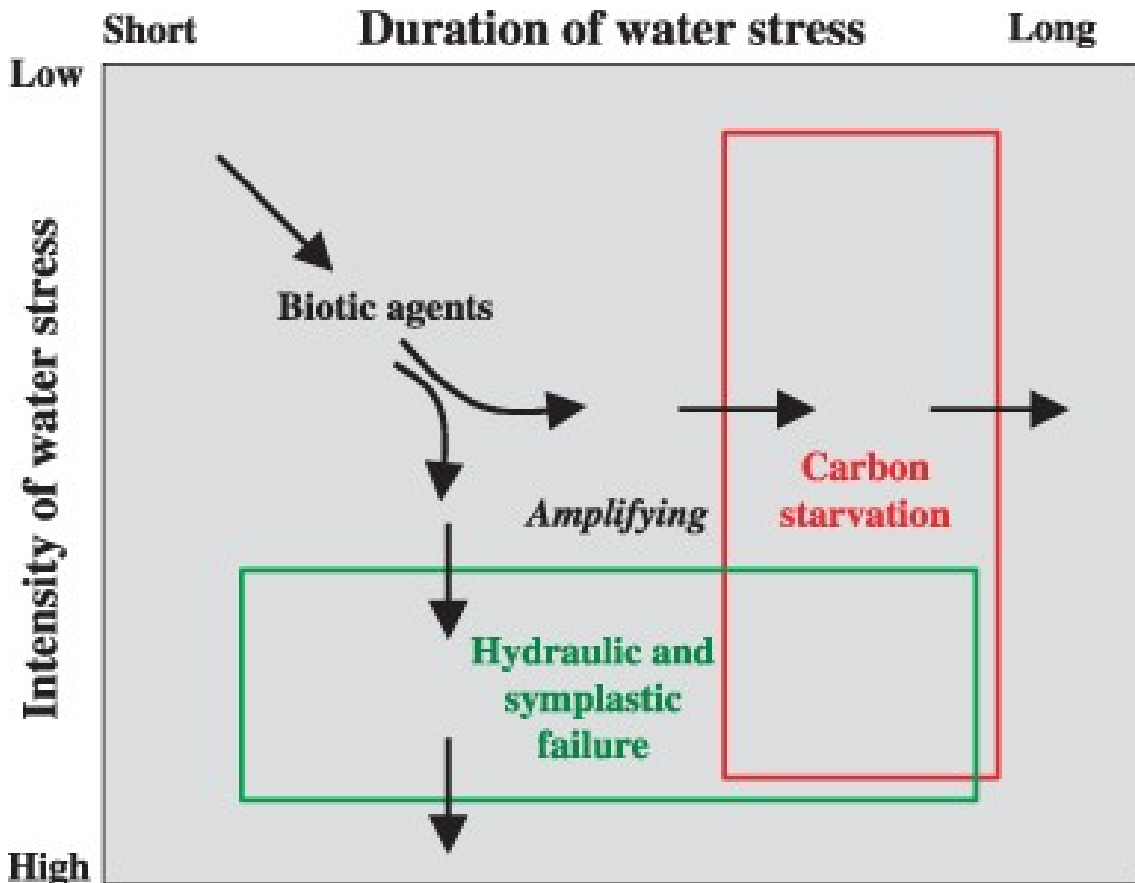
Figure 1.2: From McDowell et al. (2008): Theoretical relationship between the duration and intensity of drought, and three hypothesized mechanisms underlying mortality - carbon starvation, hydraulic failure and biotic attack.

1.3 Modelling non-structural carbohydrates

1.3.1 Satisfying a need for extra carbon

Despite their clear role in forest function, our current understanding of how NSCs are produced, stored and used remains poor (Hartmann and Trumbore, 2016). Absolute pool sizes are difficult to quantify (Quentin et al., 2015) and it is not clear how NSC reserves are distributed and transported between different plant organs under stress (Martínez-Vilalta et al., 2016; Sevanto et al., 2014). It is also not clear whether NSC storage is the passive result of asynchrony between sup-

ply and demand as described above, or whether plants also have the capacity to actively regulate NSC stores at the expense of growth and respiration (Körner, 2003; Palacio et al., 2014; Wiley and Helliker, 2012).

Nonetheless, some representation of NSC is commonly required to achieve realistic predictions of certain plant processes (Dietze et al., 2014). In particular many LSMs represent some type of labile storage pool that supports leaf flush in deciduous plants (e.g. a recent version of CLASS-CTEM, Asaadi et al. (2018); ORCHIDEE, Krinner et al. (2005); CLM5, Lawrence et al. (2018); ED2, Medvigy et al. (2009)). Without these stores of carbohydrate, leaf growth is often too slow at the start of leaf-out, resulting in lags between predicted and observed peaks of leaf area index (LAI). In the original CLASS-CTEM model (Melton and Arora, 2016), for example, GPP at the start of the growing season is based upon a 'storage LAI', until the actual LAI is sufficiently large to continue leaf flush. However, the rate of photosynthesis from this storage LAI is much slower than the reallocation rate of NSC in the updated model, resulting in significantly longer leaf-out periods (Asaadi et al., 2018). In some models this is the sole purpose of representing NSC. In ORCHIDEE (Krinner et al., 2005), for example, only deciduous trees and grasses have NSC pools, and these pools are only drawn down at the start of the growing season in order to attain reasonable leaf flushing rates. The role of NSC in evergreen trees is not considered and for the majority of the year, the NSC pool is dormant in seasonal trees. NSC certainly plays an important role in the seasonal flushing of leaves in deciduous trees and it is entirely reasonable to represent NSC in this way to improve simulated phenology. However, the role of NSC is likely to be equally large throughout the remainder of the year in both seasonal and evergreen plants, and especially during periods of environmental stress. LSMs that represent NSC purely for phenological purposes will fail to capture this role, which may be significant at a global scale.

1.3.2 Respiration and growth: sink versus source

1.3.2.1 Growth

Plant growth, in LSMs that do not represent NSC, is necessarily equal to the difference between photosynthesis and respiration, referred to as Net Primary Productivity (NPP). When respiration exceeds photosynthesis (i.e. NPP$<$0), growth rate is therefore negative, and the carbon demand of respiration is satisfied by plant biomass. However, structural compounds within a plant, such as cellulose and lignin are generally considered to be permanent, meaning that the carbon within them cannot be remobilised and used for respiration. Some LSMs rectify this problem by including a NSC pool that supports respiration when NPP is

negative (e.g. ORCHIDEE, Krinner et al. (2005); JSBACH-CN, Parida (2011)), allowing structural growth rates to remain positive. In JSBACH-CN, for example, when NPP is negative the growth rates of the structural carbon pools are set to zero and the excess carbon demand is drawn from a NSC pool. Importantly, however, when NPP is positive, the rate of structural plant growth is still determined by NPP, as it would be in a LSM that does not simulate NSC. This dependence of plant growth on carbon assimilation rate has become known as 'source-limitation', indicating the control that photosynthesis (the source of carbon) has on determining plant growth rates. Yet, it is becoming widely recognised that plant growth is more commonly limited by other factors such as temperature, nutrient and water availability, and substrate transfer rates within plants (Körner, 2003; Millard et al., 2007; Körner, 2015; Fatichi et al., 2014). Fatichi et al. (2019) describes this view, known as 'sink-limitation', with an analogy of constructing a brick wall (Fig. 1.3). The rate at which a wall can be built is unlikely to be explained entirely by the rate at which bricks are supplied. Other factors such as the supply of cement, working conditions for the builders, and transport of materials are likely to have equally large contributions. Sink-limitations on plant growth are rarely represented in LSMs but may have a significant impact on projections of future carbon uptake by forests (Friend et al., 2019).
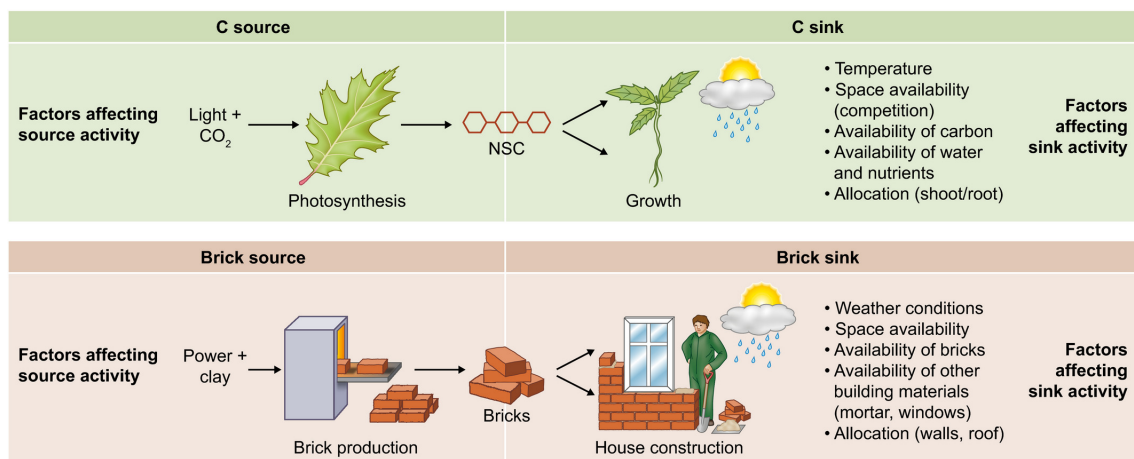
Figure 1.3: From (Fatichi et al., 2019): The construction site analogy of carbon (C) source and sink limitation in plant growth. The build-up of C in a growing plant is ultimately governed by the provisioning of C (C source; left side of the figure), and its investment into plant tissues (C sink; right side of the figure). These processes and the factors driving them can be exemplified with the construction site analogy, where C, or bricks form the key ingredient. The C source activity is mainly driven by the availability of light and atmospheric [CO2] (i.e. photosynthesis), or power and clay (i.e. brick production). Yet, for the C sink activity, where plant tissues (or buildings) are formed, the provisioning of C (or bricks) becomes only one of many limiting factors. Apart from C, favourable temperature and water availability, at least 14 other macro- and micronutrients are required (and hence can limit) the C sink strength (Körner, 2015).

Sink and source limitation are often confronted as though they are independent or contrary frameworks. However, in some sense plant growth must be both source and sink limited. Over the short-term, changes in environment may predominantly determine growth, but ultimately plants cannot grow more than they assimilate over the long-term. In the wall construction analogy, if the supply of bricks stops, eventually so too will the building of the wall. In order to account for both types of limitation, LSMs must allow environmental conditions as well as the availability of nutrients and water to affect growth, but without completely decoupling it from photosynthesis. This can be achieved mechanistically by including a dependence of growth on NSC availability. NSC stores are ultimately determined by long-term photosynthesis which couples growth to carbon assimilation. If NSC stores build up, however, the carbon available for growth is much larger than the amount supplied by instantaneous photosynthesis and so sink-limitations become more important in determining instantaneous growth rates.

The dependence of growth on NSC is less commonly represented in LSMs, although it is not non-existent. In models such as CLASS-CTEM (Asaadi et al., 2018), CLM5 (Lawrence et al., 2018) and ED2 (Medvigy et al., 2009), the NSC pool (or pools) not only supports respiration, but also has a role in determining plant growth. For example, in CLASS-CTEM (Asaadi et al., 2018), all the remaining assimilated carbon after respiration has been accounted for (i.e. all NPP) first enters three NSC pools (one each for leaf, stem and root). Carbon is then transferred from these pools to structural ones, at a rate determined by the availability of NSC within the storage pools. This flux of carbon from non-structural to structural pools is considered equivalent to plant growth, and hence plant growth in CLASS-CTEM depends on the availability of NSC. However, even in these models that include a a dependence of growth on NSC, there are rarely detailed mechanistic descriptions of how external factors like temperature and water availability affect sink strength (i.e. the demand for NSC by growth) (Fatichi et al., 2019; Körner, 2015). In CLASS-CTEM while the rate of structural growth depends on NSC availability, the sink strength is still determined by NPP. This is likely due to our relatively poor understanding, and lack of mathematical theories that describe the behaviour of plant carbon sinks (Fatichi et al., 2019; Körner, 2015). Sink strength is particularly hard to measure experimentally, in part due to the complexity of measuring NSC concentrations as mentioned above. Photosynthesis, in contrast, is more well understood owing to the easier nature of measuring leaf gas exchange (Körner, 2015). Recent studies that explore how components of plant carbon expenditure respond to environmental change (e.g. Mahmud et al., 2018; Signori-Müller et al., 2021) provide useful insights into the role of NSC and sink strength in determining plant growth and can guide model

development. However, currently the structure of many LSMs means that they will not be compatible with this development (Friend et al., 2019). A simple framework that will allow new theories to be integrated into LSMs as they are developed is therefore required.

1.3.2.2 Respiration

A similar argument can be made with respect to the dependence of plant respiration on NSC, but again, few LSMs actually include this dependence. Of the models mentioned above, in almost all (including ORCHIDEE Krinner et al. (2005); JSBACH-CN, Parida (2011); CLM5, Lawrence et al. (2018); ED2 Medvigy et al. (2009)), at least one of the NSC pools has an associated respiration rate that depends on the available carbohydrate within the pool. There is, therefore, a component of respiration that depends on NSC in these models, however, the respiration rates of the other plant components (e.g. structural leaf, stem and root) do not have this dependence. Yet the role of NSC in determining whole plant respiration rates, including those of structural components, may be particularly important (Thornley and Cannell, 2000; Cannell and Thornley, 2000). Early observations that plant carbon use efficiency (CUE: the ratio of NPP to GPP) is relatively uniform across plant species, size and environmental conditions (Waring et al., 1998) indicate a coupling between whole plant respiration and photosynthesis. This led many models (reviewed in Collalti and Prentice (2019)) to adopt a 'fixed fraction' framework, in which plant respiration was set proportional to photosynthesis. However, while CUE may be constant over sufficiently long time-scales, significant variations have been subsequently observed both temporally and spatially (Collalti and Prentice, 2019). Over short-term time-scales the ratio of respiration to photosynthesis (R:P) may change significantly in response to changes in environment such as temperature (Hansen et al., 2002; Atkin et al., 2006). The fixed fraction framework is unable to capture these changes (Atkin et al., 2007) which may be hugely important to long term predictions of global terrestrial carbon balance, given the feedbacks and non-linearities that exist within the climate system (Friedlingstein et al., 2001; Huntingford et al., 2009).

An alternative approach adopted by many LSMs (e.g. JULES, Clark et al. (2011); ISAM, (Meiyappan et al., 2015); CLM5, Lawrence et al. (2018)) is to decouple respiration and photosynthesis entirely. Respiration is commonly split into growth and maintenance components, with growth respiration typically proportional to biomass synthesis, and maintenance respiration proportional to total plant carbon or nitrogen biomass and controlled by temperature (Thornley, 1970; McCree, 1970). This approach allows changes in CUE over the short-term as maintenance respiration and photosynthesis covary due only to shared sensitivities to changes

in environment, and a shared dependence on biomass. However, linking maintenance respiration to total plant biomass can lead to unrealistically large respiration demands as biomass accumulates (Collalti et al., 2020; Thornley, 1970) and does not take into account the coupling between GPP and respiration that occurs over the long term (Gifford, 2003). In reality changes in respiration are not controlled directly by either photosynthesis or biomass, but by recent and long term NSC stores (Collalti et al., 2020; Cannell and Thornley, 2000; Thornley and Cannell, 2000). Both short term changes in CUE, and its apparent long term consistency can be explained with a simple substrate based framework (Dewar et al., 1998, 1999). An increase in the R:P ratio can be caused by an increase in temperature if respiration and photosynthesis have different sensitivities to temperature, but under the substrate framework, prolonged changes cannot be sustained. Ultimately, if respiration increases more than photosynthesis, it is down-regulated by the eventual decline in NSC. This behaviour is only possible if whole plant respiration has some dependence on NSC, at least in the limit of small NSC concentrations. Without representing this role that NSC has in determining plant metabolism, as well as supporting it, LSMs may not be able to capture the response of plant CUE to changes in climate over both the long and short-term.

1.4   What should we aim for?

Non-structural carbohydrates have an important role within the terrestrial carbon cycle, playing a significant part in both supporting and regulating plant metabolism. Storing NSC allows plants to maintain respiration and growth during periods when carbon assimilation through photosynthesis is reduced, which can occur over seasonal to multi-annual time-scales, and in particular in response to environmental stress. In addition, they have a potentially significant role in regulating plant water status and driving the recovery of plants from hydraulic damage, and as a result are a crucial component of plant responses to drought. However, comprehensive representations of NSC are missing from many LSMs, limiting their ability to predict the responses of terrestrial ecosystems to future changes in climate. An improved description of NSC utilisation and transport, and the relationship between NSC and plant respiration and growth is required in LSMs that will allow them to accurately capture the response of plant carbon expenditure to changes in climate (Friend et al., 2019).

Idealised modelling studies provide a theoretical framework that may guide model development (e.g. Rastetter et al., 1991; Thornley, 1991, 1997), and detailed mechanistic models that can successfully replicate plant growth and respiration are possible (e.g. Hemming et al., 2001; Fritts et al., 2000; Salomón et al., 2019).

However, these studies typically focus on the individual plant or species. A lack of detailed data at the ecosystem level, means that evaluating the parameters within these models for a range of species and biomes that covers all plant functional types (PFT) used in global LSMs is currently difficult (Fatichi et al., 2019; Hartmann et al., 2020). It is therefore necessary to develop a parameter-sparse model than can be calibrated against data sources that can be more effectively collected and yet captures the essential characteristics of representing a NSC pool. This will allow new developments to be built into LSMs as our understanding of the role of NSC within plants evolves.

1.5   Thesis Outline

In this chapter the current understanding of the role of NSC in plant function has been explored and the current state of NSC representation in large scale ecosystem models has been presented.

The aim of the remainder of this thesis is to present and evaluate a simple representation of NSC (The Substrate Utilisation by Growth and Autotrophic Respiration - SUGAR model) that is designed to be integrated into a LSM. The model is parsimonious yet captures the essential elements of NSC dynamics, with the dependence of both whole plant respiration and growth on NSC considered.

Chapter 2 outlines the key concepts required to build the model and briefly describes how the model may be integrated into the Joint UK Land Environment Simulator (JULES) (Best et al., 2011; Clark et al., 2011) LSM. The model equations are then presented, and by considering the model under steady-state, the possibility of evaluating the model parameters using more readily available datasets, including GPP, NPP and biomass, is explored.

In chapter 3 the ability of plants to buffer growth and respiration against variations in photosynthesis is examined at a regional scale. The behaviour and applicability of the SUGAR model to large-scale ecosystem modelling is tested using satellite data of plant productivity over the Amazon rainforest, to predict plant carbon expenditure over seasonal time-scales.

Chapter 4 investigates the role that NSC plays in buffering growth and respiration against reductions of productivity induced by extreme drought. The SUGAR model is used to simulate ecosystem carbon fluxes within an Amazonian forest under both non-stressed and stressed conditions, in conjunction with JULES, using data from a through-fall exclusion drought experiment in Caxiuanã, Brazil.

Chapter 5 looks at the role of NSC in predictions of the global terrestrial carbon sink. Specifically the variability of net biome productivity (NBP) is explored in relation to NSC. This study also allows an investigation into the separation of plant respiration into maintenance and growth components, which is typically done in most LSMs. The potential for using observed variability of atmospheric CO_2 concentrations to constrain model parameters within SUGAR is also explored.

Finally, in chapter 6, the main findings from the thesis are summarised, and the potential questions that result from these findings are presented in order to guide future research.

Chapter 2

A simple model of Non-structural Carbohydrates

2.1 Introduction

Without at least simple representations of non-structural carbohydrate (NSC) storage and utilisation, land surface models (LSM) are unlikely to accurately capture real world plant growth and respiration fluxes in the future. Despite their importance, NSC dynamics are missing from many LSMs likely owing to the scarcity of reliable datasets that show how NSCs are stored, used and transported in plants. Given our current knowledge and data availability, it is necessary to develop a parameter-sparse model that can be calibrated against data sources that can be more effectively collected than NSC data (e.g. growth and respiration data) and yet capture the essential characteristics of representing a NSC pool (e.g. decoupling photosynthesis from growth and respiration). Such an effort will not only constrain future climate projections but may also be used to stimulate further research that improves our empirical understanding of NSC storage and use.

In this chapter, SUGAR ("Substrate Utilisation by Growth and Autotrophic Respiration"), a simple model of NSC storage and utilisation, designed to be coupled to a dynamic global vegetation model (DGVM) and function as part of a land surface model (LSM), is presented. The aim of the model is to allow the decoupling of plant carbon expenditure (PCE = respiration + growth) and Gross Primary Productivity (GPP), in order to provide a more accurate representation of respiration and growth fluxes, in particular in response to environmental stress. SUGAR may be applicable to a wide range of LSMs, however, it was developed specifically to be integrated into JULES (The Joint UK Land Environment Simulator, Best et al., 2011; Clark et al., 2011), which is the land surface component of the UK Met Office Unified Model. Despite this aim, SUGAR is not coupled to JULES throughout this thesis and all subsequent simulations with SUGAR are

performed off-line. Nonetheless, before the model equations are presented, a brief description of the relevant equations in JULES is given to provide context for how SUGAR is designed to fit within a land surface scheme. SUGAR makes use of well known equations that represent the dependence of respiration and growth on temperature and substrate availability. The dependences of growth and respiration on substrate are given by the Michaelis-Menten equation, which is derived and briefly discussed. Finally, an overview of how the model parameters are evaluated throughout the remainder of this thesis is given.

2.2 JULES

The Joint UK Land Environment Simulator (JULES) is a processed-based LSM that is used both as a stand-alone model and as the land surface component of the UK Met Office weather forecast and climate models, as well as the UK community Earth System Model (UKESM Sellar et al., 2019). A full description of JULES is given in Best et al. (2011); Clark et al. (2011), however, some of the relevant equations within the model are given here to provide context for the development of a NSC sub-model.

2.2.1 Vegetation structure

JULES represents five plant functional types (PFT), or nine in more recent versions (Harper et al., 2016), in terms of a grid-box vegetation carbon density, C_v, and fractional coverage, ν. Vegetation carbon biomass is split into three components - leaf, stem and root, which are all related allometrically to the leaf area index (LAI) of each PFT:

$$C_v = L + W + R \tag{2.1}$$

$$L = \sigma_l LAI \tag{2.2}$$

$$R = \sigma_l LAI \tag{2.3}$$

$$W = a_{wl} LAI^{b_{wl}} \tag{2.4}$$

$$\tag{2.5}$$

where σ_l is specific leaf density (kgC m^{-2} per unit LAI), and a_{wl} and b_{wl} are PFT-specific parameters.

2.2.2 Respiration and growth

To understand how NSC may be represented in JULES, it is important to understand how JULES represents plant respiration and growth. Like many LSMs, since JULES does not represent any form of NSC, the sum of plant growth and

respiration (PCE) is equal to GPP.

The physiology component of JULES calculates plant respiration, R_p, which is split into maintenance, R_{pm}, and growth, R_{pg}, components:

$$R_p = R_{pm} + R_{pg} \tag{2.6}$$

Growth respiration is a fixed fraction of the Net Primary Productivity (NPP):

$$R_{pg} = \frac{r_g}{1 - r_g} \left(\Pi_G - R_p \right) \tag{2.7}$$

where r_g is a constant with a default value of 0.25.

Maintenance respiration is calculated for each plant component (leaf, stem and root) and depends on nitrogen content and temperature through a dependence on canopy dark respiration, with leaf maintenance respiration additionally depending on soil moisture. The nitrogen concentrations in stem and root are assumed to be fixed multiples (μ_{sl} and μ_{rl} respectively) of the average leaf nitrogen concentration, which allows total maintenance respiration to be written as:

$$R_{pm} = 0.012 R_{dc} \left(\beta + \mu_{sl} \frac{S}{L} + \mu_{rl} \frac{R}{L} \right) \tag{2.8}$$

where the the three terms in the brackets represent leaf, stem and root maintenance respiration respectively; the factor of 0.012 converts from (mol $CO_2 \mathrm{m}^{-2}\,\mathrm{s}^{-1}$) to (kgC $\mathrm{m}^{-2}\,\mathrm{s}^{-1}$); R_{dc} is canopy dark respiration; β is a soil moisture stress factor given by:

$$\beta = \begin{cases} 1 & \text{for } \theta > \theta_c \\ \dfrac{\theta - \theta_w}{\theta_c - \theta_w} & \text{for } \theta_w < \theta \leq \theta_c \\ 0 & \text{for } \theta \leq \theta_w \end{cases} \tag{2.9}$$

where θ_c and θ_w are the soil moisture concentrations below which photosynthesis drops below it's maximum (uninhibited) value, and becomes zero respectively

S is respiring stem carbon and is assumed to be a constant fraction of total stem carbon, W:

$$S = \frac{1}{a_{ws}} W \tag{2.10}$$

Once respiration has been accounted for, the remaining carbon (NPP) is passed to the vegetation dynamics component (TRIFFID) of JULES. TRIFFID uses NPP to increase the carbon content and fractional coverage, which together make up total plant growth. In more recent versions of JULES, the carbon allocated to

TRIFFID may be limited by available nitrogen (Wiltshire et al., 2021), causing a reduction in plant growth. However, since JULES does not contain a NSC pool, the excess carbon that cannot be allocated to growth is added to the respiration term, meaning that the equalities between growth and NPP, and between GPP and PCE are maintained. The NPP is allocated between each plant component so as to maintain the allometric scalings with LAI given in equations (2.2, 2.3, 2.4).

2.2.3   NSC in JULES

Given the allometric scaling between the three plant components (leaf, stem and root) it may be possible to represent just a single NSC pool that is assumed to be distributed evenly throughout the grid-box vegetation. Plant biomass should be separated into structural and non-structural carbon and a new plant growth term should be defined that represents the conversion of NSC to structural carbon. Growth respiration can be made equal to a fraction of this new growth term, which should depend on NSC availability. Similarly a dependence on NSC should be added to maintenance respiration (Fig. (2.2)).

2.3   Reaction kinetics

In order to model the role of NSC in LSMs it is important to understand how plant respiration and growth depend on substrate availability. Both respiration and growth are complex processes that result from the aggregate of many individual biochemical reactions. Representing these reactions individually is not practical for modelling plant behaviour at a global, ecosystem or even individual plant scale. However, several useful equations may be derived by considering the kinetics of these reactions, that may be used to describe the dependence of the aggregate process on substrate availability. Qualitatively, both respiration and growth can be described as simple enzyme reactions in which an input (NSC) is converted into a product through a reaction catalysed by an enzyme (Thornley and Johnson, 1990).

2.3.1   The Michaeilis-Menten equation

The simplest enzymatic reaction is the single-substrate scheme in which the formation of a product (P) from a substrate (S) is catalysed by an enzyme (E).

$$\text{E} + \text{S} \underset{k_r}{\overset{k_f}{\rightleftharpoons}} \text{ES} \xrightarrow{k_c} \text{E} + \text{P} \tag{2.11}$$

where E, S, ES and P are the enzyme, substrate, intermediate reaction product and final reaction product respectively; and k_f, k_r and k_c are rate constants for the forward and reverse reactions of the enzyme-substrate binding, and catalytic reaction respectively.

Under steady state when the concentration of ES is constant, the rate of ES production and decay must be equal. If we assume that the rate of each individual reaction is proportional to the concentrations of the reagents (denoted with square brackets) then we can write the following expression, equating ES production and decay:

$$k_f[\text{E}][\text{S}] = (k_r + k_c)[\text{ES}] \tag{2.12}$$

Since the enzyme is conserved in this reaction, we can assume that it's total concentration is constant and define:

$$\text{E}_0 = [\text{E}] + [\text{ES}] \tag{2.13}$$

Rearranging equation (2.13) for [E], and substituting into equation (2.12) gives the following expression for the steady state concentration of the intermediate enzyme-substrate complex in terms of the substrate concentration and total enzyme concentration:

$$[\text{ES}] = \frac{k_f \text{E}_0[\text{S}]}{k_f[\text{S}] + k_r + k_c} \tag{2.14}$$

Again assuming that the rate of reactions are linearly proportional to their reagents, the rate of the catalytic reaction under steady state can be written as:

$$v = k_c[\text{ES}] = \frac{k_c k_f \text{E}_0[\text{S}]}{k_f[\text{S}] + k_r + k_c} \tag{2.15}$$

This is commonly expressed as:

$$v = v_{max}\frac{[\text{S}]}{K_m + [\text{S}]} \tag{2.16}$$

where $v_{max} = k_c\text{E}_0$ and $K_m = \dfrac{k_r + k_c}{k_f}$.

This is known as the (single-substrate) Michaelis-Menten equation. It is a good approximation of the rate of isolated reactions described by equation 2.11, but is also widely used to approximate more complex processes that are the aggregate of many individual reactions. The Michaelis-Menten equation is commonly used to represent the substrate dependence of respiration and growth since both processes rely on enzymes and have a theoretical limiting rate above which additional carbon substrate does not increase utilisation rate (Thornley and Cannell,

2000; Thornley and Johnson, 1990; Thornley, 1971).

2.3.2 Analytical solutions to Michaelis-Menten systems

Despite its apparent simplicity, the Michaelis-Menten equation adds a relatively high level of complexity into even basic carbohydrate models. The most simple system, for example, is a finite pool of substrate that is utilised at a rate determined by Michaelis-Menten kinetics. The rate of change of the concentration of the substrate, $[S]$, in this system is given by:

$$\frac{d[S]}{dt} = -\frac{v_{max}[S]}{K_m + [S]}$$

(2.17)

As a separable ordinary differential equation, this may be solved by integration:

$$\int \frac{[S] + K_m}{[S]} d[S] = \int -v_{max} dt$$

(2.18)

This gives:

$$[S] + K_m \ln([S]) = -v_{max}t + C$$

(2.19)

where $\ln()$ is the natural logarithm and C is a constant. Assuming as initial conditions that at $t = 0$ the substrate concentration is given by:

$$[S](t = 0) = S_0$$

(2.20)

the constant C is found as:

$$C = S_0 + K_m \ln(S_0)$$

(2.21)

Eqn. (2.19) therefore, becomes:

$$[S] + K_m \ln([S]) = -v_{max}t + S_0 + K_m \ln(S_0)$$

(2.22)

Rearranging gives:

$$\frac{[S]}{S_0} + \frac{K_m}{S_0} \ln\left(\frac{[S]}{S_0}\right) = 1 - \frac{v_{max}t}{S_0}$$

(2.23)

This is a transcendental equation, meaning that an expression for $[S](t)$ cannot be written in terms of elementary functions. A solution may be given in terms of the transcendental Lambert W function (Goličnik, 2012), which is the function that satisfies the equation:

$$W(x)\exp(W(x)) = x$$

(2.24)

However, again this cannot be written as a closed-form expression. The time-course may still be plotted retrospectively by diagnosing time from an array of

substrate concentrations (Fig. 2.1). Analytical solutions are not often necessary in the field of plant or crop modelling and Michaelis-Menten systems like that given in eqn (2.17) can be solved numerically.
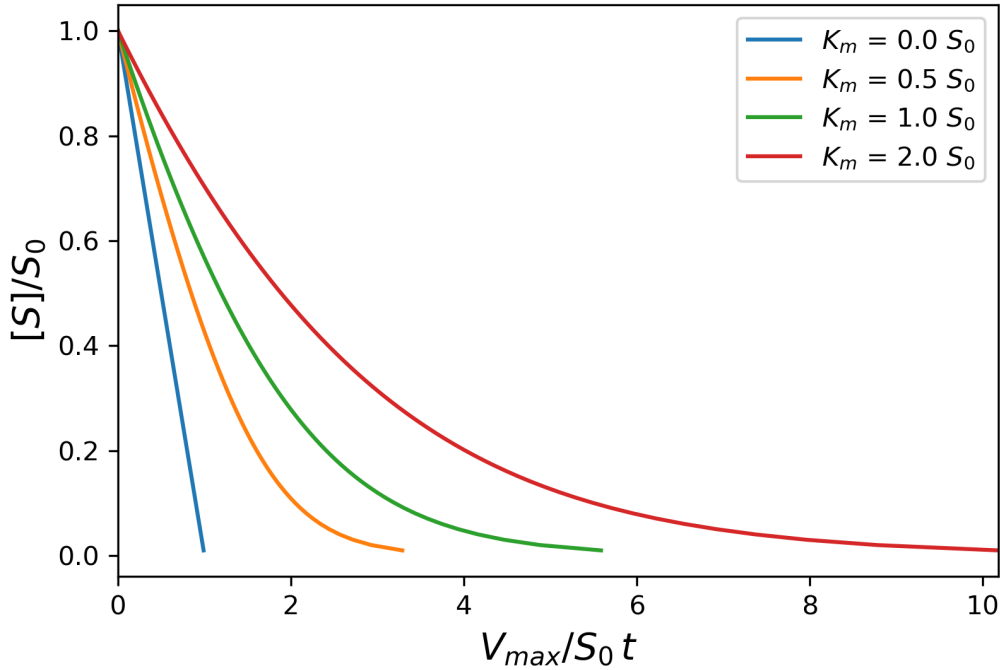
Figure 2.1: The time-course of substrate concentration ($[S]$) depletion relative to the initial substrate concentration (S_0), via the Michaelis-Menten equation, for four different Michaelis-Menten constants (K_m). The Michaelis-Menten constants are defined as a fraction of the initial substrate concentration.

2.3.3 Simplifications in the limits of substrate availability

A common simplification to the Michaelis-Menten equation is to consider the linear part of the function (e.g. Potkay et al., 2021; Dewar, 1993) in the limit that substrate availability is low relative to the saturation parameter (K_m):

$$\frac{v_{max}[S]}{K_m + [S]} \approx \frac{v_{max}}{K_m}[S], \text{ for } K_m >> [S] \tag{2.25}$$

Linear reaction kinetics may allow analytical solutions to be found, however the most common justification for using this approach is that it reduces the two parameters in the Michaelis-Menten equation (v_{max}, K_m) to just one.

Similarly, in the limit that substrate availability is saturated (or the saturation constant, K_m, is small), the rate of reaction can be approximated as independent of

substrate availability. This is known as zero-order reaction kinetics:

$$\frac{v_{max}[S]}{K_m + [S]} \approx v_{max}, \text{ for } K_m << [S] \tag{2.26}$$

Zero-order kinetics are not used to represent the substrate dependence of growth and respiration since there is trivially no difference compared to not representing any substrate dependence. However, it can be useful to consider zero-order reaction kinetics as the saturated limit of Michaelis-Menten kinetics, in order to bridge the gap between models that simulate substrate availability and those that do not. For example, it is common in LSMs to represent maintenance respiration as proportional to plant biomass, C_v. Viewing this instead as zero-order reaction kinetics in NSC, we can expect the maintenance respiration of a model that includes NSC dynamics, to behave similarly to one that does not in the limit that $K_m << [S]$.

2.4 The SUGAR Model

The 'Substrate Utilisation by Growth and Autotrophic Respiration' (SUGAR) model simulates a single pool of carbohydrate at the ecosystem scale (Fig. (2.2)) although in theory the model could be applied at multiple scales including the organ and whole plant scale. Sugars and starches are not distinguished meaning that all carbohydrate is readily available to support respiration and growth. Representing just a single pool in this way keeps the model simple and parameter sparse making integration into an LSM much easier. SUGAR is designed to sit below the photosynthesis component of a LSM. Assimilated carbon from photosynthesis (GPP) is collected by the NSC pool and the total carbon allocated to respiration and growth is then calculated and taken directly from the NSC pool. The pool is therefore always active and is constantly depleted by growth and respiration, and replenished by photosynthesis. Both growth and respiration are assumed to be single substrate enzyme reactions and depend on NSC content via the Michaeilis-Menten equation. Respiration and growth both depend on temperature via the standard Q_{10} function (Ryan, 1991). Carbohydrate content is not actively regulated by the plants in SUGAR meaning that variations in NSC stores are the passive result of asynchrony between photosynthesis and PCE caused by variations in climate.

2.4.1 Non-structural carbohydrate pool

Total plant biomass (C_v) is split into structural carbon (C_{SC}) and NSC (C_{NSC})

$$C_v = C_{SC} + C_{NSC} \tag{2.27}$$

36

(a)

Photosynthesis, Π_G

Growth, $\Pi_N = \Pi_G - R_m - R_g$

Vegetation Carbon C_v

Litterfall/Mortality, Λ

Growth Respiration
$$R_g = \frac{r_g}{1 - r_g}\Pi_N$$

Maintenance Respiration,
$$R_m = f(T, N, \theta)$$

(b)

Photosynthesis, Π_G

Vegetation Carbon C_v

Non-Structural Carbohydrate C_{NSC}

Growth, $G = G_0 F_Q C_v \dfrac{C_{NSC}}{C_{NSC} + K_m C_v}$

Structural Carbon C_{SC}

Litterfall/Mortality, Λ

Maintenance Respiration,
$$R_m = R_{m_0} F_Q C_v \frac{C_{NSC}}{C_{NSC} + K_m C_v}$$

Growth Respiration
$$R_g = \frac{1 - Y_g}{Y_g} G$$

Figure 2.2: Flow diagrams that demonstrate how SUGAR is designed to change the model structure of carbon allocation within the Joint UK Land Environment Simulator (JULES) (Best et al., 2011; Clark et al., 2011)). Arrows represent fluxes of carbon and black boxes represent carbon pools. **(a)** A representation of the current structure of carbon allocation in JULES. Maintenance respiration (R_m) depends on temperature (T), leaf nitrogen (N) and optionally, water availability (θ). Growth respiration (R_G) is equal to a constant fraction of net primary productivity (Π_N) which is equal to photosynthesis (Π_G) less total plant respiration ($R_G + R_m$). Total utilisation of carbon ($R_m + R_G + \Pi_N$) is always exactly equal to carbon assimilation by photosynthesis (Π_G). **(b)** A representation of how SUGAR would sit within JULES. Vegetation carbon (C_v) is split into structural carbon (C_{SC}) and non structural carbohydrate (C_{NSC}). Both maintenance respiration and structural carbon growth depend on temperature via a Q_{10} function (F_Q), total biomass (C_v) and non-structural carbohydrate content (C_{NSC}). Growth respiration becomes a constant fraction of growth instead of a fraction of net primary productivity.

The NSC mass fraction is then be defined as:

$$W_{NSC} = \frac{C_{NSC}}{C_v} \qquad (2.28)$$

The rate of change of NSC content (C_{NSC}) is given by:

$$\frac{dC_{NSC}}{dt} = \Pi_G - R_p - G \qquad (2.29)$$

where Π_G is canopy GPP, R_p is total plant respiration, and G is plant growth.

Using the definition of net primary productivity (Π_N):

$$\Pi_N = \Pi_G - R_p$$

equation (2.29) is written as:

$$\frac{dC_{NSC}}{dt} = \Pi_N - G \qquad (2.30)$$

2.4.2 Growth

Plant growth depends on temperature and NSC availability. The temperature dependence is assumed to follow a Q_{10} exponential relationship and the NSC dependence follows Michaelis-Menten reaction kinetics:

$$G = G_0 F_Q(T) C_v \frac{C_{NSC}}{C_{NSC} + K_m C_v} \qquad (2.31)$$

where G_0 (yr^{-1}) is the maximum specific growth rate at the reference temperature 25 °C, T (°C) is temperature, C_v (kgC m^{-2}) is total structural carbon biomass, K_m is a half saturation constant equal to the NSC mass fraction at which growth rate is half of its maximum value at the reference temperature, and $F_Q(T)$ is the Q_{10} temperature dependence given by:

$$F_Q(T) = q_{10}^{0.1(T-25)} = exp\left(ln\,(q_{10})\,\frac{(T-25)}{10}\right) \qquad (2.32)$$

where q_{10}, which is a constant taken to be 2.0 by default.

2.4.3 Respiration

Plant respiration is split into maintenance and growth components. Growth respiration is calculated as a constant fraction of plant growth:

$$R_g = \frac{1 - Y_g}{Y_g} G \tag{2.33}$$

where Y_g is the growth conversion efficiency, or yield, with a default value of 0.75 (Thornley and Johnson, 1990).

Maintenance respiration has the same temperature and NSC dependence as plant growth:

$$R_m = R_{m_0} F_Q(T) C_v \frac{C_{NSC}}{C_{NSC} + K_m C_v} \tag{2.34}$$

where R_{m_0} (yr^{-1}) is the maximum specific rate of maintenance respiration at the reference temperature 25°C.

2.4.4 Total carbohydrate utilisation

The total rate of NSC utilisation, U, is defined as the sum of plant respiration and growth:

$$U = R_p + G \tag{2.35}$$

U here is exactly equivalent to PCE and is only denoted differently for convenience and ease of reading. Using this definition, Eq. (2.29) can be written as:

$$\frac{dC_{NSC}}{dt} = \Pi_G - U \tag{2.36}$$

Since both respiration and growth have the same NSC and temperature dependence, U is given by:

$$U = \phi F_Q(T) C_v \frac{C_{NSC}}{C_{NSC} + K_m C_v} \tag{2.37}$$

where $\phi = R_{m_0} + \dfrac{G_0}{Y_g}$ is the maximum specific rate of utilisation of carbohydrate at the reference temperature 25°C.

2.5 Parameter estimation

Detailed time-series data of forest level NSC stocks are difficult to collect and are therefore scarce. This makes parameter evaluation difficult. Below is a discussion on the evaluation process for each parameter in SUGAR. Some of these parameters, for example the q_{10} parameter, have standard or commonly used values within the LSM literature, and the validity of their given values is not discussed

Symbol	Description	Units
C_{NSC}	Non-structural carbohydrate content	kgC m^{-2}
C_{SC}	Structural carbon biomass	kgC m^{-2}
C_v	Total vegetation carbon biomass	kgC m^{-2}
F_Q	Q_{10} temperature function	
G	Structural plant growth rate	kgC m^{-2} yr^{-1}
R_g	Growth respiration	kgC m^{-2} yr^{-1}
R_m	Maintenance respiration	kgC m^{-2} yr^{-1}
R_p	Total plant respiration	kgC m^{-2} yr^{-1}
T	Leaf temperature	K
U	Total non-structural carbohydrate utilisation rate	kgC m^{-2} yr^{-1}
W_{NSC}	Non-structural carbohydrate mass fraction	kgC kgC^{-1}
Π_G	Gross primary productivity	kgC m^{-2} yr^{-1}
Π_N	Net primary productivity	kgC m^{-2} yr^{-1}

Table 2.1: Definition of symbols

here. In these cases only a very brief justification is presented. For the remaining parameters, with a few assumptions the simplicity of SUGAR can be used to evaluate these parameters without the need for detailed NSC data, and instead use more commonly and readily measured variables. A summary of all parameters is given in table 2.2.

q_{10}

The q_{10} parameter represents the factor by which respiration and growth increase with every 10 ℃ of warming. The exponential Q_{10} function is commonly used to describe the temperature dependence of plant metabolism in LSMs with the standard q_{10} value of 2.0 (Ryan, 1991)

Y_g

The Y_g parameter represents the conversion efficiency of plant growth (Thornley and Johnson, 1990). By default, it is assumed to have a value of 0.75, consistent with previous estimates (Thornley and Johnson, 1990), and the parameters assumed in other LSMs (e.g. Clark et al., 2011). It is derived in Thornley and Johnson (1990) and estimated to equal 0.75. Similar parameters are used in other LSMs (e.g. Clark et al., 2011).

G_0 and R_{m_0}

These parameters represent the maximum specific rate of plant growth and maintenance respiration respectively, at the reference temperature of 25 ℃. To evaluate these parameters it is useful to define the parameter α as the ratio of G_0 to ϕ:

$$\alpha = \frac{G_0}{\phi} \tag{2.38}$$

Values for ϕ and α can be found by considering the steady-state behaviour of the model, which can then be used to determine G_0 and R_{m_0}.

ϕ

The ϕ parameter represents the maximum specific rate of carbohydrate utilisation by plant respiration and growth at the reference temperature of 25 °C. To estimate ϕ, the NSC pool is considered in equilibrium such that the rate of change of the NSC mass fraction (W_{NSC}) is zero. In reality the NSC mass fraction of a forest will never be exactly constant and variations in environmental variables will always cause at least small changes in NSC stocks. However, for a non-stressed forest it is a good assumption that over a prolonged period, τ_{obs}, the NSC mass fraction will be roughly constant. For example, we can assume that over the course of one year, a non-stressed forest will use as much carbon as it assimilates and consequently will end the year with roughly the same NSC stock with which it started. This means that averaging the model over the period τ_{obs}, changes in the NSC pool can be neglected and we can consider the mean model behaviour which is more easily evaluated.

The rate of change of W_{NSC} is given by:

$$\frac{dW_{NSC}}{dt} = \frac{1}{C_v}\frac{dC_{NSC}}{dt} - \frac{W_{NSC}}{C_v}\frac{dC_v}{dt} \tag{2.39}$$

Integrating over the period τ_{obs}, the left hand side can be set equal to zero:

$$0 = \int_{\tau_{obs}} \left(\frac{1}{C_v}\frac{dC_{NSC}}{dt} - W_{NSC}\frac{1}{C_v}\frac{dC_v}{dt} \right) dt \tag{2.40}$$

In the 'stand-alone' version of SUGAR where C_v is constant, the second term is equal to zero, and equation (2.40) becomes:

$$0 = \int_{\tau_{obs}} \left(\frac{1}{C_v}\frac{dC_{NSC}}{dt} \right) dt \tag{2.41}$$

Using the equation for the rate of change of NSC (Eq. (2.36)) this becomes:

$$0 = \int_{\tau_{obs}} \left(\frac{\Pi_G}{C_v} - \frac{U}{C_v} \right) dt \tag{2.42}$$

Substituting equation (2.37) in place of U and rearranging gives:

$$\phi \int_{\tau_{obs}} F_Q(T)\frac{W_{NSC}}{W_{NSC} + K_m}dt = \int_{\tau_{obs}} \frac{\Pi_G}{C_v}dt \tag{2.43}$$

Dividing equation (2.43) by τ_{obs} results in the temporal average of each side over the observation period.

$$\phi \left(F_Q(T) \frac{W_{NSC}}{W_{NSC} + K_m} \right)^* = \left(\frac{\Pi_G}{C_v} \right)^* \tag{2.44}$$

where the asterisk denotes a temporal average over the period τ_{obs}. I.e. for variable X:

$$X^* = \frac{1}{\tau_{obs}} \int_{\tau_{obs}} X dt \tag{2.45}$$

If it is assumed that variations in the NSC pool are small relative to it's total size, which is a good assumption for an unstressed forest in steady state, the left hand side of equation (2.44) can be approximated in terms of the temporal averages of W_{NSC} and $F_Q(T)$:

$$\phi F_Q^*(T) \frac{W_{NSC}^*}{W_{NSC}^* + K_m} = \left(\frac{\Pi_G}{C_v} \right)^* \tag{2.46}$$

Rearranging, results in the following expression for ϕ

$$\phi = \frac{W_{NSC}^* + K_m}{F_Q^*(T) W_{NSC}^*} \left(\frac{\Pi_G}{C_v} \right)^* \tag{2.47}$$

Equation (2.5) describes the assumption that given an average long term rate of photosynthesis (Π_G/C_v), and a long term average NSC mass fraction (W_{NSC}^*), a specific rate of NSC utilisation can be inferred. Evaluating ϕ, therefore requires an estimate of average specific GPP, a time series of temperature over the period of observation, and an estimate of the average NSC concentration within an ecosystem. If SUGAR is used at a single site these can be evaluated directly using GPP, biomass and temperature data where these are available. If these data are not available then the specific GPP can be approximated as the inverse of the steady state carbon residency time, $\tau = \frac{C_v}{\Pi_G}$ (e.g. Carvalhais et al., 2014), and the temperature can found using global climatology data over the same period. The average NSC pool size may be estimated directly using empirical data (e.g. for tropical forests using Würth et al., 2005).

Throughout the remainder of this thesis SUGAR is driven off-line using grid-box data of GPP, temperature and biomass. The ϕ parameter is evaluated in these simulation by first finding the average specific GPP over an initialisation period using a subset of the driving data. The average NSC mass fraction is then either estimated using empirical estimates (e.g. Würth et al., 2005), or is varied as part of a sensitivity study. It is considered a parameter in these studies and denoted f_{NSC}. Essentially the ϕ parameter has been split into two components, the tem-

perature normalised average specific rate of photosynthesis and the equilibrium NSC mass fraction, which themselves can be considered separate parameters.

α

To evaluate α, the forest is again considered under steady-state and equation (2.39) is again temporally averaged over the observation period τ_{obs}. This can then be written as:

$$0 = \left(\frac{\Pi_G}{C_v}\right)^* - \left(\frac{U}{C_v}\right)^* \tag{2.48}$$

Since for the stand-alone verion of SUGAR we are considering C_v to be constant, this becomes:

$$\Pi_G^* = U^* \tag{2.49}$$

For interest this equation simply describes the assumption that over a prolonged, steady state period, the average rate of carbon assimilation by photosynthesis is equal to the average rate of utilisation by respiration and growth.

A similar equation for long term average NPP and growth can be found by rewriting equation (2.42):

$$0 = \int_{\tau_{obs}} \left(\frac{\Pi_N}{C_v} - \frac{G}{C_v}\right) dt \tag{2.50}$$

Again dividing by the integration period, τ_{obs}, this becomes:

$$0 = \left(\frac{\Pi_N}{C_v}\right)^* - \left(\frac{G}{C_v}\right)^* \tag{2.51}$$

For the stand-alone version this gives:

$$\Pi_N^* = G^* \tag{2.52}$$

Dividing equation (2.52) by equation (2.49) yields:

$$\frac{\Pi_N^*}{\Pi_G^*} = \frac{G^*}{U^*} \tag{2.53}$$

Using the definitions of G and U from equations (2.31) and (2.37), and cancelling terms this becomes:

$$\frac{\Pi_N^*}{\Pi_G^*} = \frac{G_0}{\phi} \tag{2.54}$$

Finally this can be written as

$$\alpha = CUE^* \tag{2.55}$$

where $CUE^* = \dfrac{\Pi_N^*}{\Pi_G^*}$, is the time averaged carbon use efficiency of the non-stressed forest over the period τ_{obs}.

This can be evaluated using data from a single site where available, or using more general estimates of CUE (e.g. Chambers et al., 2004; Gifford, 1995) if not. G_0 and R_{m_0} can then be found as:

$$G_0 = \alpha\phi \tag{2.56}$$

and

$$R_{m_0} = \left(1 - \frac{\alpha}{Y_g}\right)\phi \tag{2.57}$$

K_m

Finally, the K_m parameter, represents the NSC mass fraction (W_{NSC}) at which the rate of NSC utilisation is half of it's maximum value at a reference temperature of 25 °C. It is currently not possible to evaluate K_m from empirical data. As described in section 2.3.2, the saturation effect of the Michaelis-Menten equation depends on the ratio of K_m to substrate concentration. The K_m parameter in SUGAR is therefore expressed as a fraction (a_{K_m}) of the equilibrium NSC mass fraction (f_{NSC}):

$$K_m = a_{K_m} f_{NSC} \tag{2.58}$$

where a_{K_m} is a constant. The sensitivity of SUGAR to this parameter is examined in Jones et al. (2020) within the range $a_{K_m} \in [0.1, 2.0]$, but is given a default value of 0.5, as this gives realistic NSC mass fractions (Jones et al., 2020).

2.6 Discussion and Conclusions

Many LSMs, including JULES, are unable to correctly capture plant carbon fluxes due to a tight coupling between total carbon expenditure and assimilation. SUGAR is a simple model of NSC storage designed to be integrated into a LSM and break the direct link between PCE and GPP to provide more mechanistic predictions of growth and respiration. SUGAR makes use of commonly used equations to describe the dependence of respiration and growth on temperature and substrate availability. While simple, the model is parsimonious and may be initialised and evaluated without the need for detailed NSC data. A more complex NSC model might distinguish between starch and sugar pools, or represent multiple pools for each plant organ, and actively control the input or output of NSC into pools (Martínez-Vilalta et al., 2016; Hartmann and Trumbore, 2016). However, such models would likely require representation of substrate transport between pools. NSC transport within plants is not currently well understood and evaluating parameters in these models requires the scaling of detailed NSC data to the level of trees and forests. Previously the level of uncertainty on such figures has been up to 400% (Quentin et al., 2015) and as a result, comprehensive NSC data-

Parameter	Units	Description	Evaluation
f_{NSC}	kg kg^{-1}	Equilibrium NSC mass fraction	(Wurth et al 2005)
q_{10}		Factor by which respiration and growth increase given a 10 degree warming	(Ryan 1991)
Y_g		Growth conversion efficiency	(Thornley and Johnson 1990)
a_{K_m}		Relates the half saturation NSC mass fraction (K_m) with the equilibrium pool size (f_{NSC})	Sensitivity study carried out in Jones et al. (2020)
α		Ratio of plant growth to total carbohydrate utilisation	Evaluated by setting equal to steady state carbon use efficiency (CUE*). Between 0.3-0.5 for a tropical forest (Chambers et al., 2004; Gifford, 1995)
ϕ	yr^{-1}	Maximum specific rate of NSC utilisation at 25°C	Evaluated in terms of a_{K_m} using average specific photosynthesis $\left(\frac{\Pi_G}{C_v}\right)^*$ and temperature (T) of a forest in steady state. $\phi = \frac{1+a_{K_m}}{F_Q^*(T)}\left(\frac{\Pi_G}{C_v}\right)^*$. Can also be evaluated in terms of vegetation carbon residency time τ (e.g. Carvalhais et al., 2014): $\phi = \frac{1+a_{K_m}}{F_Q^*(T)\tau}$

Table 2.2: Parameters in the SUGAR model

f_{NSC} the is fraction of NSC relative to total structural carbon and so estimates of NSC as a fraction of total dry mass should be adjusted to account for non-carbon biomass.

sets, measured through time in response to climatic variations and across enough biomes to allow all model PFTs to be evaluated are currently not available. Recent advancements in measurement protocols may allow these datasets to be reliably collected (Landhäusser et al., 2018) in the future and simple representations like SUGAR may allow more complex processes to be readily incorporated into LSMs as our understanding of them improves.

In the next chapter, the behaviour of SUGAR and its applicability to large scale ecosystem modelling will be investigated. SUGAR will be used to simulate plant carbon expenditure fluxes across the Amazon basin using predicted GPP data from an ensemble of LSMs and constrained with observations. The sensitivity of the model to the f_{NSC} parameter will be investigated in these simulations allowing the transition from modelling without, to modelling with NSC to be examined.

Chapter 3

The role of non-structural carbohydrates in the seasonality of ecosystem carbon fluxes across the Amazon rainforest.

3.1 Introduction

The Amazon rainforest is the world's largest tropical forest, storing between 69 and 102 PgC (Saatchi et al., 2007), and has a large influence on both local and global climate. Sequestering an average 0.42-0.65 $PgC\,yr^{-1}$ between the years 1990 and 2007 (Pan et al., 2011), the Amazon has represented a significant sink of atmospheric CO_2 in the recent past, and is an important mitigating factor against human-induced climate change. However, sensitivity of the forest to changes in climate, combined with the effects of fire and land use change, may mean that the Amazon sink does not persist in the future (Davidson et al., 2012; Brienen et al., 2015). Decreasing water-availability and increasing temperature both have the potential to reduce or even reverse the flux of carbon from the atmosphere into the forest (Gatti et al., 2014; Liu et al., 2017; Phillips et al., 2009). Understanding how changes in the climate influence carbon fluxes in the Amazon, and successfully representing these interactions in global climate models (GCM) is crucial to making accurate predictions of global climate in the future.

The largest axis of climate variability faced by Amazonian forests in the present day is the seasonal variation of precipitation, temperature and day length, which result in significant annual cycles of plant carbon fluxes including Gross Primary Production (GPP), plant respiration (R_p) and Net Primary Productivity (NPP). If models are to accurately predict the response of forests to future changes in climate, they must also be able to capture the response to these seasonal changes.

Yet, the seasonal cycle of carbon fluxes in the Amazon is often poorly represented in modern land surface models (LSM) (Restrepo-Coupe et al., 2016), with significant discrepancies between observations and model predictions of GPP, R_p and NPP (Harper et al., 2016). Important processes within the Amazon are therefore either missing or poorly represented in models and further development is required if accurate predictions of seasonal and future responses to climate are to be made.

There has been a large focus on modelled GPP as an area in need of improvement, in particular its response to water availability (Rogers et al., 2017). The importance of GPP should not be understated and as the gross flux of carbon into the ecosystem, it has a large impact on the net sink of carbon into the Amazon. Of equal importance, however, is what happens to carbon once it has been assimilated through photosynthesis. Even with a perfect representation of seasonal GPP, many models would be unlikely to capture the correct seasonal cycles of plant respiration and growth. Over long time-scales, the sum of respiration and growth, referred to as plant carbon expenditure (PCE), is approximately equal to GPP. However, over shorter time-scales these fluxes may diverge, with seemingly little correlation between carbon assimilation and utilisation (Doughty et al., 2015a; Restrepo-Coupe et al., 2016; Körner, 2003). Differences between carbon expenditure and assimilation may be driven by active optimisation by plants that allow the growing season to occur at the most ecologically beneficial time (Doughty et al., 2015a), or passively due to differences in the response of plant metabolism and photosynthesis to external controls, such as light, nutrient and water availability, and temperature (Fatichi et al., 2014; Wagner et al., 2012, 2016). In either case, this asynchrony between carbon assimilation and carbon expenditure must be supported by labile non-structural carbohydrates (NSC) that can deplete when demand exceeds supply and accumulate when supply is in excess. Without at least simple representations of NSC, models will remain incapable of capturing the seasonality of respiration and growth, even if photosynthesis is represented perfectly.

In this chapter the impact of NSC on the seasonal cycle of PCE is examined relative to GPP across the Amazon. SUGAR is run off-line to simulate PCE fluxes across the Amazon basin, using GPP data from an ensemble of LSMs, constrained by global fluorescence measurements from the Greenhouse Gases Observing SATellite (GOSAT) (Parazoo et al., 2014) as driving data. The sensitivity of the model to initialised NSC content within a reasonable range of possible pool sizes, and the changes the model makes to predictions of ecosystem carbon expenditure are assessed. The seasonality of predicted PCE is compared to that

of GPP and the drivers of PCE are examined.

3.2 Methods

To demonstrate how the introduction of a carbohydrate pool influences predictions of PCE, SUGAR was used to conduct a series of simulations over a six and a half year period from June 2009 to December 2015 across the Amazon basin. The model was driven with monthly GPP and temperature data and was initialised using estimates of grid-box biomass (described below). To examine the transition from modelling without, to modelling with NSC, a sensitivity study was conducted on the size of the NSC pool within SUGAR. This was done by varying the f_{NSC} parameter between simulations, within the range 0.0005-0.16. As f_{NSC} represents the initial fraction of the biomass pool that is NSC, a value of 0.0005 effectively represents a model without NSC[1], while the upper bound of 0.16 is two times a realistic estimate of the ecosystem NSC content in a tropical forest in Panama (Würth et al., 2005), representing an extreme upper limit on the effects of NSC. The range is, therefore, likely to include a realistic estimate of NSC content within the Amazon basin. Finally, the seasonality of predicted PCE is compared to that of observed leaf production, which itself is a component of PCE, at two sites within the Amazon (Wu et al., 2016).

3.2.1 Driving Data

3.2.1.1 GPP

Monthly GPP data was provided by a dataset inferred from the combination of satellite observations and vegetation models (Parazoo et al., 2014). This dataset (henceforth referred to as GOSAT GPP) uses observations of solar-induced chlorophyll fluorescence (SIF) from the Greenhouse Gases Observing SATellite (GOSAT) to constrain the output of an ensemble of eight Dynamic Global Vegetation Models (DGVM) from the TRENDY model consortium (Sitch et al., 2015). SIF is light re-emitted from leaf chlorophyll during photosynthesis, and global SIF observations from GOSAT have been shown to correlate strongly with GPP derived from flux measurements at a global scale (Frankenberg et al., 2011). Combining these observations with model output, Parazoo et al. (2014) were able to constrain seasonal and spatial variability in GPP and reduce model uncertainty by up to 40-70% in highly productive regions such as the Amazon, within the TRENDY model ensemble. Using this dataset in place of a single model, or even the original TRENDY ensemble output allows the effect of the NSC pool to be examined

---

[1]Since the NSC turnover rate is inversely related to the pool size, it is not possible to set f_{NSC} equal to zero since this results in an undefined turnover rate, so a value of 0.0005 is used.

with a reduced influence of uncertainty or deficiencies in input GPP which can be considerable (Sitch et al., 2015).

3.2.1.2 Temperature

Driving temperature was given by 'temperature at 2m' from the CRU JRA dataset (Harris, 2019) - based on the Japanese 55-year Reanalysis (JRA-55) dataset (Kobayashi et al., 2015) combined with data from the Climate Research Unit (CRU). The CRU-JRA data was re-gridded to match the spatial and temporal resolutions of the GOSAT GPP data. This data was used to drive the temperature dependence of growth and respiration in SUGAR.

3.2.1.3 Biomass

The total biomass (C_v) in each grid-box was assumed to be constant. This was a reasonable assumption given the relatively short length of the simulations. Estimates for grid-box biomass were taken from a pan-tropical above-ground biomass (AGB) dataset (Avitabile et al., 2016) which was re-gridded to the spatial resolution of the GOSAT GPP dataset.

3.2.1.4 Amazon basin

To isolate the Amazon basin region, all driving datasets were masked using the regions defined in Lavell et al. (2012) (SREX regions, Fig. 3.1), leaving only region seven to be used within the simulations.
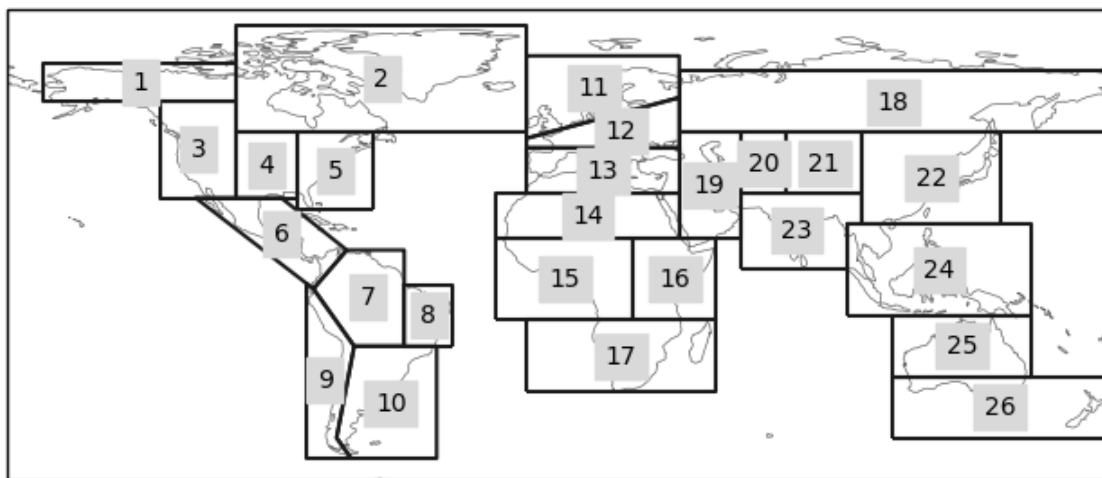
Figure 3.1: Regions defined by the Special Report on Managing the Risks of Extreme Events and Disasters to Advance Climate Change Adaptation (SREX).

3.2.2 Simulation set-up

The mean GPP over the first year of the simulation period was used with the AGB data to calculate vegetation carbon turnover time (τ) in each grid box. This was then used together with the time averaged Q_{10} function of the first year of driving temperature to evaluate the ϕ parameter in SUGAR for each grid-box. The parameters Y_g, a_{K_m} and q_{10} were kept at their default values. NPP data required to evaluate α was not available and so predicted PCE was not split into respiration and growth components. Each simulation was initialised with a different value of f_{NSC} and then spun-up to equilibrium using a 12-year repeated loop of the parametrisation year data (i.e. the first year of the simulation period).

3.2.3 Evaluation

To assess the effect that SUGAR has on predictions of PCE, a basin wide average PCE flux was compared to the basin average GPP for each pool size. An average seasonal cycle over the simulation period of GPP and PCE for each value of f_{NSC} was calculated at both a basin average and individual grid-box scale. Both the coefficient of variation and average seasonal cycle of predicted PCE were calculated for each grid-box and compared to those of GPP, in order to assess the effect of carbohydrate on seasonal variability of PCE. It is important to note that in models that do not simulate NSC storage, GPP and PCE are equivalent. This means that these comparisons not only show differences between PCE and GPP in SUGAR, but also potential differences in the prediction of PCE between SUGAR and models that do not simulate NSC. The drivers of variability of predicted PCE were also evaluated. The two possible drivers of PCE in SUGAR are carbon availability from the NSC pool which is itself driven by the carbon input from GPP, and temperature via the Q_{10} function. Therefore, the Pearson correlation coefficients of simulated PCE and driving GPP, and PCE and the Q_{10} function were calculated in each grid cell for each value of f_{NSC}. A strong correlation between predicted PCE and either variable was interpreted to mean that the variable was a strong driver of variability in PCE.

Finally, the seasonality of predicted PCE was compared to that of observed leaf production at two Amazonian evergreen forests (Wu et al., 2016). The first site (henceforth referred to as K67) is located in the Tapajós National forest near Santarém, Brazil (2.85°S, 54.97°W). The second site (henceforth referred to as K34) is located in the Reserva Cuieiras near Manaus, Brazil (2.61°S, 60.21°W) (Fig. 3.2). Wu et al. (2016) estimated an average seasonal cycle of leaf production rates at each site using litter-fall and camera-based leaf area index (LAI) observations at both sites. These were compared to the average seasonal cycle of

simulated PCE in the two grid-boxes containing each site.
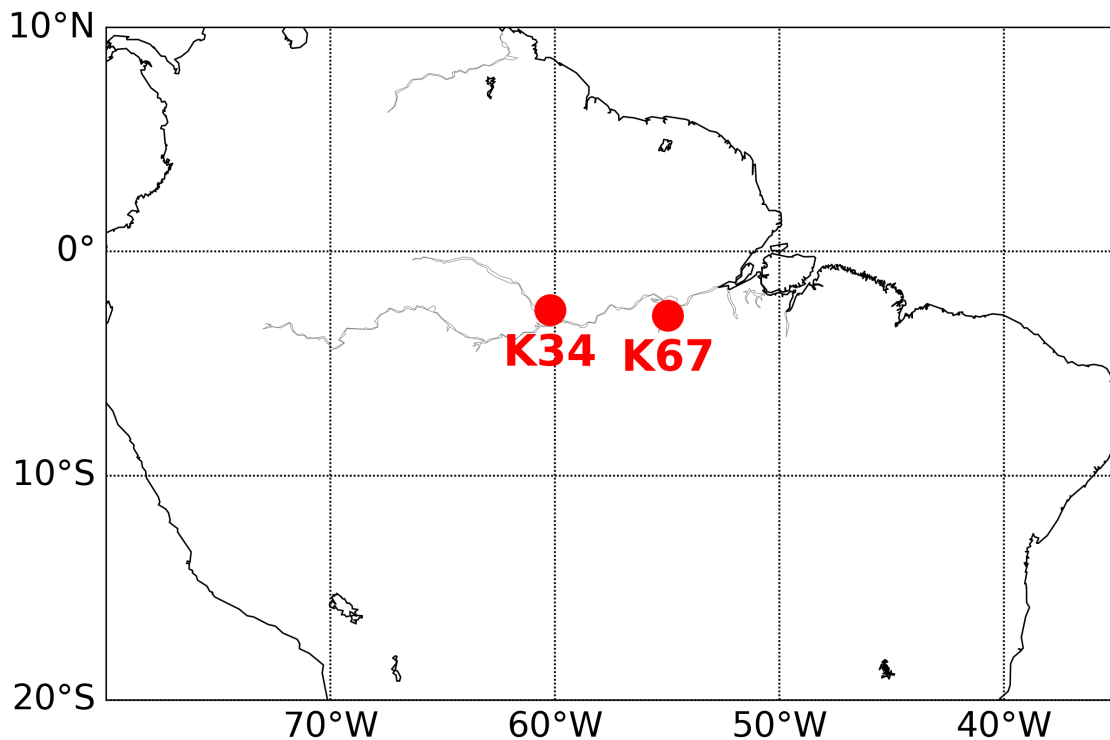
Figure 3.2: Location of two sites in the Amazon Basin at which observations of leaf production rates have been derived (Wu et al., 2016)

3.3 Results

Predictions of basin average PCE showed a significant sensitivity to the size of the initialised NSC pool (f_{NSC}). In the simulations with $f_{NSC} = 0.0005$, roughly equivalent to a model that does not represent NSC, the rate of predicted basin average PCE was almost exactly equivalent to the rate of basin average GPP from the GOSAT driving dataset (Fig. 3.3). However, as the f_{NSC} parameter was increased between simulations, the NSC pool in SUGAR caused predicted PCE to decouple from GPP, with significant differences between the two fluxes occurring in the simulations with the largest f_{NSC} values over the six and a half year period (Fig. 3.3).

The decoupling between predicted PCE and GPP was reflected in the average seasonal cycle of each flux, and SUGAR altered both the seasonal phase and amplitude of predicted seasonal PCE relative to GPP. On average the seasonal peak in the basin average GPP from GOSAT occurred in January (Fig. 3.4). In the simulations with $f_{NSC} = 0.0005$ this was mirrored in the average seasonal cycle of predicted PCE. However, as f_{NSC} was increased the mean peak in basin PCE was both dampened in magnitude and shifted in time. In the simulations
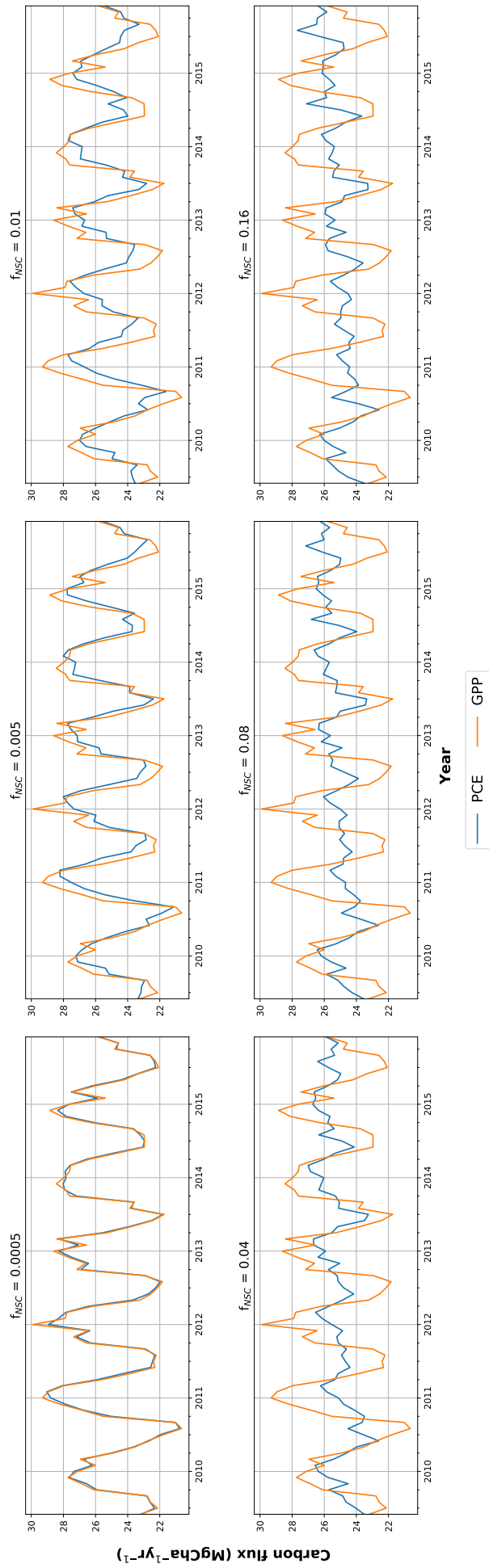
Figure 3.3: Simulated plant carbon expenditure (PCE) from SUGAR against driving gross primary productivity (GPP) (Parazoo et al., 2014) over the Amazon basin, for different initialised carbohydrate content as a fraction (f_{NSC}) of grid-box biomass (Avitabile et al., 2016).

with $f_{NSC} = 0.08$, representative of a realistic estimate of ecosystem NSC content (Würth et al., 2005), the mean seasonal peak in predicted basin average PCE no longer corresponded with the peak in basin average GPP in January, but occurred one month later in February. Additionally a second peak of comparable size occurred in August, one month after the seasonal minimum of GPP (Fig. 3.4). When the NSC pool was doubled to $f_{NSC} = 0.16$, this second peak (in August) became larger on average resulting in a 7 month difference between average seasonal peaks in PCE and GPP within the same year.

The decrease in the seasonal amplitude of predicted PCE with increasing f_{NSC} resulted in a decline in it's seasonal variability across the Amazon basin (Fig. 3.5). The coefficient of variation of the basin average GPP data was 9.51% with a maximum individual grid-box coefficient of variation of 40.9%, and a minimum of 7.47% (Fig. 3.5). When SUGAR was initialised with f_{NSC} = 0.0005, the coefficient of variation of the basin averaged PCE was similar at 9.12% (grid-box bounds: 6.57 − 37.4%, Fig. 3.5). As f_{NSC} increased the coefficient of variation decreased sharply across all grid boxes. At f_{NSC} = 0.04, the coefficient of variation across the Amazon was 3.73% with a minimum individual grid-box value of 3.59%, and a maximum value of 29.8% (Fig. 3.5). The dampening effect started to saturate at larger values of f_{NSC} and the coefficient of variation of simulated PCE decreased more slowly with increasing f_{NSC} from this point. At f_{NSC} = 0.08, the coefficient of variation of PCE across the Amazon was 3.54% (bounds: 3.78 − 25.1%, Fig. 3.5). Finally at f_{NSC} = 0.16 the coefficient of variation of simulated basin PCE was 3.63% (grid-box bounds: 3.74 - 22.9%, Fig. 3.5).

The dampening of predicted seasonal PCE caused by SUGAR occurred across all grid-boxes but was not uniform in its magnitude, and increasing the effective size of the NSC pool also reduced the spatial variation in the seasonality of PCE across Amazonia. Relative to the wetter northern Amazon, the more seasonally dry southern Amazon experiences far greater seasonal variation in GPP. This pattern was mirrored in the seasonal variation of simulated PCE (Fig. 3.5), however, with more NSC in the model the difference between PCE seasonality in the north and south declined, due to a larger decrease in seasonal variation of PCE in the southern regions. This was caused by an increase in dry season carbon expenditure when GPP was low, and a decrease in the wet season carbon expenditure when GPP was at a seasonal peak.

Alongside the decoupling between GPP and PCE, there was also a shift in the primary driver of simulated PCE. In the approximately 0% NSC mass fraction simulation ($f_{NSC} = 0.0005$), the Pearson Correlation coefficient between GPP
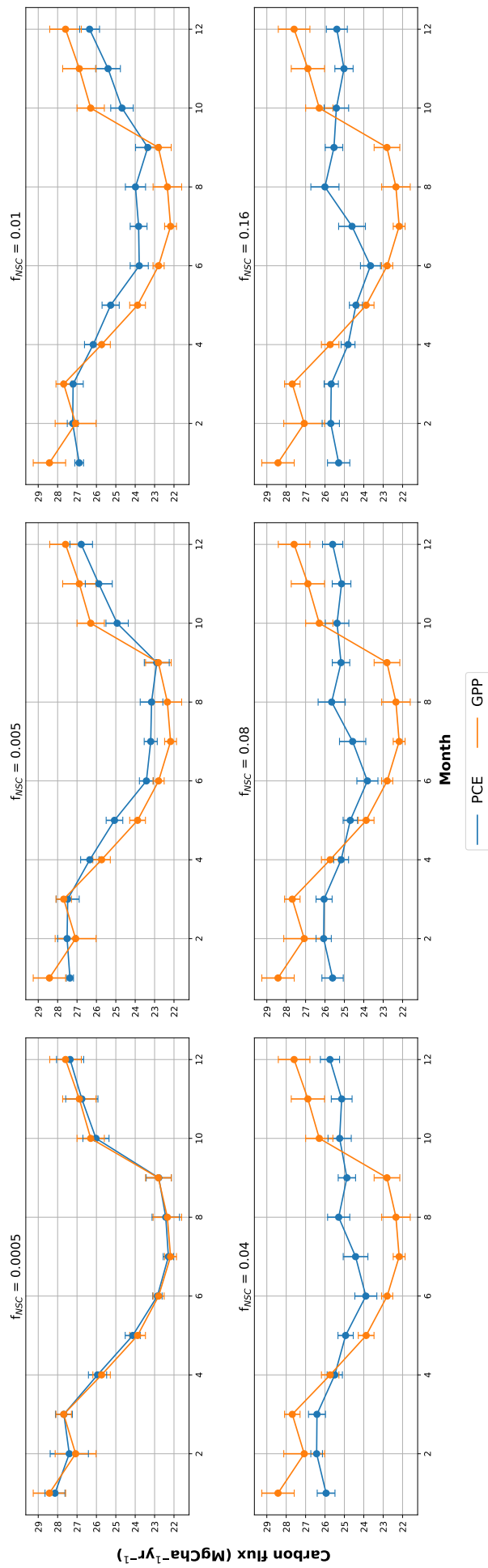
Figure 3.4: The average seasonal cycle of simulated plant carbon expenditure (PCE) from SUGAR and driving gross primary productivity (GPP) (Parazoo et al., 2014) over the Amazon basin, for different initialised carbohydrate content as a fraction (f_{NSC}) of grid-box biomass (Avitabile et al., 2016).
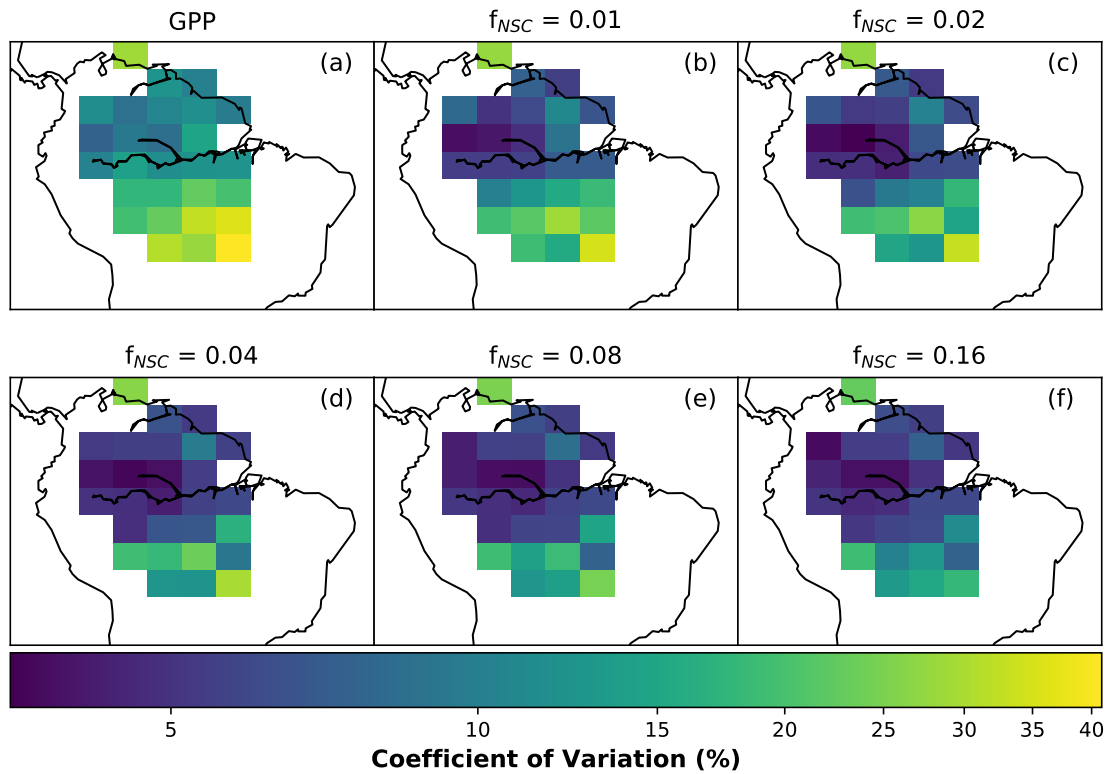
Figure 3.5: The coefficient of variation of **(a)** Gross Primary Productivity (GPP) (Parazoo et al., 2014) and **(b-f)** simulated Plant Carbon Expenditure (PCE) for different initialised carbohydrate content as a fraction of grid-box Biomass (f_{NSC}).

and predicted PCE was 0.980 on average across the Amazon, with a minimum individual grid-box value of 0.939, and a maximum value of 1.00 (Fig. 3.6). As f_{NSC} increased, the correlation between GPP and PCE declined (Fig. 3.6). In the 8% NSC mass fraction simulations ($f_{NSC} = 0.08$), the Pearson Correlation coefficient had an average value across the Amazon of 0.181, with a minimum individual grid-box value of -0.501, and a maximum of 0.997 (Fig. 3.6). This decline in the correlation between GPP and PCE not only indicates the decoupling between the two fluxes but also the declining influence of GPP on the rate of PCE in SUGAR as the NSC pool is increased. In contrast the Pearson Correlation coefficient between predicted PCE and the Q_{10} function (Eq. (2.32)) in SUGAR increased across the Amazon with increasing f_{NSC} (Fig. 3.7). In the simulations with $f_{NSC} = 0.0005$, there was little correlation between PCE and the Q_{10} function with an average Pearson Correlation coefficient of -0.0485 across the Amazon, with minimum and maximum individual grid-box values of -0.651 and 0.517 respectively (Fig. 3.7). In the simulations with $f_{NSC} = 0.08$, the Pearson Correlation coefficient had increased to an average value of 0.637, with minimum and maximum grid-box values of -0.456 and 0.956 respectively. This increase demonstrates the increase in the control of temperature over predictions of PCE via the Q_{10} function, and a shift in the primary driver of PCE from being GPP in the simulations with small NSC pool sizes, to the Q_{10} function in the simulations
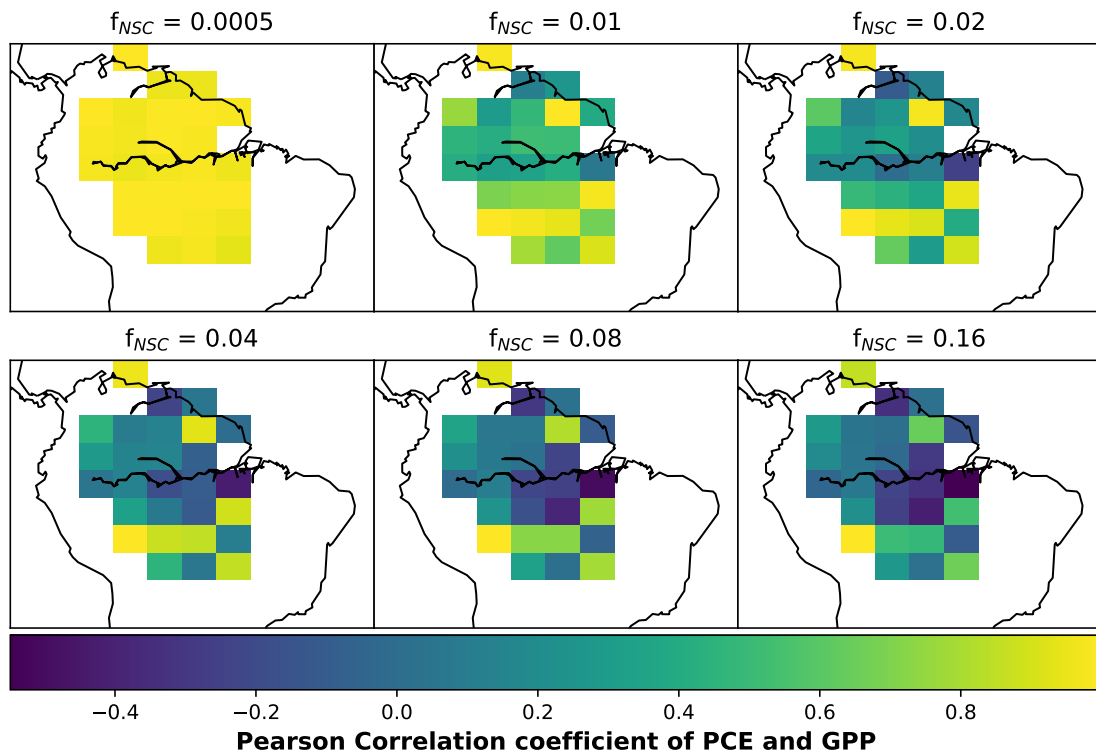
Figure 3.6: The Pearson correlation coefficient of simulated plant carbon expenditure (PCE) and driving gross primary productivity (GPP) for different initialised carbohydrate contents as a fraction (f_{NSC}) of grid-box biomass. This gives an indication of how important a driver GPP is for PCE in each grid-box.

with large NSC pool sizes.

3.4 Discussion

SUGAR alters the relationship between photosynthesis and plant carbon expenditure. In the absence of labile carbohydrate, these two fluxes are necessarily equal as the only source of carbon for respiration and growth is instantaneous assimilate from photosynthesis. This means that in models that lack any representation of NSC, PCE and GPP are always equivalent. With little or no carbohydrate, carbon expenditure in SUGAR is driven predominantly by the rate of photosynthesis, and the fluxes are equivalent (Fig. 3.3). Carbon is used by the ecosystem as soon as it is assimilated, meaning that the rate of expenditure is highly correlated with the rate of photosynthesis (Fig 3.7). This dependence of PCE on photosynthesis is often described as 'source-limitation', or 'source driven carbon dynamics' indicating the predominant role that photosynthesis (the source of carbon) has in determining the carbon balance of the ecosystem. Source-limitation is at the heart of many LSMs, likely owing to the relatively easy nature of measuring plant photosynthesis, compared to the complexity of measuring internal carbon allocation processes (Fatichi et al., 2019; Körner, 2015). Over long time scales (e.g.

57
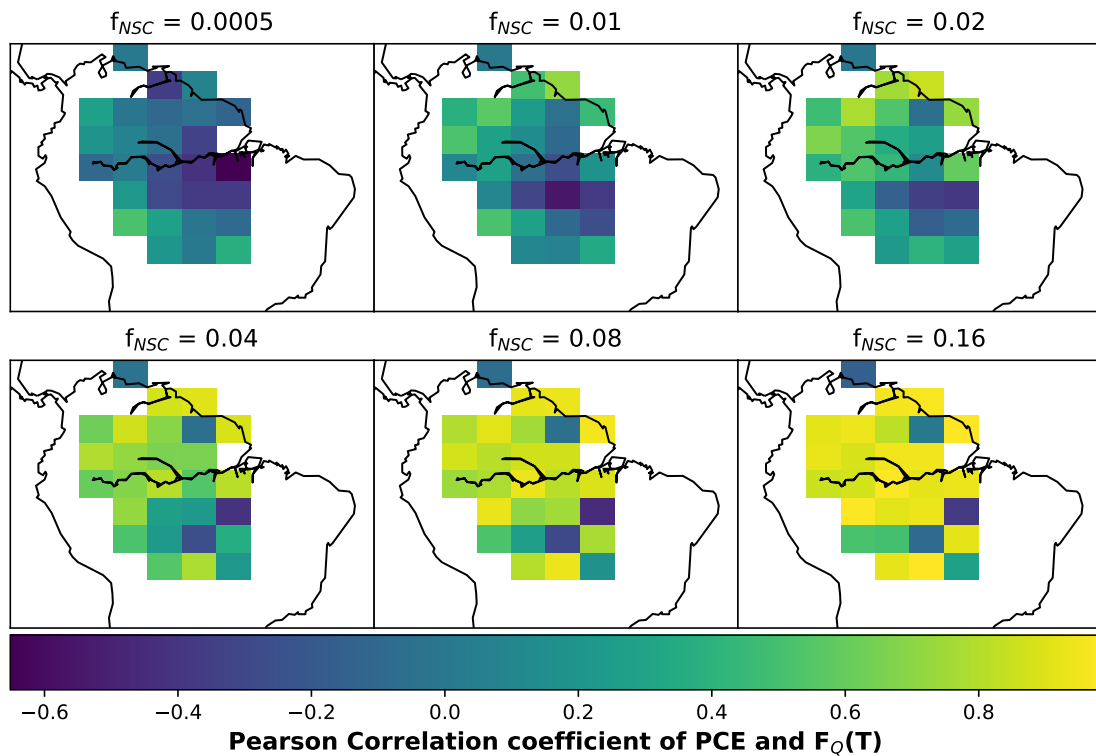
Figure 3.7: The Pearson correlation coefficient of simulated plant carbon expenditure (PCE) and driving Q_{10} (F_Q) for different initialised carbohydrate contents as a fraction (f_{NSC}) of grid-box biomass. This gives an indication of how important a driver the Q_{10} function is for PCE in each grid-box.

> 1 year) the equality between PCE and GPP may hold, and the total amount of carbon assimilated through photosynthesis will be approximately the same as the total amount expended by respiration and growth (PCE). However, on shorter time scales (e.g. seasonal or diurnal time scales) PCE and GPP can diverge significantly with carbon being expended either when physiologically needed or when environmental conditions allow; and not simply when it is made available through photosynthesis (Doughty et al., 2015a; Restrepo-Coupe et al., 2016).

Increasing evidence suggests that components of PCE, in particular plant growth, are often more strongly limited by the rate at which they can use carbon, referred to as their 'sink strength', rather than the rate at which carbon is supplied (Fatichi et al., 2014; Körner, 2003; Wiley and Helliker, 2012; Palacio et al., 2014). Limitation by sink-strength, or 'sink-limitation', means that PCE is more commonly driven by environmental factors, such as temperature and water availability, than it is by photosynthesis. This can result in differences between GPP and PCE both through time and across space, as the two fluxes respond differently to temporal variations and spatial gradients in climate. Sink-limitation is only possible if theses differences between photosynthesis and carbon expenditure can be supported by labile NSC pools. In SUGAR we see a transition from source to sink-
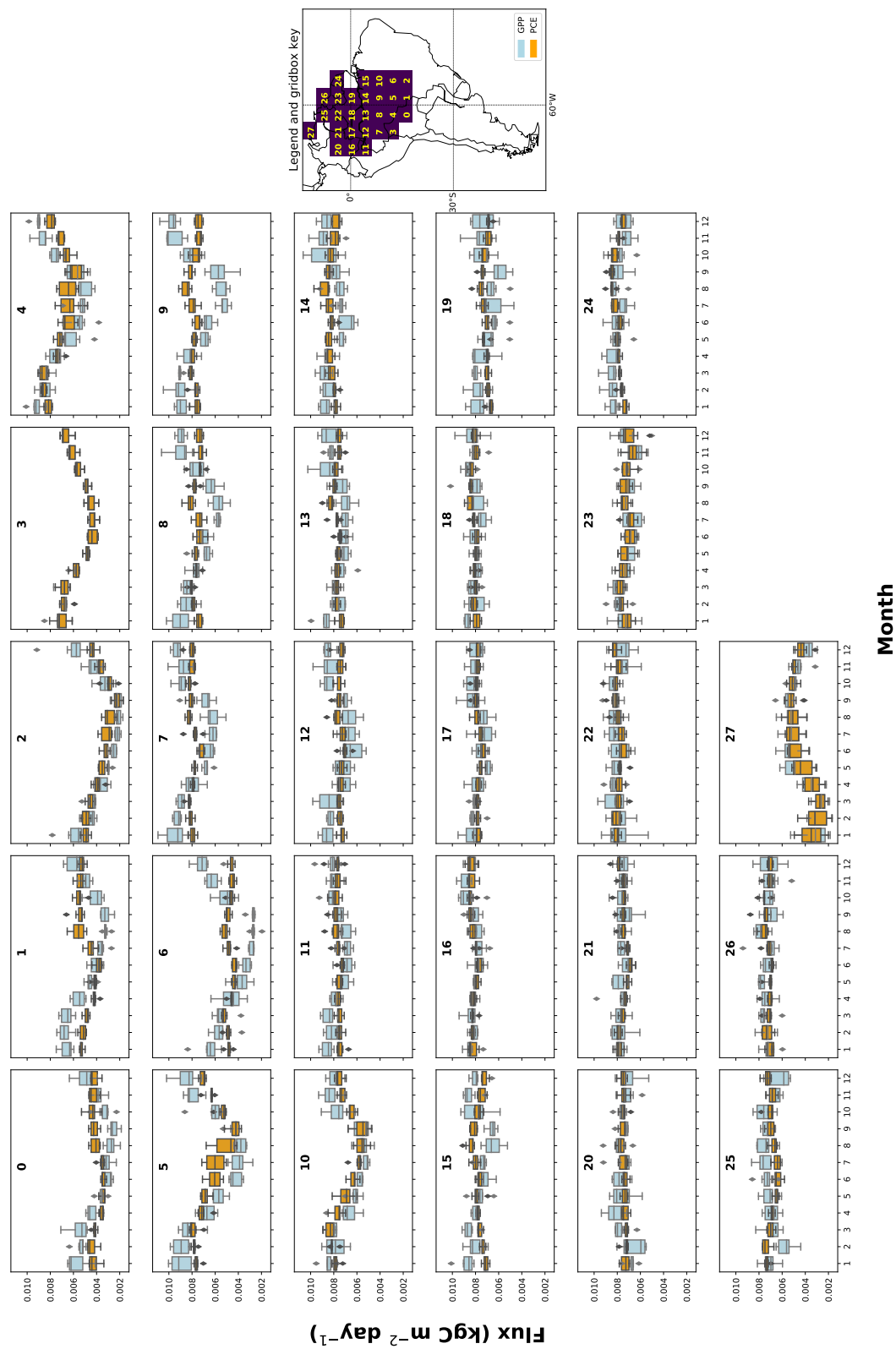
Figure 3.8: The mean seasonal trend of simulated plant carbon expenditure (PCE) and forcing gross primary productivity (GPP) (Parazoo et al., 2014) for each gridbox in the $f_{NSC} = 0.08$ SUGAR simulations. The map key shows which plot corresponds to which grid-box.
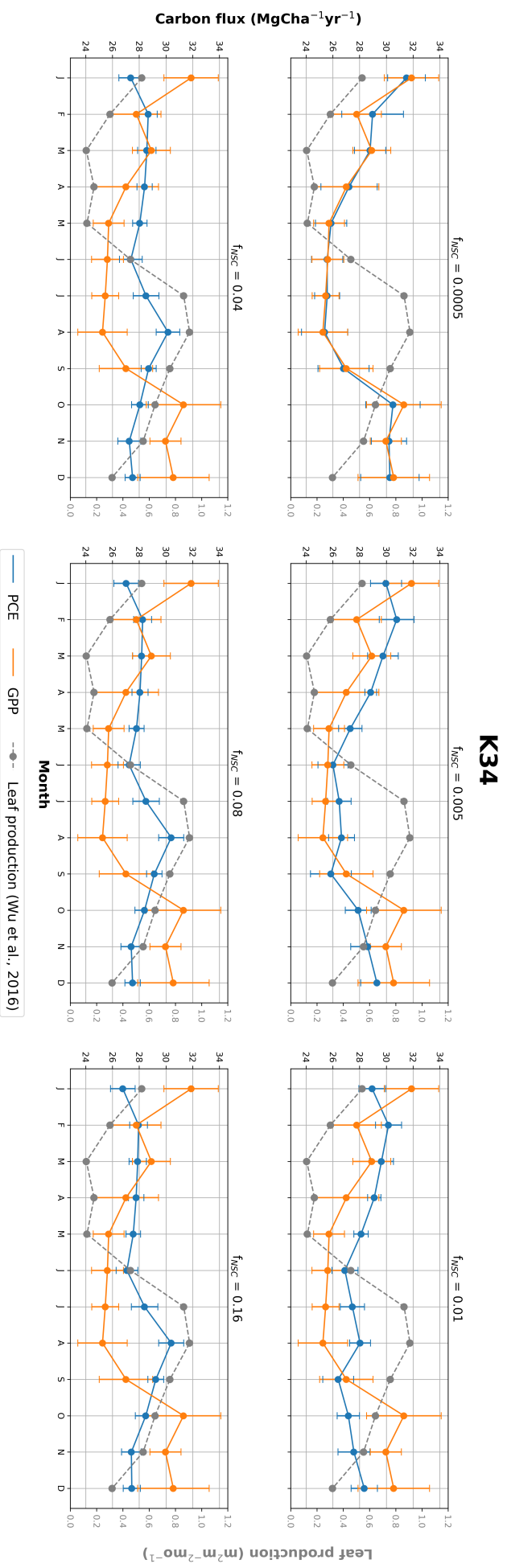
Figure 3.9: The average seasonal cycle of simulated plant carbon expenditure (PCE) from SUGAR for a range of initialised carbohydrate concentrations, compared to the observed seasonal cycle of leaf production (Wu et al., 2016) at the K34 site in the Reserva Cuieiras, Brazil.
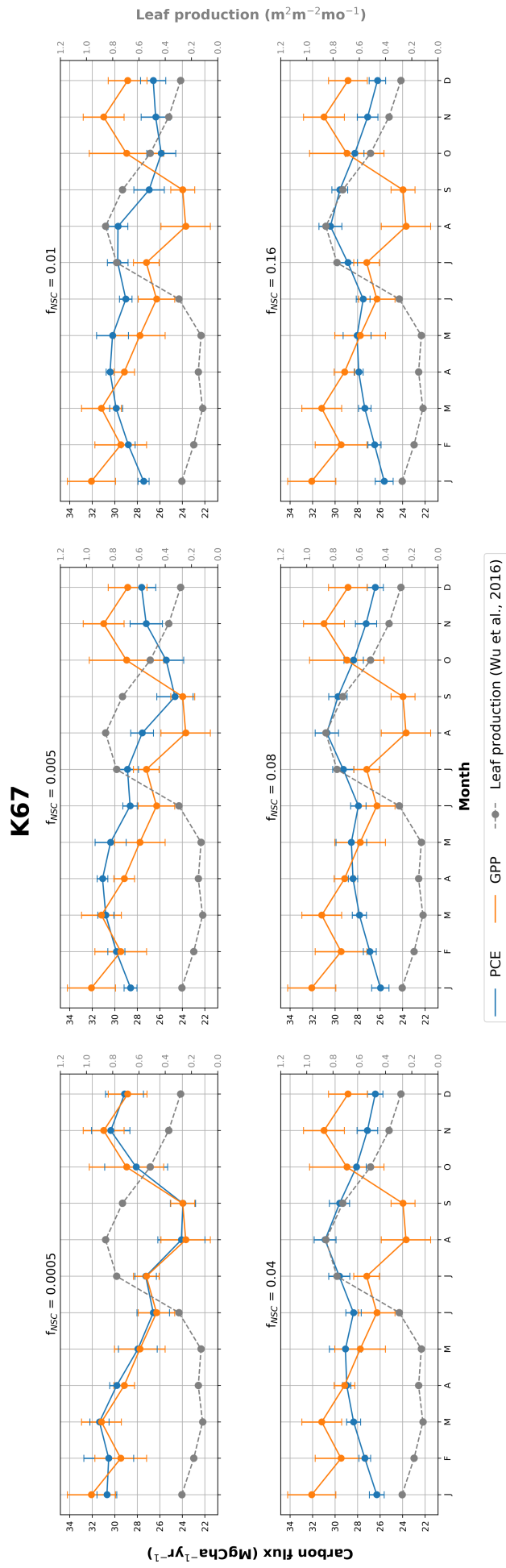
Figure 3.10: The average seasonal cycle of simulated plant carbon expenditure (PCE) from SUGAR for a range of initialised carbohydrate concentrations, compared to the observed seasonal cycle of leaf production (Wu et al., 2016) at the K67 site in the Tapajós National forest, Brazil.

limitation by adding more carbohydrate to the ecosystem. As the f_{NSC} parameter was increased, PCE in SUGAR became less carbon limited (Fig 3.6) and more controlled by the Q_{10} that controls its response to temperature (Fig 3.7). This allowed PCE and GPP to diverge over the seasonal time-scale and across spatial gradients. In the simulations with the largest f_{NSC} values, this resulted in a significant change in the seasonality of predicted PCE (Fig. 3.3), and the spatial patterns of PCE variability across the Amazon (Fig. 3.5).

At the basin scale, the average seasonal cycle of predicted PCE in SUGAR exceeded that of the driving GPP, for five months between May and September, when the model was initialised with f_{NSC} values of 0.04 and above (Fig. 3.4). In addition, there was a significant shift in the average seasonal peak of PCE relative to GPP, with peak carbon expenditure moving from January, when GPP was also at its seasonal maximum, to August, only a month after the seasonal minimum of GPP (Fig. 3.4). This shift from January to August was fully realised in the simulations with the largest initialised NSC pool, although it is difficult to draw much significance from this simulation since the initialised carbohydrate pool was twice that of a realistic estimate. However, it aptly demonstrates the upper bound of the transition of predicted PCE with increasing NSC. Similar asynchrony between PCE and GPP has been observed across the Amazon. Doughty et al. (2015a) found that PCE exceeded GPP for at least four months of the year at two sites within the Amazon. In Caxiuanã, Brazil PCE exceeded GPP between April and August, while in Tambopata, Peru this occurred between August and November (Doughty et al., 2015a). While these differences occur over short time-scales, they may be significant over the long-term, in particular if the asynchrony is driven by extreme stress events such as drought (Martínez-Vilalta et al., 2016; Adams et al., 2013; Galiano et al., 2011). Maintaining PCE during periods of reduced GPP is a key part of plant survival as many components of PCE are integral to plant function. Developing simple representations of NSC such as SUGAR, that allow PCE to decouple from GPP in LSMs, is therefore vital for improving the accuracy of future projections of the Amazon.

Capturing the correct seasonality of PCE is of course key to accurately simulating growth and respiration fluxes, but may also be crucial for predicting the seasonality of photosynthesis. Wu et al. (2016) found that the variability of climate alone was insufficient to fully explain the seasonality of photosynthesis at various sites across the Amazon. The timing of peaks in LAI, as well as the age and quality of leaves were found to be primary drivers of GPP over seasonal time-scales. The rate of leaf production, as well as the rate of leaf senescence, are therefore key variables in predicting plant productivity across the Amazon, and this creates

an important feedback between carbon expenditure and productivity. At two of the sites (K34 and K67) observed by Wu et al. (2016), leaf production peaked in the dry season, several months before the peak in observed GPP (Figs 3.9 & 3.10). This pattern may be a sign of active strategies by plants that aim to optimise carbon gain from photosynthesis given the seasonality of light, temperature and precipitation (Kikuzawa, 1995), and these strategies likely rely on significant stores of NSC within plants as well as subsoil water reserves (Elliott et al., 2006; Nepstad et al., 1994).

Interestingly the peak in leaf production observed by Wu et al. (2016) is matched by the predicted peak of PCE in SUGAR in the corresponding grid-boxes of each site, for realistic estimates of f_{NSC} (Figs 3.9 & 3.10). The comparison of a single component of carbon expenditure to total PCE must be done with caution, as the proportions of total PCE allocated to each process within a plant can vary significantly throughout a year, particularly in response to changes in water-availability (Chaves et al., 2002; Doughty et al., 2015a). The seasonality of total PCE may therefore differ greatly from that of a single component such as leaf production. Nonetheless, the agreement between SUGAR and these observations may provide insight into the drivers for leaf growth across the Amazon. The timing of peak leaf production rates is attributed to an optimisation strategy that maximises photosynthetic carbon gains. However, it seems likely that there are still one or more environmental indicators that trigger this increased leaf production and allow the optimisation to occur. In the SUGAR simulations with f_{NSC} values above 0.04, the primary driver of PCE was temperature via the Q_{10} function. It is possible that changing temperatures also signal the increase in leaf production seen at the K34 and K67 sites. However, the seasonality of insolation has previously been found as a predominant driver of leaf production in non-water-limited forests across the Amazon (Wagner et al., 2017), and given the strong correlation between incoming solar radiation and maximum air temperature (Wagner et al., 2017), it is also possible that the temperature response in SUGAR is acting as a proxy for incoming light radiation. A better understanding of the physiological mechanisms behind leaf growth is required to correctly represent the environmental drivers of both PCE and GPP.

As well as changing the timing (or phase) of the peak of PCE, SUGAR also altered its seasonal amplitude, reducing the overall variability of PCE across the Amazon. This effect was most pronounced in the semi-arid regions of the southern Amazon where there is a strong seasonal cycle in GPP (Fig. 3.8), corresponding to a strong seasonal pattern of precipitation. Semi-arid regions provide the largest contribution to the global carbon sink anomaly, in part due to this high

variability in GPP (Poulter et al., 2014; Ahlström et al., 2015). Yet variability in terrestrial carbon uptake is not only determined by the variability of GPP but also by that of plant respiration, heterotrophic respiration from soils and carbon loss from disturbance and land-use change. The seasonality of GPP varies significantly across the Amazon as ecosystems span climatic gradients (Wagner et al., 2016). However spatial patterns of respiration and growth may differ greatly due to their contrasting responses to these gradients relative to photosynthesis (Liu et al., 2017; Girardin et al., 2016; Doughty et al., 2015a). Capturing the difference between GPP and PCE spatially as well as temporally is therefore crucial to modelling the variability of terrestrial carbon uptake and representing the contribution of semi-arid regions to the global carbon sink. Given the significant role that terrestrial carbon uptake has on the global carbon balance (IPCC, 2013), accurately predicting future variability in atmospheric CO_2 concentrations (Cox et al., 2013) may be reliant on a sub-model such as SUGAR which can allow this de-coupling to occur. Further research examining the role of NSC-based approaches in large scale ecosystem models is required and we must focus on improving our understanding of NSCs and how to model them.

3.5   Conclusions

In this chapter, we have seen how SUGAR is able to decouple GPP from PCE across the Amazon basin by shifting the primary driver of carbon utilisation from being the rate of carbon assimilation by photosynthesis, to the direct control of temperature via the Q_{10} function in SUGAR. This was described as a transition from source to sink limited carbon dynamics and we saw the importance of this in relation to predictions of terrestrial carbon uptake by LSMs both spatially and through time. In the next chapter, the accuracy of SUGAR at predicting ecosystem carbon fluxes under both steady-state and extreme climatic conditions is evaluated using observational data from a through-fall exclusion (TFE) drought experiment and corresponding control forest in Caxiuanã, Brazi. Results from both SUGAR and The Joint UK Land Environment Simulator (JULES) are compared with observations for the site, allowing the role of NSC in supporting respiration and growth during drought to be investigated.

Chapter 4

Simulating the responses of a tropical forest to drought

4.1 Introduction

The frequency and severity of droughts are predicted to increase across large parts of the globe as a result of climate change (Marengo et al., 2018; Hartmann et al., 2013). The effects of drought on vegetated ecosystems are well documented (Phillips et al., 2009; Bastos et al., 2018; Luo et al., 2018; Gloor et al., 2018; Schwalm et al., 2012), yet their sensitivity to the droughts of the future is highly uncertain. Key questions relate to how forests will respond to increasing drought length and severity (McDowell et al., 2008), as well as the effect that repeated droughts, occurring in quick succession may have on ecosystem responses (Anderegg et al., 2020). Plants can be resilient to less severe and short-term droughts as they combat excessive water loss by closing stomata (Martínez-Vilalta et al., 2014; Sperry and Love, 2015; Tyree and Sperry, 1989), and manage the resulting loss in productivity by making use of stores of non-structural carbohydrates (NSC) (O'Brien et al., 2015). However, over the long-term, or if the decline in water availability is particularly severe, drought may cause significant increases in forest mortality as plants become more likely to succumb to hydraulic failure or carbon starvation, and become more vulnerable to disturbance from biotic attack and fire (Rowland et al., 2015; Meir et al., 2018; Nepstad et al., 2007; McDowell et al., 2008). Our understanding of these long-term/severe drought responses stems largely from experimental studies in which soil moisture is artificially reduced by preventing rainfall from reaching the forest floor. These experiments, referred to as through-fall exclusion (TFE), allow more severe and prolonged drought conditions to be studied than can be achieved by observing natural droughts alone. TFE experiments have provided significant insight into the response of forests to the potential droughts of the future, however, due to the small number of experiments that have actually been carried out, particularly in

the tropics where only eight have been reported (Meir et al., 2015), determining the mechanistic processes behind these responses remains a challenge.

The 'Esecaflor' experiment in Caxiuanã, Brazil is a large-scale TFE experiment in the Amazon rainforest. As the longest running tropical TFE experiment, it has not only provided unique insight into the response of the Amazon to extreme drought, but also become a useful tool for evaluating process-based vegetation models such as those that exist within the land surface model (LSM) component of global climate models. Accurately capturing the response of the forest to the TFE experiment is an important benchmark that allows us to assess the capacity of LSMs to predict future responses to drought. However, previous simulations using five process-based terrestrial biosphere models (CLM3.5, (Levis et al., 2004; Oleson et al., 2008); ED2, (Medvigy et al., 2009); IBIS v2.6.4, (Foley et al., 1996; Kucharik et al., 2000); JULES v2.1 (Best et al., 2011; Clark et al., 2011) and SiB3, (Sellers et al., 1996; Baker et al., 2008)) reveal significant deficiencies in predictions of the experiment (Powell et al., 2013). While the five models were able to successfully capture the behaviour of a corresponding control plot associated with the experiment, the response of the forest in the TFE plot was poorly represented in all five model simulations. Each model failed to correctly capture the loss of above ground biomass (AGB) through mortality as a result of the drought, and responses of carbon fluxes and allocation, including autotrophic respiration and net primary productivity (NPP), over both the short and long term were also not captured by the models. These mismatches between predictions and observations have been attributed to a lack of drought induced mortality mechanisms within models; an over sensitivity of photosynthesis to soil water stress, resulting in an overestimation of productivity declines in response to the drought; and deficiencies in the phenological cycle within the models, which has an important role in determining whole canopy level carbon fluxes. However, the role of other factors, including the dynamics of NSC have been so far left unexplored.

Observations suggest that during the early stages of the experiment, the TFE forest was using significantly more carbon than was being supplied through photosynthesis, as Plant Carbon Expenditure (PCE - the sum of plant growth and respiration) exceeded Gross Primary Production (GPP) by $7.0\pm4.5\,\mathrm{MgC\,ha^{-1}\,yr^{-1}}$ in the third year of the experiment (Metcalfe et al., 2010). This implies an important role for NSCs, which are typically used to support this type of asynchrony between supply and utilisation during the drought. However, it has also been observed that trees that died as a result of the experiment showed no significant signs of depleted NSC stores relative to trees in the control plot (Rowland et al., 2015). Resolving these apparently contradicting observations remains a

challenge as detailed observations of NSC concentrations over the course the experiment are not available due to the high complexity and uncertainty involved in collecting this data. Comprehensive representations of NSC and its role in determining plant respiration and growth rates are also missing from previous modelling studies of the experiment, including within the five models used in Powell et al. (2013). The role of NSC dynamics in the response of the forest to the experiment, and its contribution to the discrepancies between model predictions and observations remain unclear.

In this chapter, the role that NSC dynamics has on model predictions during the drought is assessed. New simulations of the TFE experiment and corresponding control plot are carried out using a more recent version of one of the five models used in Powell et al. (2013), namely version 5.2 of the Joint UK Land Environment Simulator (JULES). The output from these simulations is then used to drive SUGAR off-line to produce a post-processed set of model predictions that account for the effect of NSC on ecosystem carbon fluxes in each plot. The outputs from both JULES and SUGAR are evaluated against observations from the TFE experiment (Metcalfe et al., 2010; da Costa et al., 2014) as well as a new time-series of NPP derived from data collected in Rowland et al. (2015). In addition to investigating the role that NSC may have had in the ecosystem response to the TFE experiment in Caxiuanã, this chapter represents an opportunity to evaluate the capability of SUGAR at predicting carbon fluxes, both under steady-state, and extreme climate conditions.

4.2 Methods

4.2.1 The Caxiuanã drought experiment

The TFE experiment is located in the Caxiuanã National Forest, Pará State, Brazil (1°43'3.5"S, 51°27'36"W), where measurements of meteorology and plant physiology of two 1 ha plots began in 2001. In January 2002, panels were introduced into one of the plots, excluding c. 50% of rainfall from the soils and subjecting the plot to an artificial drought. Measurements of meteorology and forest physiology continue to the present day, providing a detailed dataset of forest response to drought. At the start of the experiment, total estimated above-ground biomass was 213.9 ± 14.2 MgC ha^{-1} in the control forest, and 200.6 ± 13.2 MgC ha^{-1} in the TFE plot. After 13 years of the drought treatment, biomass loss to mortality in the TFE plot had increased by $41.0\pm2.7\%$ relative to 2001 values (Rowland et al., 2015). Observations and modelling studies at the site suggest that while GPP declined in response to the artificial drought, PCE was maintained at close to pre-drought levels during at least the first 3-4 years of the experiment (Metcalfe

et al., 2010; Fisher et al., 2007). NSC reserves are thought to have sustained PCE during this time and it is estimated that the forest had access to c. 20 $MgC\,ha^{-1}$ of available NSC (c. 8% of live biomass) during the drought (Metcalfe et al., 2010). This discrepancy between PCE and GPP in the TFE plot cannot be captured by LSMs without simulating some kind of NSC storage. A full summary of the experimental set up and the most recent collection of results from the site is available in Meir et al. (2018).

4.2.2 JULES simulations

4.2.2.1 Paramtetrisation

JULES version 5.2 was first used to simulate the control plot from 2001-01-01 to 2016-12-09 using a pre-existing parametrisation of the site. This initial simulation predicted much lower values of GPP than observations (Metcalfe et al., 2010; da Costa et al., 2014) and so the effective leaf nitrogen content in JULES was increased by increasing the 'vint' and 'vsl' parameters. These represent the intercept and slope, respectively, of the linear relationship between V_{cmax} and leaf nitrogen. vint was increased from 7.21 to 12.0 and vsl from 19.22 to 25.0. This increased V_{cmax}, bringing predicted GPP in-line with observations. This increase in V_{cmax} however, also increased predicted plant respiration in JULES, causing predicted carbon use-efficiency to drop below observed values. This was solved by reducing the 'fd' parameter, which controls the linear relationship between dark respiration and V_{cmax}, from 0.01 to 0.0075. The same parametrisation was then used to simulate both the control and TFE plots over the same period. Both simulations were spun up for 176 years using a repeated loop of the control meteorological data.

4.2.2.2 Driving data

JULES was driven with hourly meteorological data collected from the site (da Costa et al., 2010, 2018) over the simulation period. Mean annual rainfall during this period was between 1772.6 and 2967.1 mm. To simulate the effect of the drought experiment, precipitation in the TFE driving data was halved from January 1, 2002, in line with estimates of average exclusion rate. Daily incident radiation varied from 419.8 $W\,m^{-2}$ to 731.1 $W\,m^{-2}$. Specific humidity, long-wave radiation and air pressure were not collected but were be either estimated or calculated from other meteorological variables. Air pressure was assumed constant at 101325.0Pa (Atmospheric pressure at sea level). This is a reasonable assumption as, although there will have been some variation in reality, JULES is not particularly sensitive to changes in air pressure in the likely range. Specific humidity (q) was calculated

from relative humidity (rh), temperature (T) (°C) and air pressure (p):

Specific humidity is defined as the ratio of water vapour mass (m_w) to total air mass ($m = m_v + m_d$, where m_d is dry air mass).

$$q = \frac{m_v}{m_v + m_d} \tag{4.1}$$

This can be written in terms of the mixing ratio (w) which is defined as the ratio of water vapour mass to dry air mass.

$$q = \frac{w}{w + 1} \tag{4.2}$$

where $w = \dfrac{m_v}{m_d}$

We can consider water vapour to be an ideal gas under normal atmospheric conditions, which allows us to write its equation of state as:

$$e = \rho_v R_v T \tag{4.3}$$

where e is the partial pressure of water in the air (or partial vapour pressure); ρ_v is the density of water vapour in the air (i.e. the mass of water vapour, m_v, per unit volume of air.); $R_v \approx 461.5\,\mathrm{J\,kg^{-1}\,K^{-1}}$ is the specific gas constant of water vapour; and T is temperature.

Rearranging Eq. (4.3) and the equivalent equation for dry air, to find ρ_v and dry air density (ρ_d), we can write the water vapour mixing ratio in terms of the partial vapour pressure and total air pressure (p):

$$w = \frac{e R_d}{(p - e) R_v} \tag{4.4}$$

where $R_d \approx 287.1\,\mathrm{J\,kg^{-1}\,K^{-1}}$ is the specific gas constant of dry air.

Relative humidity (RH) is defined as the ratio of the water vapour mixing ratio, w, to its equivalent value at saturation (w_s) and is commonly expressed as a percentage:

$$RH = 100 \frac{w}{w_s} \tag{4.5}$$

Rearranging Eq. (4.5) for w and substituting into Eq. (4.2), we find an expression for q in terms of RH and w_s:

$$q = \frac{w_s rh}{w_s rh + 1} \tag{4.6}$$

where $rh = \dfrac{RH}{100}$

Using Eq. (4.4) we can find an expression for w_s in terms of the saturated partial vapour pressure (e_s), and write q as:

$$q = \frac{\epsilon e_s rh}{\epsilon e_s rh + p - e_s} \tag{4.7}$$

where $\epsilon = R_v / R_d \approx 0.622$

Finally we can use the August-Roche-Magnus formula to approximate e_s in terms of temperature:

$$e_s = 611.2 \exp\left(\frac{17.67T}{T + 243.5}\right) \tag{4.8}$$

Both relative humidity and temperature were measured at the site, while air pressure was estimated as described above. Long-wave radiation was calculated from measured temperature using linear relationships taken from Powell (2015). A summary of all the data used to drive JULES is given in table 4.1

Variable name	Physical variable	Units	Source
sw_down	Downward short-waveradiation	W m^{-2}	Measured directly on site
lw_down	Downward long-waveradiation	W m^{-2}	Calculated using linear regressions on temperature for each month.
tot_rain	Total rainfall	$\text{kg m}^{-2}\,\text{s}^{-1}$	Measured directly on site. Converted from mm h^{-1} to $\text{kg m}^{-2}\,\text{s}^{-1}$.
tot_snow	Total snowfall	$\text{kg m}^{-2}\,\text{s}^{-1}$	Set to zero
t	Temperature	K	Measured directly on site. Converted from ℃ to K
wind	Wind speed	m s^{-1}	Measured directly on site.
pstar	Air pressure	Pa	Not measured on site. Assumed to be constant at 101325.0 Pa (Mean pressure at sea level).
q	Specific humidity	kg kg^{-1}	Calculated using relative humidity (measured on site); temperature and estimated air pressure.

Table 4.1: A summary of the meteorological variables used to drive JULES at Caxiuanã

4.2.3 SUGAR simulations

Gridbox GPP (gpp_gb) and grid-box temperature at 1.5 m above canopy height (t1p5m_gb) outputs from JULES were then used to drive SUGAR off-line in each plot. In both control and TFE simulations the forests were considered to be in equilibrium, and the total plant biomass (C_v) was assumed to be constant. This was a reasonable assumption in the control plot given the relatively short simulation period. The assumption is less reliable in the TFE plot but was necessary to allow the effect of the NSC pool to be examined in isolation. The aim of these simulations was to examine how SUGAR compares to JULES in its response to the drought experiment. With the exception of the f_{NSC} and a_{K_m} parameters, SUGAR was therefore parametrised using the first year of output data from JULES (i.e. the year before panels were installed in the TFE plot) rather than observations from Caxiuanã. The average predicted GPP and biomass of the simulated forest were used to evaluate ϕ. The parameter α was evaluated by finding the average CUE of the simulated forest. This was then used to evaluate R_{m_0} and G_0. The NSC pool in both plots was initialised to 8% of the simulated biomass, in-line with estimates of total available NSC in the TFE plot (Metcalfe et al., 2010). Finally, to test the sensitivity of SUGAR to the parameter a_{K_m}, the simulations were repeated using a range of a_{K_m} values between 0.1 and 2.0.

4.2.4 Model Evaluation

Snapshot fluxes (NPP, R_a, PCE) from JULES and SUGAR were evaluated against observations from Metcalfe et al. (2010) and da Costa et al. (2014) for the periods 2005 and 2009-2011. Model predictions from JULES and SUGAR were calculated by taking the mean of each flux over each period. Observations for 2005 are from Metcalfe et al. (2010) and observations from 2009-2011 are from da Costa et al. (2014). Simulated photosynthesis in JULES responded almost instantly to the introduction of the panels on the TFE plot which meant that NPP, R_a and PCE changed significantly in both models between 2002 and 2005. To demonstrate this change predicted fluxes during the 2002-2004 period were also calculated for each model. Observations for this period are not available to such a comprehensive degree as they are for 2005 and the 2009-2011 period. For this reason the model predictions for 2002-2004 were compared to the 2005 observations. This is reasonable in the control plot where it is plausible that the forest was in steady state (Metcalfe et al., 2010) and so fluxes from 2005 will be similar to those during the 2002-2004 period. In the TFE plot while there were some significant changes in observed carbon fluxes during the first 3 years of the experiment, (for example the production of leaves, flowers and fruits, and fine wood (Rowland et al., 2018; Meir et al., 2018)), the forest largely resisted the effects

of the drought during this period (significant increases in mortality were not seen until 2005 (Rowland et al., 2015; Meir et al., 2018)) and so we can similarly expect fluxes from 2002-2004 to be comparable to those from 2005. Nonetheless, care should be taken with these comparisons.

Predicted plant growth from each model was also evaluated against an observed time-series of NPP from each plot. Observed NPP was calculated using total local litter-fall and AGB increment (Rowland et al., 2018). The use of AGB in place of total biomass increment means that this NPP time-series did not include root increment. This was accounted for in both models by removing the root component of plant growth. Since SUGAR does not disaggregate any fluxes into organ level components, root growth was removed using the allometric scaling within JULES.

Litter-fall was collected on a monthly basis in each plot. The dataset was gap-filled using linear interpolation (Fig. 4.1).
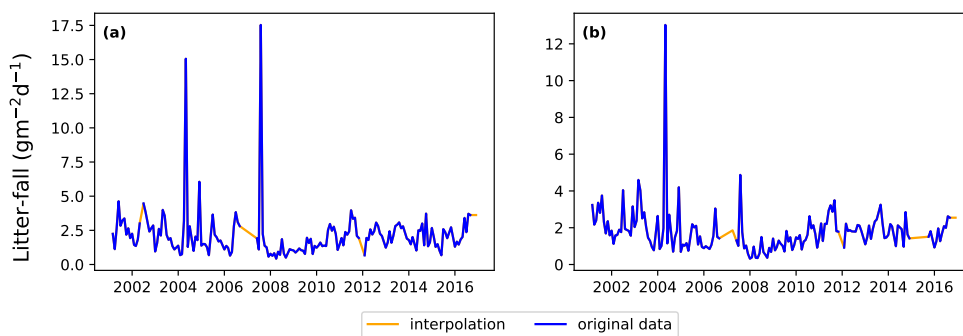
Figure 4.1: Interpolated litter-fall observations at Caxiuanã in (a) the control plot and (b) the through-fall exclusion (TFE) plot.

An ensemble of eight allometric equations (Table 4.2) were used to estimate AGB increment from trunk diameter at breast height (DBH) data that was measured on all trees with DBH>10cm, every 1 to 3 years over the period of 2000 to 2015 (Rowland et al., 2015). Trees adjacent to perimeter trenches, dug around both plots to prevent through-flow of soil water into the plots, were excluded from the datasets (Rowland et al., 2015), leaving a total measured plot size of 0.64ha. The resulting biomass was scaled to 1.0ha. If a tree grew into the DBH $\geq$10cm class during the experiment it was counted as a 'new recruit' and its DBH data was then measured. This meant that the calculated AGB increment included a recruitment flux which manifested as a positive flux of carbon each time a tree was recruited. This recruitment flux was due to a change in the sample population and not due to a change in physiology, and was therefore removed. Similarly if a tree died during the experiment it was removed from the dataset for the remainder of the mea-

surement period. This loss of carbon by mortality was also removed, isolating the plant growth component of AGB increment. The 95% confidence intervals from the ensemble of allometric equations were used as an estimate of error, although in reality the uncertainty in this data is likely to be much larger.

Author	Equation	a	b	c	d	E
Brown (1997)	$a + bD + cD^2$	42.69	-12.8	1.242		
Brown (1997)	$\exp(a + b\log_e(D))$	-2.134	2.53			
Carvalho Jr. et al. (1998)	$1000a\exp(b + c\log_e(D/100))$	0.6	3.323	2.546		
Araújo et al. (1999)	abD^c	0.6	4.06	1.76		
Chambers et al. (2001)	$\exp(a + b\log_e(D) + c\log_e(D)^2 + d\log(D)^3)$	-0.37	0.333	0.933	-0.122	
Baker et al. (2004)	$\exp(a + b\log_e(D) + c\log_e(D)^2 + d\log(D)^3)(\rho/0.67)$	-0.37	0.333	0.933	-0.122	
Chave et al. (2005)	$\exp(a + b\log_e(D) + c\log_e(D)^2 + d\log(D)^3)(\rho)$	-1.499	2.148	0.207	-0.0281	
Chave et al. (2014)	$\exp(a - 0.976E + b\log_e(D) + c\log_e(D)^2 + d\log(\rho))$	-1.803	2.673	-0.0299	0.976	-0.0510307

D = Diameter at breast height (dbh); ρ = Wood density; a, b, c, d, E are constants.

Table 4.2: Ensemble of allometric equations used to calculate above-ground biomass at the Caxiuanã drought experiment.

4.3 Results

4.3.1 Simulations in a tropical moist forest

In the simulations of the control plot, in which the forest was not subject to any artificial drought stress, JULES and SUGAR produced similar results of long term NPP accumulation (Fig. 4.2), that were both consistent with observations. By the end of the NPP observation period (2014-12-17), JULES predicted a total accumulated NPP of 155.6 $\mathrm{MgC\,ha^{-1}}$ and SUGAR 154.7 $\mathrm{MgC\,ha^{-1}}$. Both results were consistent with observations (Fig. 4.2, 161.5$\pm$22.0 $\mathrm{MgC\,ha^{-1}}$) from the site. There were some small differences between JULES and SUGAR on an inter-annual time-scale, but in general the models predicted comparable annual mean values of control plot PCE, Ra and NPP (Fig. 4.4). During the first three years of the experiment (2002, 2003, 2004), JULES predicted an annual mean PCE of 35.13 $\mathrm{MgC\,ha^{-1}\,yr^{-1}}$, and SUGAR predicted 34.79$\pm$0.17 $\mathrm{MgC\,ha^{-1}\,yr^{-1}}$. Both these results lay within the confidence intervals of the observations from the site (Fig. 4.4, 33.0$\pm$2.9 $\mathrm{MgC\,ha^{-1}\,yr^{-1}}$). The two models differed most in the natural drought years of 2005, 2010 and 2015 in which predicted annual GPP was at its lowest. In 2005 JULES predicted a decrease (relative to the 2002-2004 period) in annual mean PCE to 33.32 $\mathrm{MgC\,ha^{-1}\,yr^{-1}}$ (-5.15%) whereas SUGAR predicted an increase to 36.13$\pm$0.27 $\mathrm{MgC\,ha^{-1}\,yr^{-1}}$ (+3.85%). The decrease in JULES PCE was caused by a decrease in predicted GPP in 2005. In SUGAR this decrease in GPP was buffered by NSC storage (Fig. 4.5), and an increase in the annual mean temperature drove the increase in predicted PCE. Both results were close to the observed value although the SUGAR result was outside the observed confidence intervals by 0.64%. In 2010 average annual rainfall was 1772.6 $\mathrm{mm\,yr^{-1}}$, the lowest in the 16 year period (c. 25% decrease on the 16-year mean 2324.2 $\mathrm{mm\,yr^{-1}}$). This caused a decline in predicted GPP on the control plot from 35.92
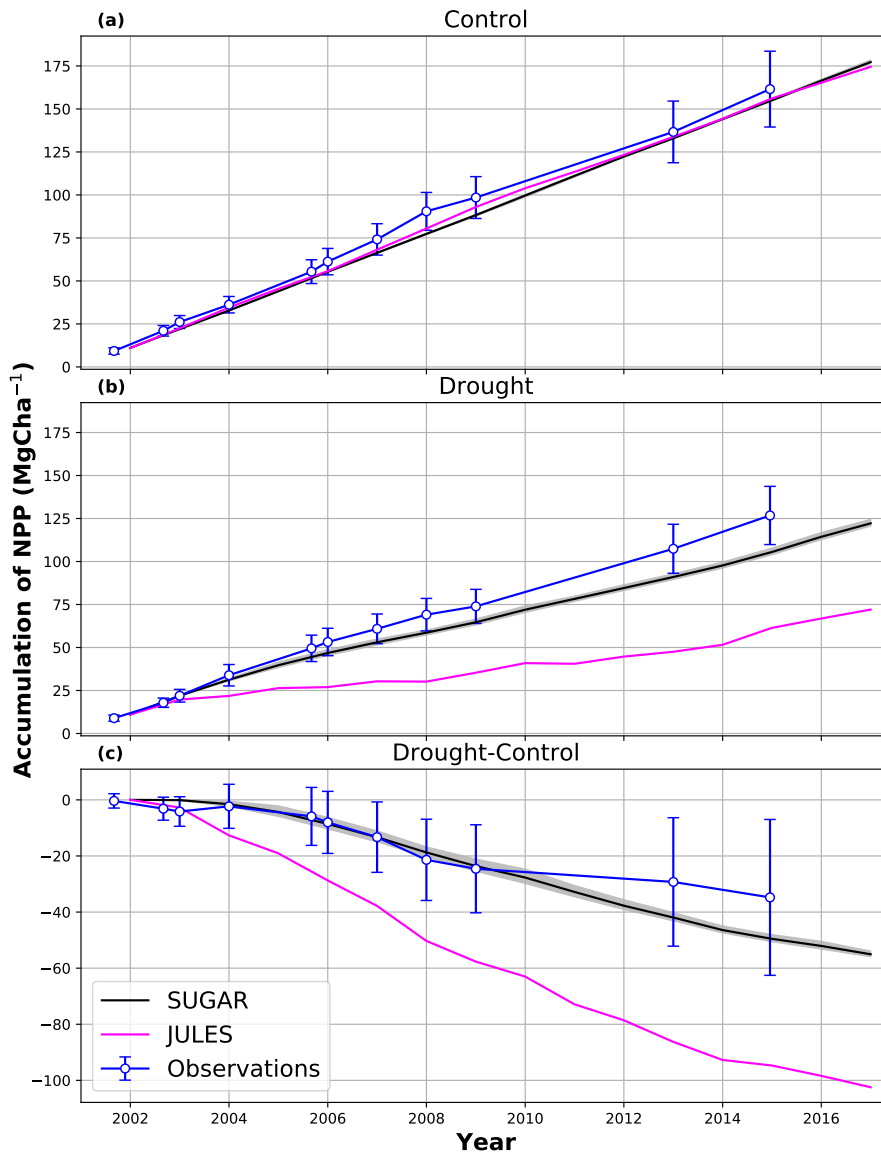
Figure 4.2: Accumulated Net Primary Productivity (NPP) at Caxiuanã in (a) Control plot, (b) Through-fall exclusion (TFE) plot and (c) The difference between the drought and control forest (TFE-control). Observations are calculated as the accumulated sum of above-ground biomass increment change and total local litterfall (Rowland et al., 2018). The presented confidence intervals are the sum of the litterfall measurement error and the 95% confidence intervals of biomass increment calculated from 8 allometric equations using trunk diameter at breast height (DBH) data from Caxiuanã. The uncertainty envelope on SUGAR represents the maximum and minimum of an ensemble of simulations in which parameter a_{K_m} was varied between 0.1 and 2.0.

$MgC\,ha^{-1}\,yr^{-1}$ in 2008 to 32.94 $MgC\,ha^{-1}\,yr^{-1}$ in 2010. Consequently, JULES predicted a mean PCE of 33.60 $MgC\,ha^{-1}\,yr^{-1}$ over the period 2009-2011 which lay below observed values. SUGAR was able to buffer the forest against the 2010 decline in GPP and allows elevated PCE in 2010 (36.36±0.36 $MgC\,ha^{-1}\,yr^{-1}$) relative to 2008 (34.52±0.52 $MgC\,ha^{-1}\,yr^{-1}$). This allowed SUGAR to maintain a mean PCE value over the 2009-2011 period of 36.00±0.54 $MgC\,ha^{-1}\,yr^{-1}$ which

was close to observations (Fig. 4.4). The largest difference between the two
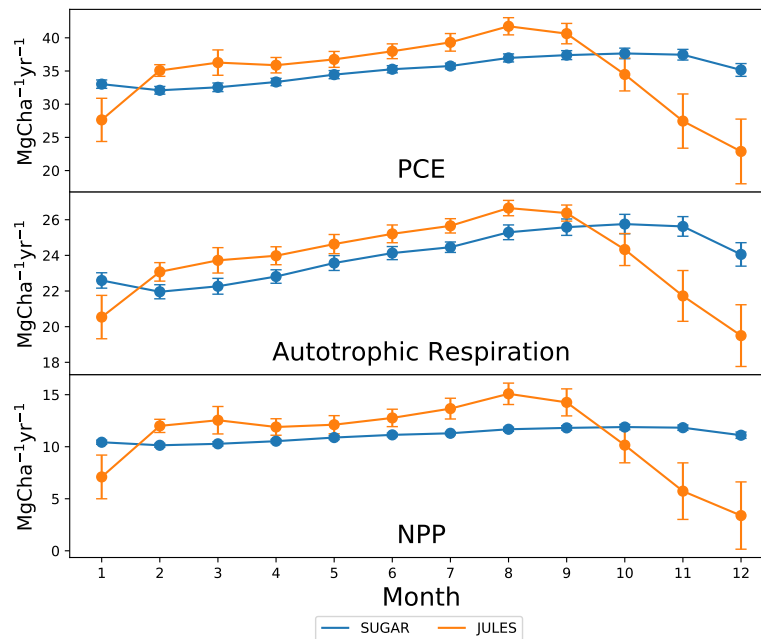
Figure 4.3: The average seasonal cycle of control plot Plant Carbon Expenditure (PCE = NPP+R_a), Autotrophic respiration (R_a) and Net primary productivity (NPP) predicted by The Joint UK Land Environment Simulator (JULES) and the Substrate Utilisation by Growth and Autotrophic Respiration (SUGAR) model.

models in the control plot was their prediction of the seasonal cycles of PCE, autotrophic respiration and NPP (Fig. 4.3). SUGAR predicted a much less variable seasonal cycle in all three fluxes relative to JULES, with a coefficient of variation of 5.74% for each flux, compared to 16.7%, 9.41% and 33.3% for PCE, R_a and NPP in JULES respectively. On average the fluxes in JULES all peaked in August with seasonal maximums of 41.7$\pm$1.30 MgC ha^{-1} yr^{-1}, 26.7$\pm$0.43 MgC ha^{-1} yr^{-1} and 15.1$\pm$1.03 MgC ha^{-1} yr^{-1} respectively. Seasonal minimums occurred in December with values of 22.9$\pm$4.87 MgC ha^{-1} yr^{-1}, 19.5$\pm$1.73 MgC ha^{-1} yr^{-1} and 3.39$\pm$3.23 MgC ha^{-1} yr^{-1} respectively. In SUGAR; PCE, R_a and NPP all peaked in October and the seasonal maximums were lower than those of JULES at 37.6$\pm$0.80 MgC ha^{-1} yr^{-1}, 25.8$\pm$0.55MgC ha^{-1} yr^{-1} and 11.9$\pm$0.25 MgC ha^{-1} yr^{-1} respectively. Similarly the seasonal minimums in SUGAR occurred in February and were larger than those in JULES with values of 32.1$\pm$0.58 MgC ha^{-1} yr^{-1}, 22.0$\pm$0.40 MgC ha^{-1} yr^{-1} and 10.1$\pm$0.18 MgC ha^{-1} yr^{-1} respectively.

4.3.2   Simulating responses to drought

In the TFE plot simulations, SUGAR and JULES diverged significantly in their predictions of NPP, PCE and Ra, with SUGAR more accurately capturing observations than JULES (Figs. 4.2&4.4). JULES was able to capture NPP accumu-
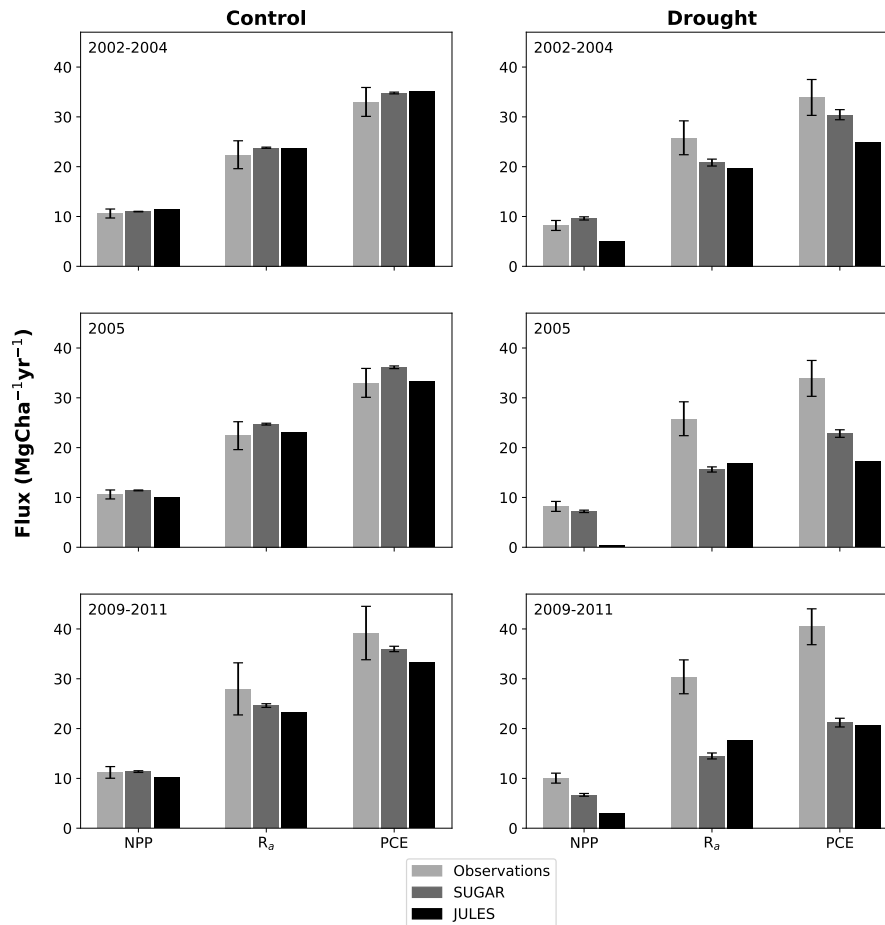
Figure 4.4: Net primary productivity (NPP), Autotrophic respiration (R_a) and Plant Carbon Expenditure (PCE = NPP+R_a); for the periods 2002-2004, 2005 and 2009-2011. The left column is from the control plot and the right is from the through-fall exclusion (TFE) plot. The error bars on the SUGAR fluxes represent the maximum and minimum of an ensemble of simulations in which the a_{K_m} parameter was varied between 0.1 and 2.0.

lation for approximately 1 year after the start of the drought treatment, however, from 2003 onwards, predicted NPP accumulation dropped significantly below the confidence intervals of the observations (Fig. 4.2). This was driven predominantly by a sharp decline in GPP in response to the declining water availability. SUGAR was able to capture NPP accumulation for much longer and predictions remained within the confidence intervals of the observations until the start of 2009 (Fig. 4.2). By the end of the observation period JULES predicted a total of 60.6 MgC ha^{-1} of accumulated NPP and SUGAR 105.22 MgC ha^{-1}. Neither result lay within observed confidence intervals of the observations (Fig. 4.2, 126.8±16.9 MgC ha^{-1}) although the SUGAR result represented a significant improvement relative to JULES.

During the first 3 years of the experiment, SUGAR was able to buffer a significant decline in predicted GPP on the TFE plot, which dropped from 34.90

MgC ha^{-1} yr^{-1} in 2001, to a minimum of 19.61 MgC ha^{-1} yr^{-1} in 2003 (-43.8%). Since JULES does not contain an NSC storage component and PCE is equal to GPP, PCE in JULES also dropped by 43.8%, from 34.90 MgC ha^{-1} yr^{-1} in 2001 to 19.61 MgC ha^{-1} yr^{-1} in 2003. As a result JULES predicted a mean PCE value of 24.84 MgC ha^{-1} yr^{-1} over the first three years of drought treatment (2002, 2003, 2004). These values were outside the confidence intervals of the observations and 26.7% below the mean PCE value observed in the TFE plot (33.9$\pm$3.6 MgC ha^{-1} yr^{-1}, Fig. 4.4). SUGAR was able to maintain PCE at a higher level than JULES during these first three years by drawing upon a mean 5.60$\pm$1.01 MgC ha^{-1} yr^{-1} of NSC each year to support growth and respiration (Fig. 4.5). This resulted in a mean PCE of 30.44$\pm$1.01 MgC ha^{-1} yr^{-1} over the period 2002-2004, which lay within the observed confidence interval (Fig. 4.4). The NSC buffering effect in SUGAR continued in 2005 with SUGAR expending 5.59$\pm$0.76 MgC ha^{-1} yr^{-1} more carbon than JULES during that year. This meant that the predicted annual mean PCE in SUGAR was 22.82$\pm$0.76 MgC ha^{-1} yr^{-1} compared to 17.23 MgC ha^{-1} yr^{-1} in JULES. Both results lay below the lower bound of the observed confidence intervals (33.9$\pm$3.6 MgC ha^{-1} yr^{-1}, Fig. 4.4), however, the SUGAR result represented a significant improvement relative to JULES. In the latter years of the drought simulations (2009 onwards), the NSC pool became significantly depleted (Fig. 4.5) and the buffering effect in SUGAR (described above) diminished. Consequently, on annual time-scales, the mean PCE in JULES and SUGAR during the 2009-2011 period were similar (20.76 and 21.20pm0.87 MgC ha^{-1} yr^{-1} respectively), although the allocation of carbon to respiration and growth was different, with SUGAR expending more (6.70$\pm$0.28 MgC ha^{-1} yr^{-1}) carbon on growth than JULES (3.06 MgC ha^{-1} yr^{-1}). This difference in allocation allowed SUGAR to predict the observed NPP with more skill than JULES, however it meant that respiration predictions were reduced relative to JULES and the observations.

4.3.3 Reduced soil-moisture stress in JULES

The ability of SUGAR to accurately capture PCE responses to drought in these simulations is partially dependent on the GPP used to run it. Photosynthesis in JULES has a high sensitivity to reductions in soil moisture (eg., Harper et al., 2016; Williams et al., 2018). In the TFE simulations JULES predicted a total reduction in GPP of 17.68 MgC ha^{-1} between 2001 to 2005, an average of 4.42 MgC ha^{-1} yr^{-1} each year. Combining the observed PCE rates (Metcalfe et al., 2010) in the TFE plot with the predicted GPP by JULES implies that the forest was using an average of 10.96 MgC ha^{-1} yr^{-1} carbon more than it is assimilating in the first four years of the drought. Assuming that JULES correctly captured the response of GPP to the drought, this implies that the forest had access to at
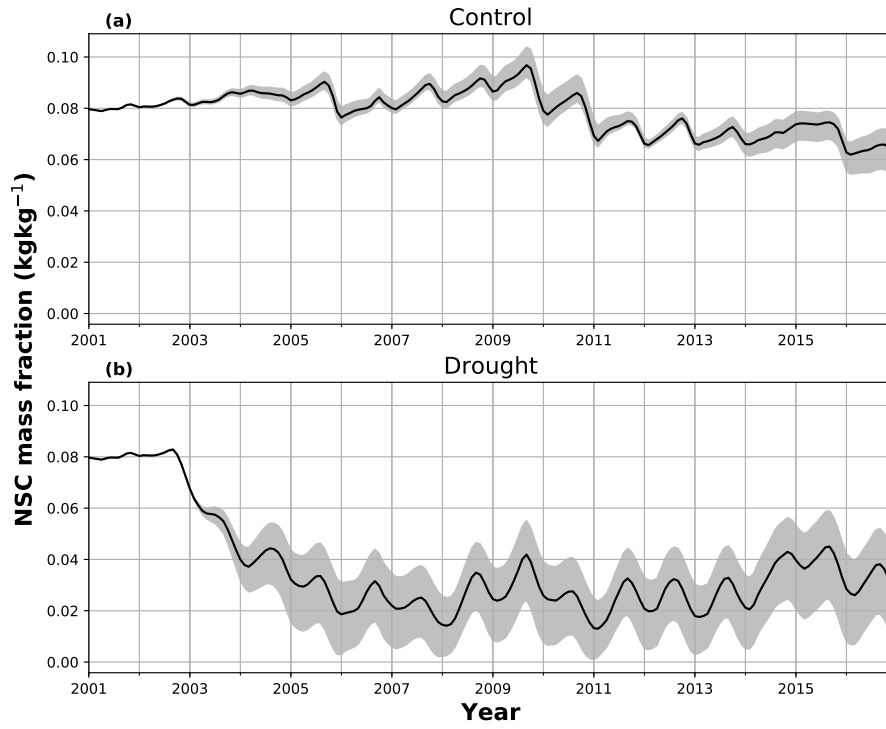
Figure 4.5: The effect of the non-structural carbohydrate (NSC) saturation parameter (a_{K_m}) in SUGAR on simulated NSC as a fraction of total carbon biomass, in (a) the control plot and (b) the TFE plot. The mean, maximum and minimum from an ensemble of simulations where a_{K_m} is varied between 0.1 and 2.0 are presented.

least $43.86 \mathrm{MgC\,ha^{-1}}$ of NSC, c. 22% of estimated forest biomass. Such a high NSC content is unlikely for tropical forests, which are more likely to have reserves close to 10% (Würth et al., 2005). The more likely explanation for this difference between predicted GPP and observed PCE, is that JULES overestimated the decline in photosynthesis in response to the drought. To test this, the drought stress in JULES was artificially reduced by 50% and the simulations were repeated.

Photosynthesis in JULES is scaled by a factor, β, that depends piece-wise linearly on soil-moisture concentration (θ) (Clark et al., 2011).

$$\beta = \begin{cases} 1 & \text{for } \theta > \theta_c \\ \dfrac{\theta - \theta_w}{\theta_c - \theta_w} & \text{for } \theta_w < \theta \leq \theta_c \\ 0 & \text{for } \theta \leq \theta_w \end{cases} \tag{4.9}$$

where θ_c and θ_w are the soil moisture concentrations below which photosynthesis drops below it's maximum (uninhibited) value, and becomes zero respectively.
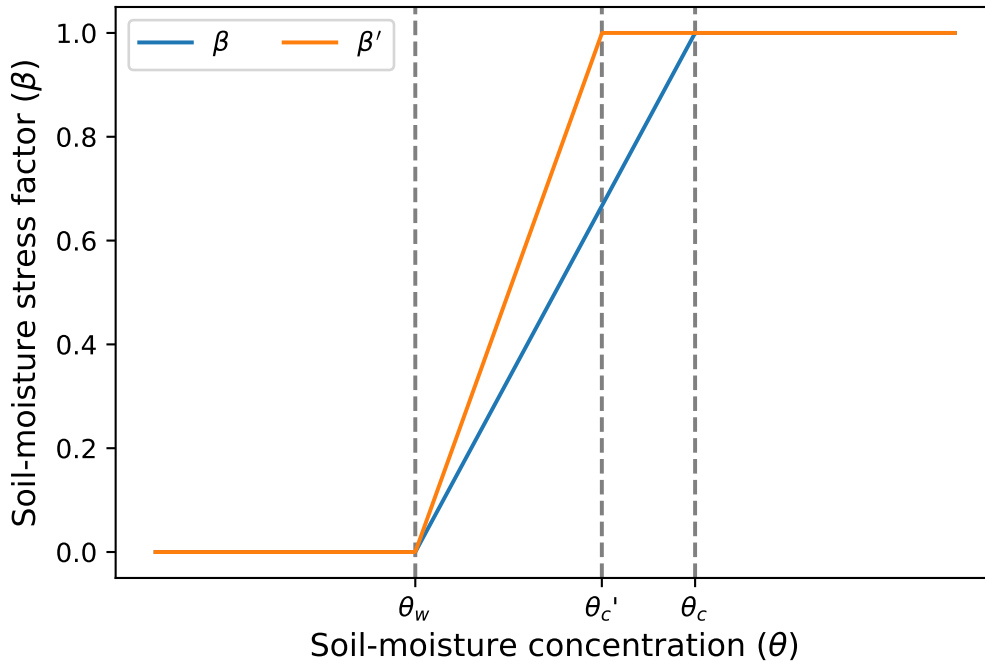
Figure 4.6: The soil-moisture stress (β) and adjusted soil-moisture stress (β') as a function of soil moisture concentration (θ).

To reduce the sensitivity of β to soil-moisture an altered β-factor was defined as:

$$\beta' = min\left\{1.0, 1.5 \times \beta\right\} \tag{4.10}$$

This is equivalent to defining a new value for θ_c (Fig. 4.6):

$$\theta'_c = \frac{2}{3}\left(\theta_c - \theta_w\right) + \theta_w \tag{4.11}$$

The new beta-factor means that soil-moisture stress does not start to occur until a lower soil-moisture concentration, therefore reducing the sensitivity of predicted photosynthesis to drought. The time-series of β and β' throughout both control and TFE simulations is shown in Fig. 4.7.

As expected, changing β in this way reduced the effect of the drought on predicted photosynthesis. Total annual PCE was consistently higher in both plots than it was in the original simulations. In the control plot the change was small but allowed both SUGAR and JULES to better capture PCE towards the end of the experiment, while slightly reducing the accuracy of PCE predictions during the early stages (Fig. 4.8). In the TFE plot the change was larger and both JULES and SUGAR captured early experiment PCE much better than in the previous simulations. However, PCE in both models still dropped significantly below observed levels during the latter stages of the experiment, potentially suggesting

79
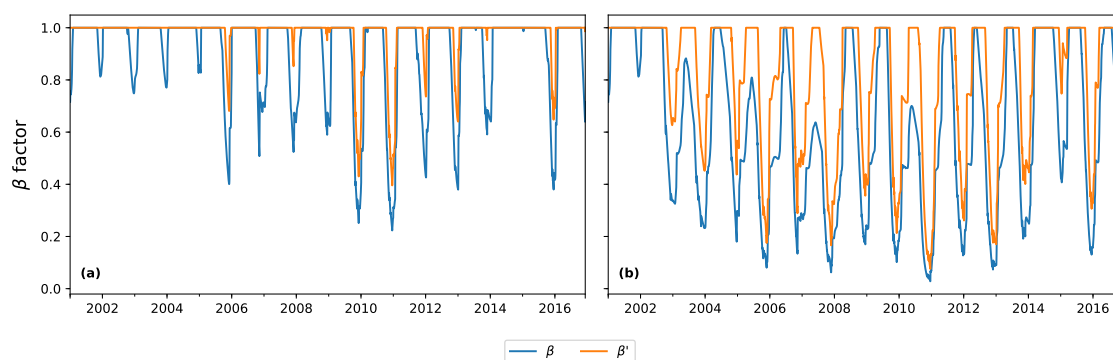
Figure 4.7: The soil-moisture stress (β) and adjusted soil-moisture stress (β') in (a) the control plot simulations and (b) the through-fall exclusion (TFE) plot simulations.

that the sensitivity of β to soil-moisture is still too high. The allocation of carbon between respiration and growth in SUGAR suffered with too much going to growth. This meant that SUGAR overestimated NPP accumulation in the TFE plot, while JULES more accurately captured it.

4.4 Discussion

SUGAR and JULES predicted very similar long-term NPP accumulation, and comparable annual mean fluxes of NPP, R_a and PCE in the natural climate conditions of a tropical moist forest. However, there were larger differences between SUGAR and JULES on shorter time-scales, due to the buffering of the natural variability in GPP by SUGAR. While carbon fluxes were similar over a year or longer, SUGAR significantly changed their seasonal cycle, with both the amplitude and phase of the seasonal variation being notably different with the addition of the NSC pool. The top panel in Fig. 4.3 shows the difference in the seasonal cycles of PCE within JULES and SUGAR. However, since PCE in JULES is equivalent to GPP, we can also view this panel as a demonstration of the decoupling between PCE and GPP in SUGAR. Doughty et al. (2015a) showed a similar decoupling on a seasonal scale in multiple sites across South America including Caxiuanã. While peaks in photosynthesis of many tropical forests are typically driven by the seasonality of radiation, the seasonal cycle of plant growth is commonly driven by variation in precipitation (Wagner et al., 2016). On its own JULES is unable to capture this asynchrony since the discrepancy between supply and demand must be supported by a NSC pool. This means that even if JULES were able to perfectly capture the seasonal cycle of GPP it would be unlikely to capture the seasonal cycles of plant respiration and growth. Accurately capturing these seasonal patterns may be crucial to accurately predicting the response of tropical forests to future climate change. These results, therefore, highlight the importance of substrate-based modelling to better capture the responses to nat-

80
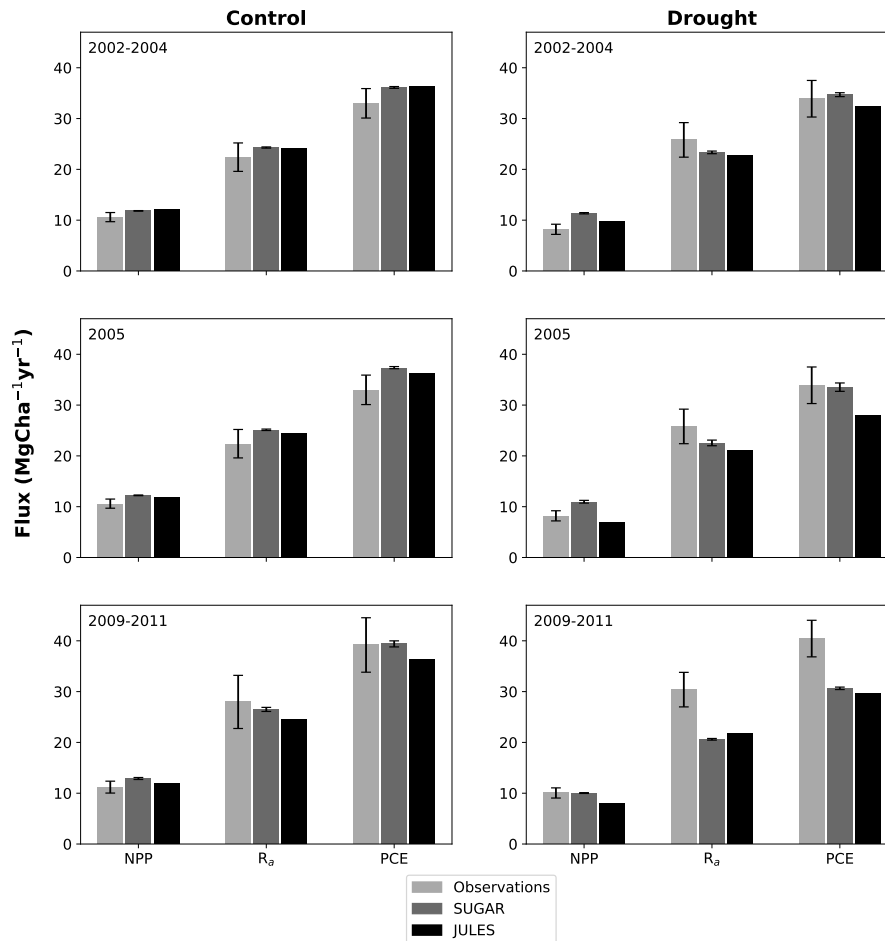
Figure 4.8: Net primary productivity (NPP), Autotrophic respiration (R_a) and Plant Carbon Expenditure (PCE = NPP+R_a); for the periods 2002-2004, 2005 and 2009-2011. The left column is from the control plot and the right is from the through-fall exclusion (TFE) plot. Soil moisture stress has been artificially reduced in JULES by 50% and the resulting GPP has been used to drive SUGAR.

ural variation, even under current climate conditions and without extreme events.

In the TFE plot, SUGAR made significant improvements to the prediction of ecosystem carbon fluxes, particularly for accumulated NPP. This improvement was caused by a combination of two processes that occur in SUGAR and that are not present in JULES. The first process is the utilisation of the NSC pool during the early stages of the experiment. SUGAR expended a mean 5.53 $\mathrm{MgC\,ha^{-1}}$ more carbon than was assimilated through photosynthesis in the first three years of drought (2002-2004) and a further 5.80 $\mathrm{MgC\,ha^{-1}}$ in 2005. This allowed an increase in both growth and respiration relative to JULES and was consistent with the analysis in Metcalfe et al. (2010), which suggests the TFE plot was expending 7.0±4.5 $\mathrm{MgC\,ha^{-1}\,yr^{-1}}$ more than it was accumulating in 2005, implying that NSC stores were being depleted in response to the drought (Fig. 4.5). Signori-Müller et al. (2021) found significant dry-season reductions in the total NSC contents of leaves and branches across multiple sites in the Amazon. These were largely attributed
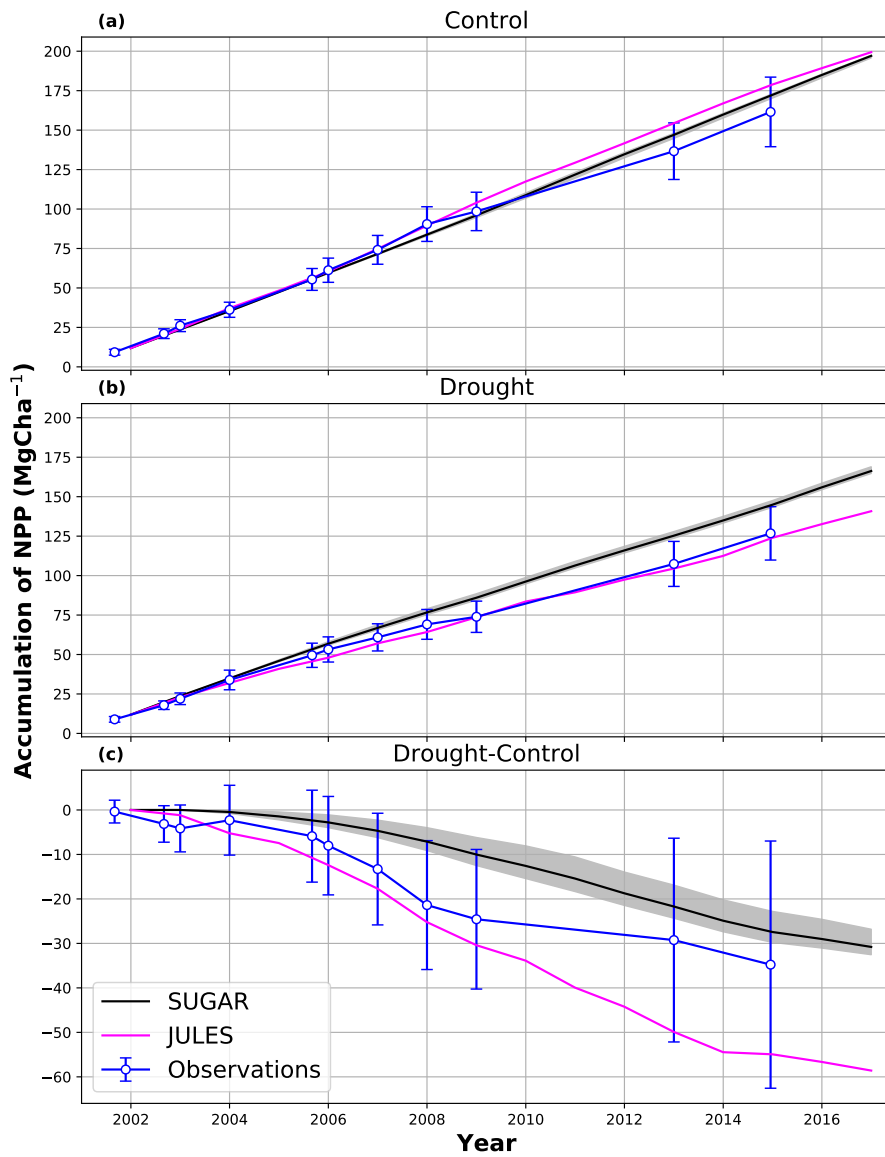
Figure 4.9: Accumulated Net Primary Productivity at Caxiuanã in (a) Control plot, (b) TFE plot and (c) The difference between the drought and control forest (TFE-control). Soil moisture stress has been artificially reduced in JULES by 50% and the resulting GPP has been used to drive SUGAR. Observations are calculated as the accumulated sum of biomass increment change and local litter-fall (Rowland et al., 2018). The presented confidence intervals are the sum of the litter-fall measurement error and the 95% confidence intervals of biomass increment calculated from 8 allometric equations using trunk diameter at breast height (DBH) data from Caxiuanã.

to the limitation of photosynthesis by declining water availability combined with the continued carbon demand of respiration and growth (Signori-Müller et al., 2021), and support the results predicted by SUGAR in the TFE plot. However, alongside the reductions in total NSC, Signori-Müller et al. (2021) also observed significant shifts in the ratio of soluble sugars to starch in response to declining water-availability, with almost all measured species greatly increasing their proportions of soluble sugars during the dry season. SUGAR is currently unable to capture these shifts as these different types of NSC are not distinguished. Yet, shifts in NSC composition represent an important adaptation by plants, as soluble sugars are frequently used to maintain hydraulic function via osmotic regulation. The dynamic allocation of carbon to soluble sugars and starches may have important feedbacks on plant water-status, which in turn can effect photosynthesis and greatly impact forest responses to drought. Further work is required to include these processes within SUGAR as these advances may have the potential to greatly improve simulations of ecosystem responses to drought.

The second process that occurred in SUGAR, and aided the prediction of NPP accumulation was the down regulation of respiration in response to the depleting NSC pool. In the JULES simulations, photosynthesis declined much faster than respiration and, since growth is equal to GPP – Ra in JULES, this meant that NPP dropped significantly as GPP declined in response to the drought. The result of this effect was that in two years (2005 and 2007), the predicted annual mean NPP by JULES, was negative. Negative NPP is generally considered to be unrealistic, particularly over the time-scale of a year (Roxburgh et al., 2005), and since JULES does not contain a labile carbon pool to support the deficit, missing carbon was taken from the structural pool. The physical interpretation of this is that trees in JULES respire away their structural carbon and shrink. While there is some evidence of recycling and remobilisation of structural compounds, the magnitude of structural carbon being allocated to respiration (via the resulting negative NPP) in these JULES simulations was not realistic. In SUGAR, respiration declined due to the depletion of the NSC pool. This down-regulation of Ra meant that a larger proportion of instantaneous GPP was available for NPP, resulting in larger predictions of NPP in SUGAR than JULES, despite similar estimates of total PCE. While this latter process aided the prediction of NPP in SUGAR, it should be noted that observations from Caxiuanã actually indicate an increase in TFE plot respiration between 2005 and 2011 (Metcalfe et al., 2010; da Costa et al., 2014), likely associated with an increase in stem and root respiration rates (Rowland et al., 2021). SUGAR is currently unable to capture this increase and this is likely due to the simplicity of the assumptions made within the model. For example, it has been assumed that plant growth is directly dependent on carbohydrate availability

and temperature only. Water stress can reduce plant growth in SUGAR, but only indirectly by inhibiting photosynthesis and causing a decrease in available carbon. However, in reality plant growth can be affected directly by decreasing water availability through the inhibition of cell expansion (Balducci et al., 2013; Hsiao, 1973; Boyer, 1970). This decline in growth may even occur before declines in photosynthesis which can cause a build up of NSC and eventually result in an increase in respiration (Fatichi et al., 2014). This is not to suggest that this specific process comprehensively explains the observed increases in respiration on the drought plot at Caxiuanã, but such interactions between NSC utilisation and the environment are likely to have been important during the TFE experiment. Neither SUGAR nor JULES are able to capture these processes currently, however, SUGAR provides a basis upon which these interactions may be implemented in models like JULES, potentially resulting in further improvements to predictions of forest responses to drought.

The sensitivity of photosynthesis to water-availability is a significant component of modelling forest drought responses, and has been highlighted as a key source of error between model predictions and observations at Caxiuanã (Powell et al., 2013). The difference between observed PCE and predicted GPP by JULES in the TFE plot in the original simulations was roughly 50% larger than suggested by Metcalfe et al. (2010) and implied an unrealistic amount of stored NSC. Reducing the sensitivity of photosynthesis to soil-moisture stress in JULES improved predictions of PCE, R_a and NPP in the TFE plot by JULES, in particular in the early stages of drought (Fig. 4.8). It might be possible for JULES to accurately capture both respiration and NPP in both plots over the entire drought experiment by further tuning of the sensitivity of photosynthesis to soil moisture. However, when tuning model responses in this way, it is important to ask what the physiological meaning is behind the changes being made. In this case we are not seeing improved results because of the inclusion of an important process that was previously missing. Nor has the representation of an already existing process been improved in a way that has any grounding in plant physiology. 'Artificial' model development like this can be useful, as it has been here, in demonstrating deficiencies in the structure or parametrisation of models. However, while reducing the sensitivity of photosynthesis to water-stress has improved predictions of NPP and respiration in these simulations, it would be unreasonable to expect these improvements to be universal across all sites and drought scenarios. Recent developments in modelling stomatal responses to soil moisture (Mencuccini et al., 2019; Eller et al., 2018, 2020; Sperry et al., 2017) have proven to be more capable of capturing forest transpiration during drought (Eller et al., 2018), and may have the potential to significantly improve GPP predictions in LSMs such as JULES.

This may allow more accurate and robust simulations of the TFE experiment at Caxiuanã using JULES in the future. However, there is a clear link between plant hydraulics and labile carbon storage, given stomatal closure comes at the cost of a reduction in carbon assimilation. The ability of a plant to store and use labile carbon is crucial to its ability to survive, and recover from, drought-induced stomatal closure (Sala and Mencuccini, 2014; O'Brien et al., 2014; Trugman et al., 2018). Without including at least simple representations of NSC storage, the potential of this recent work to improve the representation of stomatal behaviour in response to drought in LSMs, is unlikely to be realised.

4.5   Conclusions

A significant proportion of previous discrepancies between observations and model predictions of tropical forest responses to drought is associated with deficiencies in the representation of photosynthesis in LSMs. However, the work in this chapter reveals that there is also an important role for NSC in these predictions, and that this role cannot be neglected in future model developments. Despite the simplicity of SUGAR, it makes significant changes to the predictions of carbon fluxes in response to drought and demonstrates the potential impact that substrate-based approaches to plant modelling could have on future predictions of ecosystem carbon fluxes, in particular during periods of drought.

Additional work is required to further improve predictions of the TFE experiment at Caxiuanã, in particular the role of water-availability in directly regulating plant growth must be explored. Significant improvements are being made to the representation of stomatal behaviour during drought. However, given the theoretical relationship between stomatal control and NSC, this work must be accompanied by the development of simple models such as SUGAR, which may form the basis for more complex processes to be introduced into LSMs like JULES that allow more accurate predictions of vegetation drought responses.

The aim of the next chapter, is to assess the role of NSC in determining ecosystem carbon fluxes on a global scale. Output from four LSMs will be used to drive a simplified version of SUGAR off-line to predict respiration and NPP fluxes across the globe. The effects of SUGAR on these predictions will be examined and the possible changes to estimates of global terrestrial carbon uptake, that including NSC in the four LSMs could make, will be explored. This allows the possibility of using the variability of atmospheric CO_2 concentrations to constrain model parameters within SUGAR to be investigated.

Chapter 5

The effects of NSC on predictions of the global terrestrial carbon sink

5.1 Introduction

5.1.1 The Growth-Maintenance Respiration Paradigm

Due to the complexity of respiratory processes within plants, truly mechanistic representations of autotrophic respiration (R_a) do not currently exist, and nor would they be practical within current state of the art land surface models (LSM). Nonetheless, capturing variation in plant respiration is an integral component of modelling the climate and so several simple approaches have been proposed. The most common approach is the so called growth maintenance respiration (GMR) paradigm (Thornley, 1970), in which plant processes are split into two distinct categories, each with their own separate respiratory demands. Growth processes are defined as those that result or aid in the synthesis of new plant biomass, while maintenance processes are defined as those that maintain pre-existing biomass. This separation results in a corresponding separation of total respiration into two distinct fluxes which can be represented independently. This framework is widespread due to its simplicity (a useful property for representations of plant processes at a global scale) but also its apparent consistency with observations. Experiments by McCree (1970) suggest that under controlled environmental conditions, variations in R_a can be described by the following equation:

$$R_a = kP + cW \tag{5.1}$$

where P is photosynthesis, W is plant dry mass and, k and c are coefficients that are constant under constant environmental conditions, but may vary with changes in temperature for example. The dependence of R_a on photosynthesis, indicated by the first term on the right hand side of equation (5.1), is interpreted as the respiratory cost associated with converting substrates (derived from photosynthesis)

into new biomass, and equated to growth respiration. The dependence of R_a on biomass, indicated by the second term on the right hand side of equation (5.1), is interpreted as a demonstration of the respiratory cost of maintenance, which is assumed to increase with plant size.

Despite the prevalence of the GMR paradigm within LSMs, it has faced criticism (Thornley, 2011; Amthor, 2000). While it may be reasonable to split plant processes into growth and maintenance categories on a functional basis, at a biochemical level the distinction between growth and maintenance respiration is less clear (Thornley, 2011). Both sets of processes require energy in the form of ATP, and many processes in both categories also require matter, either to produce new biomass (growth) or to replace old biomass (maintenance). The metabolic processes that produce ATP and the anabolic processes that synthesise carbon compounds are qualitatively the same in growing and non-growing plants (Thornley, 2011). From this viewpoint, attributing the two terms in equation (5.1) to two distinct respiratory processes makes little sense and suggests an alternative interpretation of McCree's equation (equation 5.1) is required.

A simple framework proposed by Thornley (2011) represents respiration as just a single component that depends on the availability of labile substrate in the form of non-structural carbohydrate (NSC). When the availability of NSC is large, respiration is able to completely decouple from photosynthesis, with environmental factors such as temperature controlling its rate (Collalti et al., 2020). Under constant environmental conditions, changes in photosynthesis do not significantly alter the concentration of NSC and with constant substrate concentrations, respiration becomes proportional to biomass. Conversely, in the absence of significant NSC stores, the rate of respiration is dependent on the supply of carbon from photosynthesis and becomes a constant fraction of Gross Primary Productivity (GPP) (Collalti et al., 2020). Under more intermediate NSC availability, this framework is able to capture the influence of both photosynthesis and biomass on respiration, and importantly can be used to explain McCree's equation (Thornley, 2011). While a potentially more mechanistic approach, this framework has received little attention in large scale modelling studies. This may be in part due to the difficulty of representing labile carbon storage. In particular the evaluation of NSC turnover rates and pool sizes (Collalti et al., 2020) are difficult to determine due to the large error associated with direct NSC measurements at an ecosystem or even whole plant scale (Quentin et al., 2015). In order for this approach to be examined, an alternative method for evaluating these uncertainties is therefore required.

5.1.2   Terrestrial carbon uptake and the Global Carbon Budget

A crucial part of predicting future climate is the development of reliable estimates of stocks and fluxes of carbon in the global system. These estimates are integral to limiting the increase in the concentrations of greenhouse gases in the atmosphere and reducing the risk of the most severe emissions scenarios. The Global Carbon Project (GCP) is a global research project with the aim of developing an accurate overview of the global carbon cycle that not only details the patterns within observations of carbon stocks and fluxes, but also describes the processes and interactions that govern and control these patterns. Each year the GCP produces a "Global Carbon Budget" (GCB) that outlines the most up to date estimates of carbon stocks and fluxes globally (Friedlingstein et al., 2019). However, estimates of the difference between sources (from fossil fuel, industry and land-use change emissions) and sinks (into the land and ocean) of carbon to and from the atmosphere do not currently match the observed changes in atmospheric CO_2 concentrations. This results in a "budget imbalance" that represents the uncertainty within both our understanding and empirical assessment of the global carbon cycle. The exact source of this uncertainty is not clear, but it has been attributed largely to deficiencies in process-based models used to estimate carbon uptake by both the land and ocean, due to its high inter-annual and semi-decadal variability, and lack of significant long-term trend (Bastos et al., 2020; Friedlingstein et al., 2019). We may, therefore, tentatively view the GCB budget imbalance as a metric of the accuracy of these models, and use it as benchmark for future developments within these models.

In this chapter the applicability of this benchmark for evaluating the role of NSC in simulating plant carbon fluxes is investigated. A simplified version of the SUGAR model is driven off-line with the output of four LSMs from the TRENDY model consortium, which supports the terrestrial carbon uptake component of the GCB. In this version of SUGAR, plant respiration is represented as a single component that depends on temperature and substrate availability. The output from SUGAR is compared to the original TRENDY outputs and the relationship between the GMR paradigm and the single component respiration framework is examined at a global scale. The role that NSC turnover rates play in this relationship is investigated by examining the variability of predicted Net Primary Productivity (NPP). The potential of using the GCB budget imbalance to evaluate these changes and potentially constrain model parameters is examined by calculating new estimates of NBP based on the updated predictions of NPP by SUGAR, and comparing to an 'implied land carbon sink', which is calculated using the budget imbalance from GCB 2019 (Friedlingstein et al., 2019).

5.2 Methods

5.2.1 TRENDY LSMs

Simulations from a group of four LSMs were used to drive a modified version of SUGAR off-line. The LSMs used were; CLASS-CTEM (Melton and Arora, 2016), LPJ-GUESS (Smith et al., 2001, 2014), JULES-ES-1.0 (Best et al., 2011; Clark et al., 2011) and ISAM (Meiyappan et al., 2015) and the simulations used were all completed as a part of the TRENDY v.8 project. The four LSMs were chosen from the wider TRENDY consortium due to two common properties:

1. None of the versions of the models used contain any representation of NSC or labile carbon reserves.

2. All four models follow the GMR paradigm and separate respiration into growth and maintenance components, with growth respiration a simple fraction of NPP.

Most models in the TRENDY consortium split respiration into growth and maintenance components. However, these components were not outputted separately as part of the TRENDY v.8 project. It was important, therefore, that maintenance and growth respiration could be calculated from the NPP and total autotrophic respiration outputs. This was possible with the four chosen TRENDY LSMs since growth respiration is a simple fraction of NPP in these models. In JULES-ES-1.0 and LPJ-GUESS this fraction is constant with a value of one third. CLASS-CTEM and ISAM differ slightly as the value of this fraction depends on whether NPP is positive or negative. When NPP is negative, growth respiration is set to zero in both models. When NPP is positive, growth respiration is equal to one third of NPP in ISAM and equal to 0.176 (3/17) times NPP in CLASS-CTEM. These representations allow growth respiration to be calculated from NPP output from each LSM, which then allows maintenance respiration to be found from total respiration. A summary of the representation of both growth and maintenance respiration in each LSM is given in table 5.1. Other models in the TRENDY consortium that (a) do not have representations of NSC and (b) separate respiration according to the GMR paradigm (e.g. CABLE-POP: Haverd et al., 2018) would have also been suitable for this study, however, more complex dependences in the growth respiration coefficient meant that growth and maintenance respiration could not be separated using just the TRENDY v.8 outputs.

5.2.2 Modifications to the SUGAR model

The standard SUGAR model uses a simple Q10 function to describe the temperature dependence of both respiration and growth. There has been much dis-

cussion on the responses of plants to temperature, in particular the response of respiration (Huntingford et al., 2017). However, this was not the focus of this study, and changing the temperature dependence of respiration in the four LSMs would likely result in significant changes to its variability, that would be difficult to separate from the effects made by the NSC pool. Therefore, to isolate the impact of NSC, the temperature dependence of maintenance respiration in each LSM was used. To simplify the model further, the Michaelis-Menten NSC dependence in standard SUGAR was replaced with linear reaction kinetics. This removes the saturation parameter (K_m) from SUGAR and directly links the equilibrium pool size (f_{NSC}) to the NSC turnover rate. This results in just a single tuning parameter which allows for a more simple sensitivity analysis to be carried out. The maintenance respiration ($R_{m_{SUGAR}}$) in this simplified version was given by:

$$R_{m_{SUGAR}} = R_{m_{TRENDY}} \frac{W_{NSC}}{f_{NSC}} \tag{5.2}$$

where $R_{m_{TRENDY}}$ is the maintenance respiration of each TRENDY LSM, and f_{NSC} is a constant.

As in the standard version of SUGAR, a new plant growth term, G, was defined that depends on temperature and NSC availability. In SUGAR growth and maintenance respiration have the same temperature and NSC availability and are therefore proportional. In order to maintain this property, the growth was given by:

$$G_{SUGAR} = g_0 R_{m_{TRENDY}} \frac{W_{NSC}}{f_{NSC}} \tag{5.3}$$

where g_0 is a constant.

Growth respiration was then made proportional to the new plant growth term. The constant of proportionality or growth respiration coefficient was assumed to be the same as in the TRENDY LSMs.

$$R_{g_{SUGAR}} = \frac{r_g}{1 - r_g} G_{SUGAR} \tag{5.4}$$

where r_g is the growth respiration coefficient from each LSM given in table 5.1.

Since maintenance respiration and plant growth have the same dependence on NSC, temperature and biomass in SUGAR, the total autotrophic respiration can be written as:

$$R_{a_{SUGAR}} = \left(1 + \frac{r_g g_0}{1 - r_G}\right) R_{m_{TRENDY}} \frac{W_{NSC}}{f_{NSC}} \tag{5.5}$$

We can view this as a single component of respiration, with the first term in the brackets representing maintenance respiration now scaled by the size of the NSC pool, and the second term representing growth-respiration.

5.2.3 Numerical simulations

Simulations were carried out over a 118 year period from January 1901 to December 2018 on a monthly time-step. The NSC mass fraction, W_{NSC}, was updated each time-step using prescribed annual biomass and prescribed monthly GPP ($\Pi_{G_{TRENDY}}$) from each TRENDY LSM, using the following equation:

$$\frac{dC_{NSC}}{dt} = \Pi_{G_{TRENDY}} - R_{m_{SUGAR}} - G_{SUGAR} - R_{g_{SUGAR}} \quad (5.6)$$

Equation (5.6) was updated using the forward euler method. The time-step of one month was split into 500 sub-steps of roughly 1.5 hours each. This was only necessary for the smallest values of f_{NSC} (i.e. the fastest turnover rates), but for consistency this was used for every simulation. This process was carried out for all grid-boxes where the initial grid-box biomass was greater than $1\,\text{kgC m}^{-2}$. Since the turnover time of NSC is inversely related to its pool size which is itself related to the initial biomass in each gridbox, C_v values below this threshold resulted in large turnover rates which were numerically unstable, even when the time-step was subdivided 500 times.

5.2.4 Parameter calibration

Since the value from each TRENDY LSM was used for the r_g parameter, there were only two parameters that needed to be calibrated, g_0 and f_{NSC}. The g_0 parameter was first calibrated for each grid-box following the principles described in chapter 2 and Jones et al. (2020), using the first ten years of TRENDY data from the 118 year period. The parameter in each grid-box was given by:

$$g_0 = \frac{\int_{\tau_{10}} \Pi_{N_{TRENDY}} dt \int_{\tau_{10}} C_{v_{TRENDY}} dt}{\int_{\tau_{10}} \Pi_{G_{TRENDY}} dt \int_{\tau_{10}} R_{m_{TRENDY}} dt} \quad (5.7)$$

where $\Pi_{N_{TRENDY}}$ and $\Pi_{G_{TRENDY}}$ are the NPP and Gross Primary Productivity (GPP) outputs from each TRENDY model respectively; and τ_{10} is the ten year period from 01/01/1901 to 01/01/1911.

To assess the role of NSC turnover time, a sensitivity study was carried out for the f_{NSC} parameter. Forty values of f_{NSC} were tested that were split evenly on a log-scale between 0.001 and 1.0, with a maximum value of 0.838. The lower bound represents a NSC pool with a fast turnover and was the smallest pool size

that could be simulated with a reasonable time-step. The behaviour of these simulations was qualitatively similar enough to the model with an infinitely fast NSC turnover rate (f_{NSC} = 0) to not warrant any lower values. The upper bound is an unrealistically large estimate of NSC mass fraction. Setting it close to one ensures that all realistic estimates of NSC mass fraction are captured within the tested range. A value of 1.0 was not used since this represents the case when 100% of biomass is NSC, which is not possible to represent mathematically, when the structural biomass is non-zero.

5.2.5 Analysing NPP variability

Predictions of plant respiration were used to calculate updated predictions of NPP, by subtracting from the GPP data from the four TRENDY LSMs. The effect of the SUGAR model on these predictions of NPP was then assessed at a global scale, looking both spatially and at global averages. First the inter-annual variability (IAV) of the global average NPP from the four original TRENDY LSMs was calculated. This was done by de-trending the annual TRENDY NPP data using a quadratic fit and then taking the variance. The same was done for SUGAR and each value of f_{NSC}. The percentage change in IAV of global average NPP caused by SUGAR, relative to the original TRENDY models, was then calculated and plotted against f_{NSC}.

The variance of NPP is given by:

$$var\{NPP\} = var\{GPP\} + var\{R_a\} - 2Cov\{GPP, R_a\} \qquad (5.8)$$

where $var\{GPP\}$ and $var\{R_a\}$ are the IAV of GPP and R_a respectively; and $Cov\{GPP, R_a\}$ is their covariance. SUGAR does not affect predictions of GPP and so a change in the IAV of predicted NPP can be associated with either a change in the IAV of R_a or a change in the covariance of R_a with GPP. The IAV of R_a, and the covariance of R_a and GPP from SUGAR were therefore also calculated, as described above. The percentage changes in the IAV of NPP, the IAV of R_a, and the covariance of R_a and GPP, relative to the TRENDY LSMs were then plotted spatially for four values of f_{NSC}: 0.001, 0.01, 0.1 and 0.5. This allowed the change in IAV of global mean NPP to be analysed, first in terms of which regions contributed most to this change, and second whether the change was driven predominantly by a change in the IAV of autotrophic respiration, or by a change in the covariance of GPP and respiration.

5.2.6 Comparing to global Net Biome Productivity

Data from the GCB was used to evaluate the changes made to global NPP by SUGAR on the four TRENDY LSMs. First, the inter-annual difference between the original TRENDY NPP output and the updated prediction of NPP from SUGAR was added to the NBP output from each TRENDY LSM:

$$NBP_{SUGAR} = NBP_{TRENDY} + \Delta NPP \qquad (5.9)$$

where ΔNPP is the inter-annual difference between NPP predicted by SUGAR and the original TRENDY output. To calculate ΔNPP, both TRENDY and SUGAR NPP fluxes were first de-trended using a quadratic fit, in order to isolate inter-annual differences and remove any changes to the long term trend caused by SUGAR. The justification for this is that net biome productivity depends on both NPP and soil respiration. However, soil respiration rates are not directly independent of NPP on short time-scales. Large changes in the long term trend of NPP would likely result in a significant response from soil respiration which would not be captured in these uncoupled simulations. By just using de-trended differences, this error is minimised. Updated global datasets of NBP were then created for each TRENDY LSM using the updated estimates of NBP from SUGAR, and the original TRENDY data for grid-boxes where SUGAR had not been used (i.e. all grid-boxes with initial $C_v < 0$). These merged datasets were then summed to produce a global mean NBP flux for each value of f_{NSC}.

An implied land carbon sink from GCB was calculated by assuming that the budget imbalance within the GCB was exclusively associated with errors within predictions of the land sink. Assuming that there was no error associated with observations of carbon emissions from fossil fuels and land-use change, and no error within the predictions of the ocean carbon sink, an implied land sink was calculated as:

Implied land sink $=$ fossil fuel and industry $+$ land-use change emissions

$-$ atmospheric CO_2 growth $-$ ocean sink

This is essentially the rate that carbon must have been absorbed into the land, assuming our measurements and predictions of all other carbon fluxes and stocks within the climate system are correct. This implied land C sink is shown in Fig 5.1 along with the original predictions of NBP from each of the four chosen TRENDY LSMs. In general the four TRENDY models tend to over estimate the variability of NBP over the period of 1959 to 2018.

The affect of SUGAR on these predictions was assessed by calculating the rel-
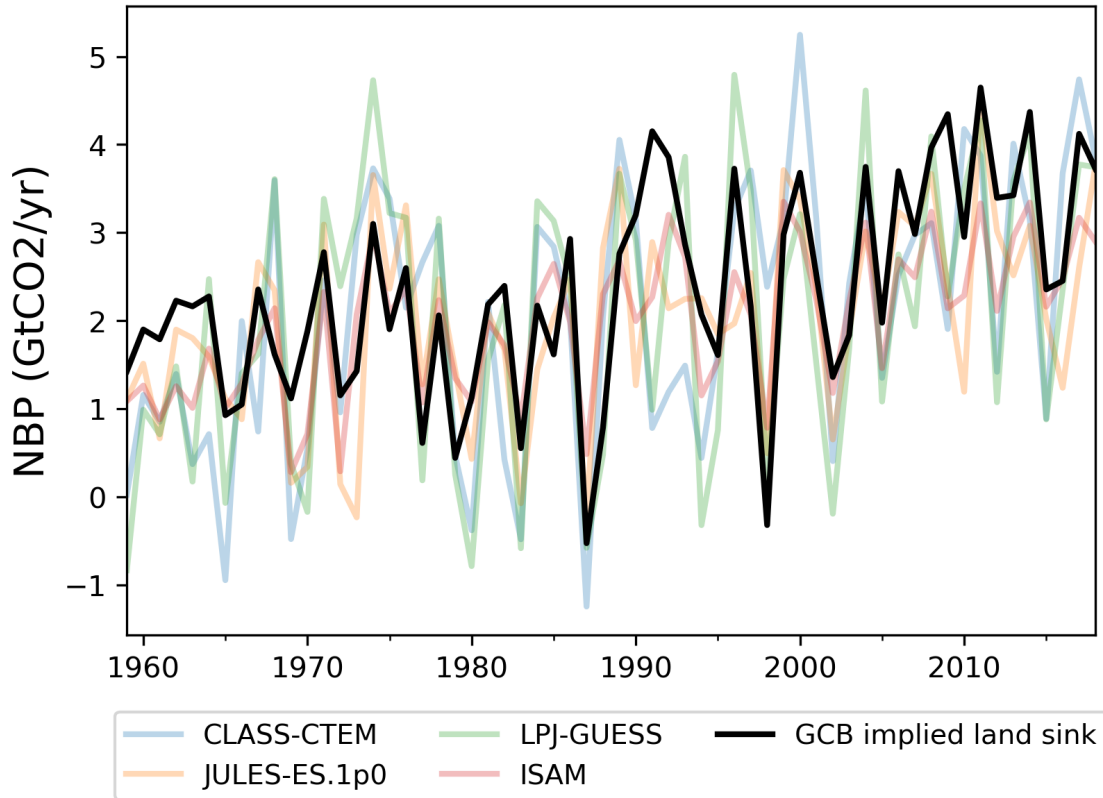
Figure 5.1: Predicted net biome productivity (NBP) from four LSMs from the TRENDY v.8 project (Sitch et al., 2015), compared to the implied land sink from the global carbon budget (GCB) 2019 (Friedlingstein et al., 2019).

ative change in the root mean square error (RMSE) between predicted and observed NBP. This was done by first calculating the RMSE between the implied land sink from GCB2019 and the predicted NBP in each TRENDY LSM. Data from the years 1990 and 1991 were not included to remove the effect of the eruption of Mount Pinatubo which was not captured in the LSMs. The same was then done with predictions from SUGAR for each value of f_{NSC}. A percentage change in RMSE relative to the original TRENDY models was then plotted against f_{NSC} for the output of each SUGAR post-processed LSM.

5.3 Results

5.3.1 Inter-annual variability of NPP: global mean

The addition of the NSC pool into the TRENDY LSMs had a significant effect on the IAV of global mean NPP. For the slowest turnover rates/largest NSC pool sizes, there was a large increase in the IAV of global NPP relative to the original TRENDY LSMs (Fig. 5.2). The ensemble mean saw a maximum increase of 42.7% in the IAV of NPP at a f_{NSC} value of 0.49. The largest increase in IAV was in LPJ-GUESS which saw a maximum increase of 69.2% when f_{NSC} was

equal to 0.59. In contrast, when the turnover rate of NSC was fast/NSC pool size
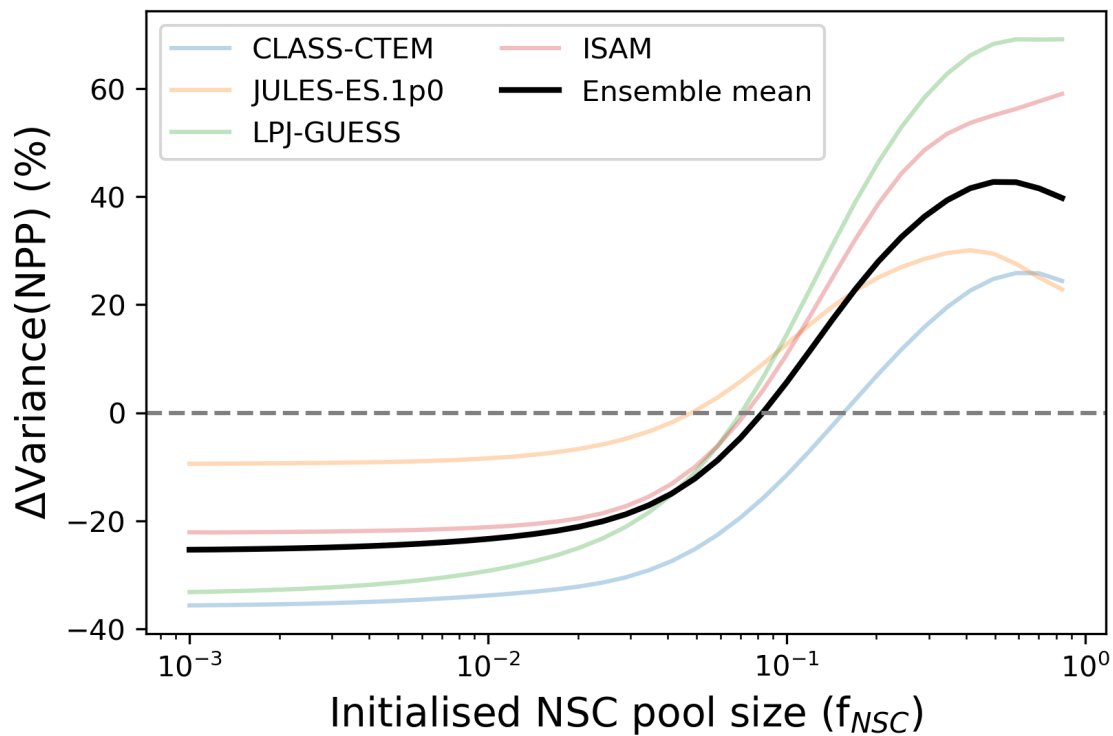
Figure 5.2: The percentage change in the inter-annual variance of predicted global net primary productivity (NPP) against initialised non-structural carbohydrate (NSC) mass fraction f_{NSC} from a simplified version of the SUGAR model. The percentage change is relative to the inter-annual variance of global NPP from four land surface models (LSM) which have been used to drive the SUGAR model.

was small, all four models saw a significant decrease in the IAV of global mean NPP (Fig. 5.2). This decreases was largest in CLASS-CTEM which saw a 35.7% decrease in IAV for the smallest f_{NSC} value of 0.001. For the ensemble mean, this maximum decrease was still significant at 25.4%.

An important feature of Fig. 5.2 is the point at which each curve crosses the x-axis. This represents the NSC turnover rate/pool size at which the IAV of global NPP was unchanged relative to the original TRENDY LSMs. This point was similar across all four models, occurring when f_{NSC} was approximately equal to 0.1. Using linear interpolation, the f_{NSC} values at which each model curve crossed the x-axis were calculated as: CLASS-CTEM: 0.156; JULES-ES.1p0: 0.0481; LPJ-GUESS: 0.0706; ISAM: 0.0735.

5.3.2 Inter-annual variability of NPP: spatial analysis

To understand the change in IAV of global mean NPP it was useful to examine how the variability of NPP changes spatially (Fig. 5.3). First, at $f_{NSC} = 0.5$,

representing slow NSC turnover/large NSC pool size, the increase in the IAV of NPP seen previously in the global mean, was also seen both spatially across all models (Fig. 5.3). In the ensemble mean the relative increase in IAV was most pronounced across the tropics. It should be noted that this does not necessarily mean that the topics have the largest contribution to the change in IAV of the global mean NPP seen in Fig. 5.2, since the changes presented are relative to the original variability in TRENDY and not absolute change. The relative change in the tropics was significant across all four models, however, in LPJ-GUESS there were also large relative changes across the northern hemisphere and sub-tropics (Fig. 5.3).
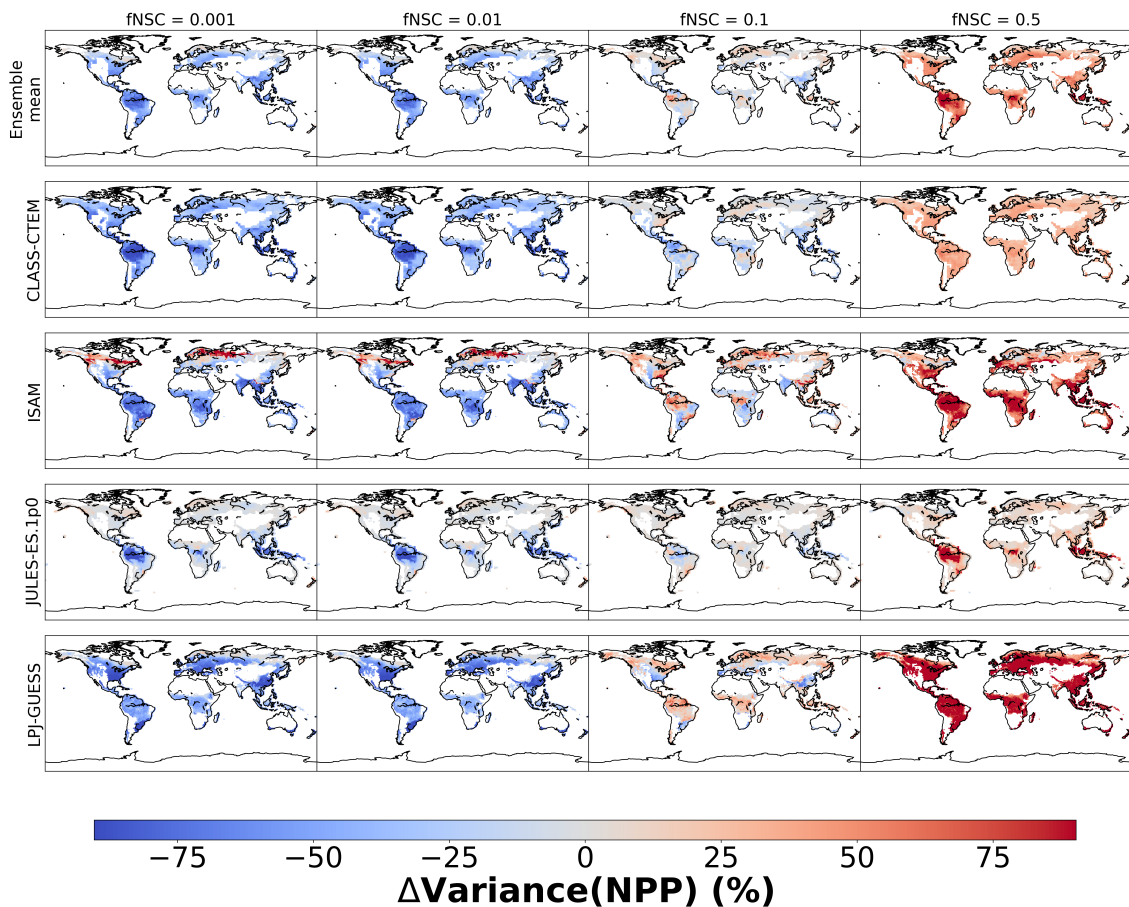
Figure 5.3: The percentage change in the inter-annual variance of predicted net primary productivity (NPP) against four initialised non-structural carbohydrate (NSC) mass fractions (f_{NSC}) from a simplified version of the SUGAR model. The percentage change is relative to the inter-annual variance of NPP from four land surface models (LSM) which have been used to drive the SUGAR model.

The change in the IAV of NPP can be associated with a change in either the IAV of R_a, or the covariance of GPP and R_a, according to equation (5.8). An increase in the IAV of R_a results in an increase in the IAV of NPP, while an increase in the covariance of GPP and R_a decreases the IAV of NPP. The percentage change in the IAV of R_a was far less uniform with respect to the sign of the change,

96

both spatially and across models, than that of NPP (Fig. 5.4). In the ensemble mean, the increase in the IAV of NPP was consistent with an increase in the IAV of R_a across the Amazon basin, however, for many other regions, the IAV of R_a decreased in contrast to the increase in the IAV of NPP. This indicates that the increase in IAV of NPP was driven predominantly by the relative change in the covariance of GPP and R_a, the sign of which was consistently negative both spatially and across models (Fig. 5.5). The decrease in the covariance of GPP and R_a was again most pronounced across tropical regions in most models, with the exception once more being in LPJ-GUESS where significant decreases were also seen in northern latitudes and the subtropics (Fig. 5.5).
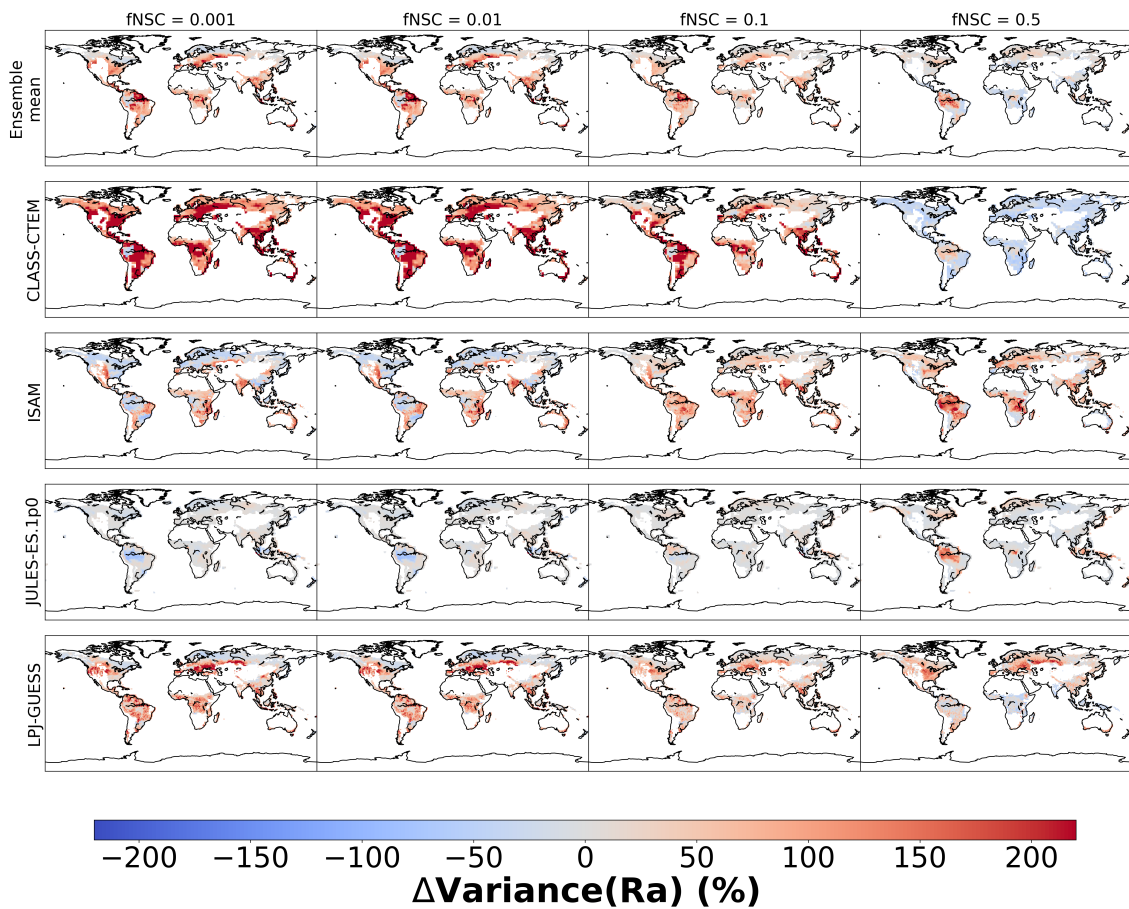
Figure 5.4: The percentage change in the inter-annual variance of predicted autotrophic respiration (R_a) against four initialised non-structural carbohydrate (NSC) mass fractions (f_{NSC}) from a simplified version of the SUGAR model. The percentage change is relative to the inter-annual variance of R_a from four land surface models (LSM) which have been used to drive the SUGAR model.

At $f_{NSC} = 0.001$, representing the fastest NSC turnover rates/smallest pool sizes, the decrease in the IAV of global mean NPP (Fig. 5.2) was again a largely consistent result both spatially and across models (Fig. 5.3). The main exception to this was a significant increase in IAV across northern regions in ISAM. The cause of this exception is not yet clear.
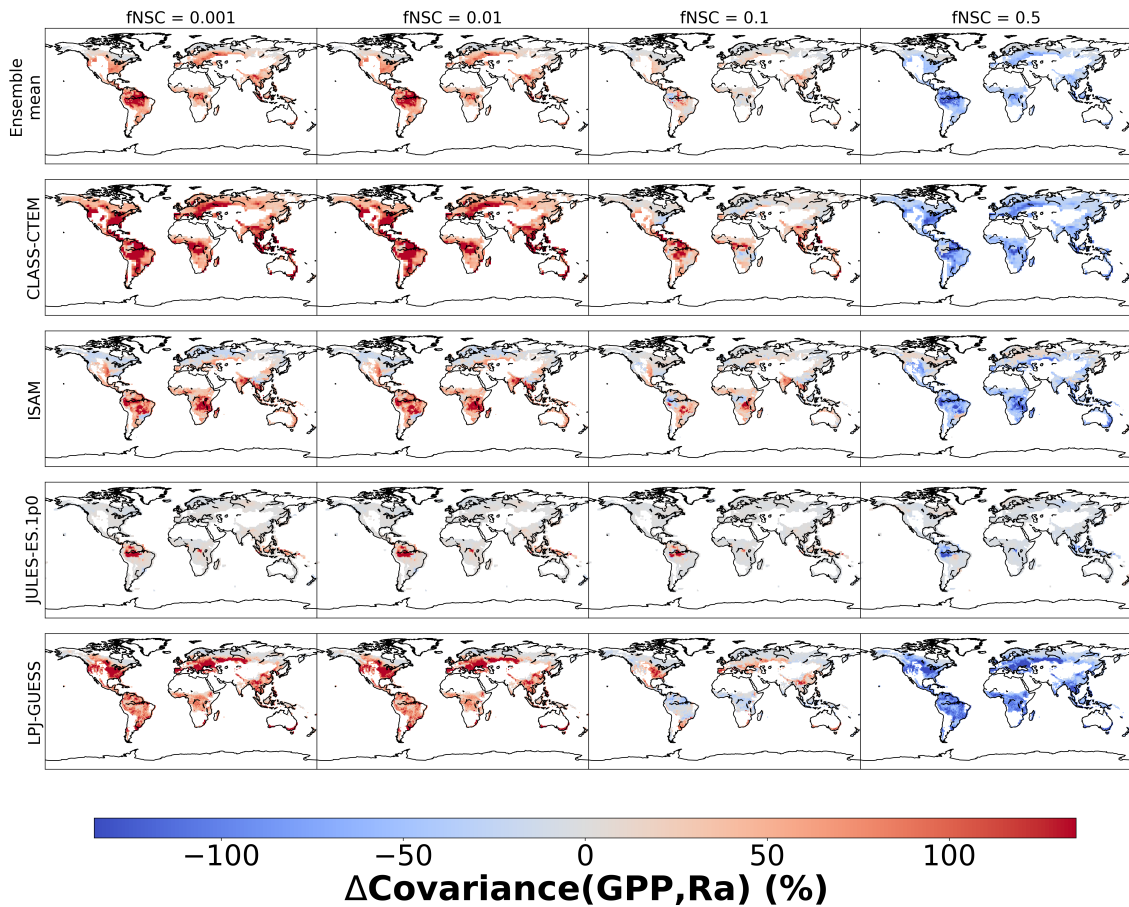
Figure 5.5: The percentage change in the covariance of annual gross primary production (GPP) and predicted annual autotrophic respiration (R_a), against four initialised non-structural carbohydrate (NSC) mass fractions (f_{NSC}) from a simplified version of the SUGAR model. The percentage change is relative to the equivalent covariance from four land surface models (LSM) which have been used to drive the SUGAR model.

The mostly consistent decrease in the IAV of NPP was again in contrast to the heterogeneity in the sign of the change in IAV of R_a (Fig. 5.4). At this smaller f_{NSC} values, several regions across all models saw significant increases in the IAV of R_a which was in contradiction to the decrease seen for NPP. Again, this indicates that the change in the covariance of GPP and R_a, which was positive across most regions and models, was the predominant driver of the change in IAV of NPP. The increase in the IAV of NPP seen across northern latitudes in ISAM was also consistent with decreases in the covariance of GPP and R_a. Finally, at the two intermediate f_{NSC} values (0.01 and 0.1), the transition from a decrease to an increase in the IAV of global mean NPP (from small f_{NSC} values to large) is seen spatially (Fig. 5.3). This transition did not occur uniformly in space or across models.

5.3.3 Comparing to observations of the land carbon sink
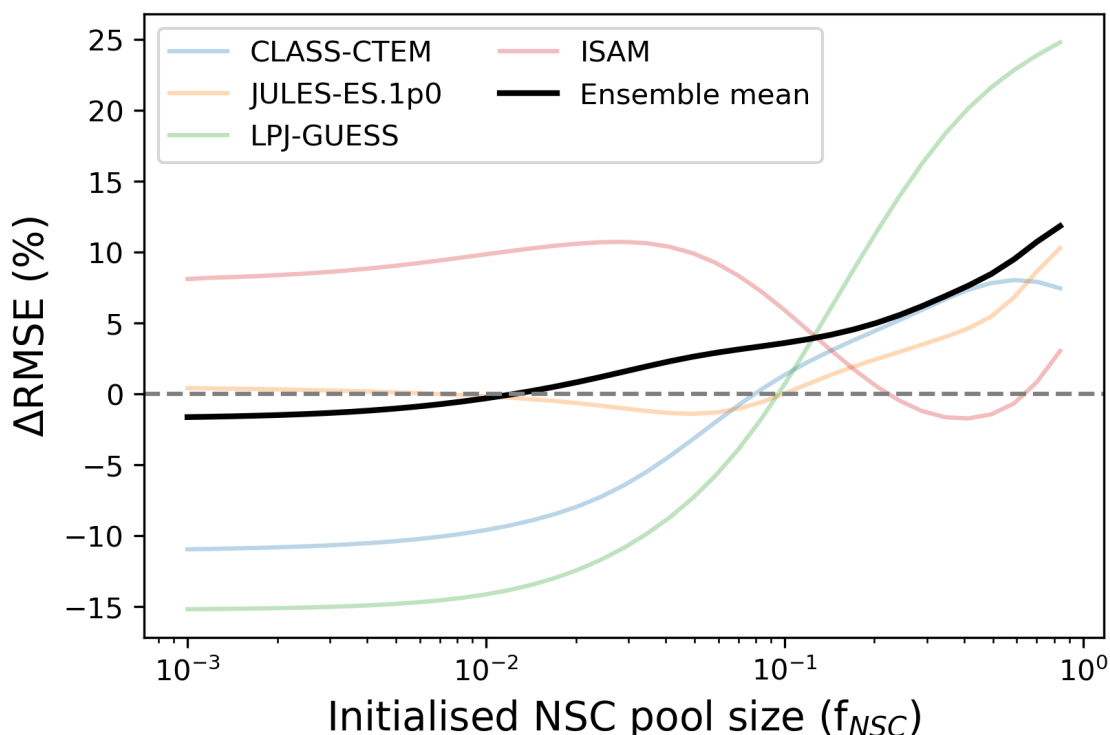
Figure 5.6: The percentage change in the root mean square error (RMSE) between predicted and observations of global net biome productivity (NBP) against initialised non-structural carbohydrate (NSC) mass fraction. The predicted NBP is from a simplified version of the SUGAR model, driven by four land surface models (LSM). Observations are the implied land sink from the Global Carbon Project. The percentage change is relative to the RMSE between observations and the predicted NBP from the four original LSMs.

The changes made to predicted NBP relative to the original LSMs and observations varied significantly between models (Fig. 5.6). In CLASS-CTEM and LPJ-GUESS, significant improvements to predicted NBP were achieved using the smallest values of f_{NSC}. In both models, the maximum reduction in the RMSE between observations and predictions occurred at the smallest tested value of f_{NSC} ($f_{NSC} = 0.001$). At this value LPJ-GUESS saw a decrease of 15.2% in the RMSE, and CLASS-CTEM saw a decrease of 10.9%. However, above $f_{NSC} = 0.0953$ in LPJ-GUESS, and above $f_{NSC} = 0.0796$ in CLASS-CTEM, the predictions of NBP by SUGAR less accurately captured the GCB obsevations than the original LSMs, with the RMSE increasing as f_{NSC} increased above these values in both models. In JULES-ES-1.0 and ISAM, improvements to the predictions of NBP were less significant and occurred at different values of f_{NSC}. In JULES-ES-1.0, the RMSE between predictions and observations was reduced, relative to the original model, for f_{NSC} values between 0.00711 and 0.0100. The maximum decrease of 1.33% occurred at an f_{NSC} value of 0.0492. In ISAM the RMSE was reduced relative to the original model for f_{NSC} values between 0.225 and 0.636,

with a maximum reduction of 1.72% occurring at f_{NSC} = 0.412. The NBP predicted by SUGAR at these optimal values of f_{NSC} are compared with the original prediction by each LSM and the GCB observations in Fig. 5.7.
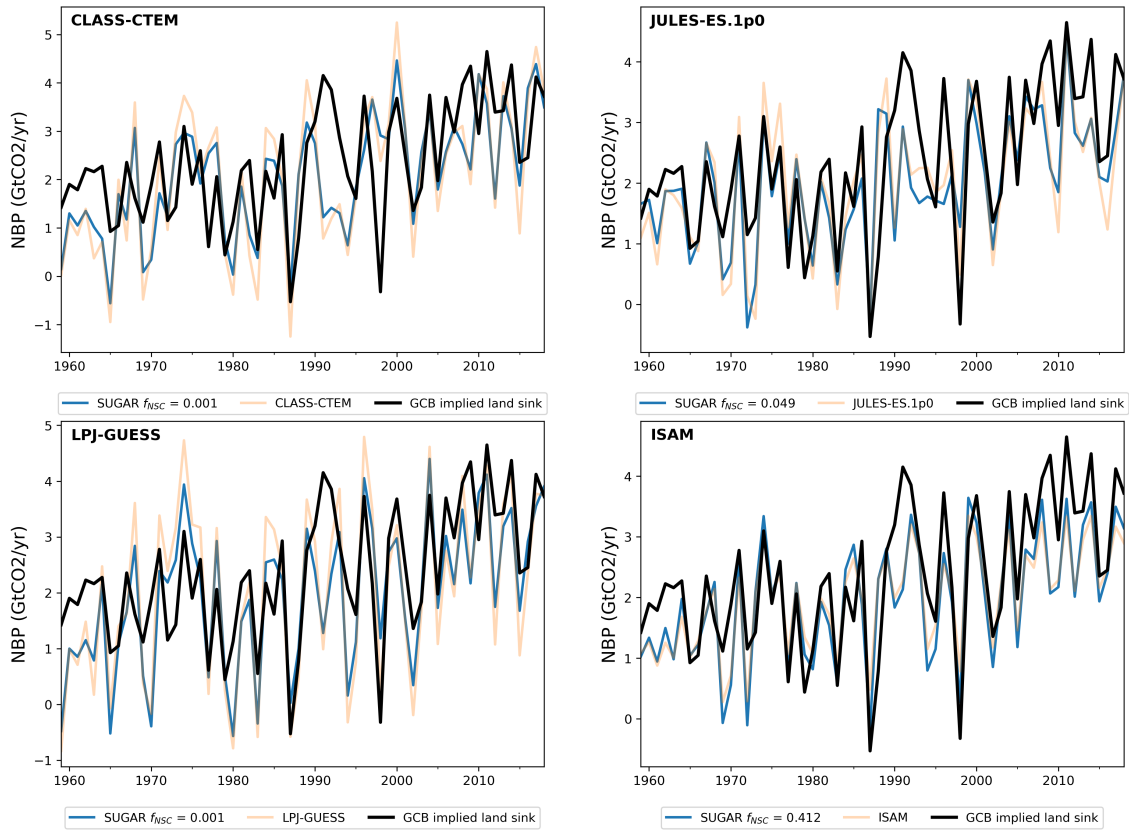
Figure 5.7: The Net Biome Productivity (NBP) predicted by four land surface models (LSM) from the TRENDY model consortium (orange), and the NBP predicted by the SUGAR model (blue) with an initialised non-structural carbohydrate (NSC) mass fraction (f_{NSC}) that optimises the prediction of NBP relative to observations from the Global Carbon Budget (GCB). The f_{NSC} values that optimise the prediction of NBP by SUGAR for each TRENDY LSM are: for JULES-ES-1.0, f_{NSC} = 0.0492; for CLASS-CTEM, f_{NSC} = 0.001; for LPJ-GUESS, f_{NSC} = 0.001; and for ISAM, f_{NSC} = 0.412.

5.4 Discussion

In order to understand the changes made by SUGAR to the variability of predicted NPP it is useful to consider the extreme limits of f_{NSC}. When NSC turnover is slow (i.e. f_{NSC} is large) the rate of respiration in SUGAR is driven predominantly by its temperature and biomass dependences, which in these simulations come from the $R_{m_{TRENDY}}$ factor in equation (5.2). Covariance between R_a and GPP in this limit, is due only to their shared dependence on temperature and biomass and there is no direct relationship between the two variables. The dependence of photosynthesis on other factors such as light and water availability in the four LSMs, mean that the variability both seasonally and inter-annually of respiration

and photosynthesis may be significantly different in this limit. We see a decrease in their covariance relative to the original TRENDY models as f_{NSC} increases, as the influence of photosynthesis on respiration declines. This complete decoupling of GPP and R_a may be particularly important in tropical regions where the variation of GPP can differ greatly from that of temperature (Wagner et al., 2016), and may explain the significant relative change in the covariance of GPP and R_a seen in these regions (Fig. 5.3). In the opposite limit of fast NSC turnover (i.e. f_{NSC} is small), photosynthesis becomes the most important driver of respiration, and the influence of temperature and biomass via the $R_{m_{TRENDY}}$ factor is negligible. This results in a general increase in the covariance between GPP and R_a, as the two variables become more tightly correlated. It should be noted that since the magnitude of covariance depends on the magnitude of the variables, a change in the long-term trend (and therefore magnitude) of respiration in SUGAR may also result in a change in the covariance between GPP and R_a, that not does not necessarily indicate a change in the correlation between the two variables. This may explain the apparent decrease in covariance seen in some regions and models at low f_{NSC} values, in particular across northern latitudes in ISAM, which is in contradiction to the increasing correlation between the two variables that should occur in this limit of fast NSC turnover rate.

These two opposing extremes of fast and slow NSC turnovers are significant. In the limit that f_{NSC} tends to zero (i.e. the turnover rate tends to ∞), respiration in SUGAR becomes a constant fraction of GPP, as NSC is utilised as soon as it is assimilated. Importantly, since respiration is a constant fraction of GPP, it is also always proportional to NPP, and so in this limit we can view SUGAR as a purely growth respiration model. In the opposing limit, where f_{NSC} is large and the turnover rate of NSC is slow, respiration is controlled by its own dependences on temperature and biomass, and we can view SUGAR in this limit as a purely maintenance respiration model. These limits allow us to connect the single respiration flux in SUGAR to the GMR paradigm used in the TRENDY LSMs. The GMR paradigm is an interpretation of empirical observations that, at a constant temperature, changes in respiration can be described by both changes in biomass and changes in photosynthesis (McCree, 1970), as described by equation (5.1). The split of respiration into growth and maintenance components is an attempt to account for this balance between photosynthesis and biomass as primary drivers of respiration. This balance is commonly altered via the growth and maintenance coefficients (k and c from eq. (5.1) respectively), however, the physical interpretation of these coefficients is not clear, which makes justifying their values difficult. The single component respiration framework provides a more mechanistic explanation that the apparent split in the control of respiration between photo-

synthesis and biomass is determined by the turnover rate of substrate (Thornley, 2011; Collalti et al., 2020). At intermediate NSC turnover rates, SUGAR is in the transition shown in Figure. 5.5, where respiration moves from being controlled predominantly by photosynthesis at fast NSC turnover rates to being controlled predominantly by biomass and temperature at slow NSC turnover rates. The point at which the variability of global mean NPP predicted by SUGAR is the same as that in the original TRENDY LSMs may be viewed as the point at which this alternative interpretation is equivalent to the GMR paradigm. It is interesting to note that the value of f_{NSC} at which this happened, was of the order of 0.1 for all four LSMs. It is difficult to say with any certainty whether this holds any significance. However, a mass fraction of 0.1 is a good estimate of the average concentration of NSC at an ecosystem level within a tropical rainforest (Würth et al., 2005), and given the large proportion of total global biomass made up by tropical forests, may also be a reasonable estimate of the average ecosystem NSC content at a global scale. If we assume that the maintenance-growth split within these four LSMs has been parametrised to match the observed split in the control of respiration by photosynthesis and biomass, then these values may support the idea that the single component respiration framework is a more mechanistic way to explain variation in total plant respiration.

An aim of this study was to explore the possibility of using global observations of terrestrial carbon uptake to constrain the turnover rate of NSC within SUGAR. In all four LSMs the RMSE between predicted and observed NBP was reduced by the addition of the NSC pool in SUGAR, for at least a small range of f_{NSC} values. In some of the LSMs the maximum reduction in this RMSE was quite large, in particular in LPJ-GUESS and CLASS-CTEM where the RMSE was reduced by by up to 15.2% and 10.9% respectively. However, it is important to analyse the significance of these reductions and the f_{NSC} values associated with them. First, for LPJ-GUESS and CLASS-CTEM, the RMSE between predicted and observed NBP saw the largest reduction as f_{NSC} tended towards zero and NSC turnover rates became large. The resulting constraint on NSC concentrations, suggests that plants do not store any form of reserve compounds and that all carbon is utilised as soon as it is assimilated. This limit is equivalent to setting respiration equal to a constant fraction of GPP, an approached used in some models (Collalti and Prentice, 2019) and referred to as the 'fixed fraction hypothesis' (Waring et al., 1998; Collalti et al., 2020). However, this conflicts with observations that plants often contain significant amounts of reserve carbon (Würth et al., 2005; Hoch et al., 2003) and that carbon utilisation rates can diverge from carbon assimilation rates over both seasonal and multi-annual time-scales (Doughty et al., 2015a). In contrast, in ISAM, the maximum reduction in RMSE occurred when f_{NSC} was equal

to 0.412, suggesting that on average more than 40% of plant biomass is made up of NSC. While plants are capable of storing large quantities of non-structural compounds, such high concentrations of NSC are unlikely. Ecosystem level NSC concentrations are difficult to determine but estimates are usually close to ~10% of total plant biomass (Martínez-Vilalta et al., 2016). For example, an estimate of 8% was reported for a semi-deciduous tropical forest (Würth et al., 2005), while the most recent estimate of NSC concentrations in temperate forests is at c. 4% (Furze et al., 2019). Finally, in JULES-ES-1.0, the maximum reduction in RMSE occurred at an f_{NSC} value of 0.0492, implying an average NSC mass fraction of around 5% globally. This is a far more realistic estimate, however, its reliability must be thoroughly examined. Several of the factors that we might use to explain the unrealistic values of f_{NSC} that emerge from the other LSMs, also apply to JULES-ES-1.0, meaning we cannot rule out getting the right (or at least realistic) answer for the wrong reason. Nonetheless as a proof of concept this is an encouraging result.

Several limitations in this study limit the use of the GCB budget imbalance to constrain NSC turnover. The first is the calculation of NBP predictions in SUGAR. NBP is the balance between fluxes into and out of the land surface. Two significant components of this are the net flux of carbon absorbed by plants (NPP) and the flux of carbon out of the soil by heterotrophic respiration (R_H). These two components are not independent as the rate of R_H is closely related to the input of carbon into the soils through plant litter-fall, which itself is determined by NPP. To calculate predictions of NBP in SUGAR, changes in the inter-annual variability of in NPP were added to the original predictions of NBP from each TRENDY LSM, however, this did not take into the account the relationship between NPP and R_H. Accounting properly for this relationship would require SUGAR to be coupled to each LSM and the TRENDY simulations to be repeated, which may produce significantly different predictions of NBP to those presented here. This should motivate the community to consider the role of NSC in LSMs so that fully coupled simulations can be realised. Another limitation was the use of grid-box fluxes from the TRENDY LSMs to drive SUGAR. One of the main assumptions made in these simulations was that the f_{NSC} value used within SUGAR was uniform across the globe meaning that every ecosystem was initialised with the same NSC mass fraction. However, significant variation in the amount of NSC stored by plants has been seen across ecosystems and plant species (Martínez-Vilalta et al., 2016; Dietze et al., 2014). An improvement to these simulations may be to represent NSC on a plant function type (PFT) basis instead of at the grid-box level. This would allow the spatial and inter-species variation in NSC content to be accounted for and result in more accurate constraints on NSC turnover. Finally,

the effect that the variability of both predicted GPP and maintenance respiration in each LSM has on the predictions made by SUGAR is large. The variability of respiration and NPP predicted by SUGAR is ultimately determined by contributions from the GPP and R_m inputs from TRENDY. Deficiencies in the predictions of these two variables therefore limits the ability of SUGAR to accurately predict respiration and NPP fluxes, and highlights the need to develop the representation of respiration and NSC in these LSMs, in conjunction with developments in the representation of photosynthesis.

5.5   Conclusions

This work highlights the potential impact that representing the dependence of respiration and growth on NSC may have on the variability of carbon fluxes even on inter-annual time-scales. The apparent dependence of respiration on photosynthesis and biomass may be explained by a simple substrate-based framework which represents an alternative interpretation to the GMR paradigm. The growth-maintenance split within the four TRENDY LSMs used in this chapter may also indicate an average global NSC mass fraction of around 10%. The use of atmospheric CO_2 observations to constrain parameters within SUGAR is difficult due to the many other processes associated with the global carbon cycle that introduce uncertainty into observations and model predictions. Further work is needed if this method is to be successful, however, it highlights the potential of using the variability of carbon fluxes to constrain components of NSC dynamics.

Model	Maintenance Respiration	Growth Respiration	Reference
CLASS-CTEM	$R_{m_L} = s_L V_m f_{25}(Q_{10}) f_{par}$ $R_{m_i} = 2.64 \times 10^{-6} s_i l_{v,i} C_i f_{25}(Q_{10})$ where: $i = S, R$ (stem or root) $l_{v,i}$ = live fraction of stem or root C_i = stem or root carbon mass s_i = base respiration rate (constant) V_m = maximum catalytic capacity of rubsico $f_{par} = \frac{1}{k_n}\left(1.0 - e^{-k_n LAI}\right)$	$R_g = \epsilon_g max\{0, GPP - R_m\}$ where: $\epsilon_g = 0.15$	(Melton and Arora, 2016)
LPJ-GUESS	$R_{m,t} = 0.0548 r \frac{C_t}{cton_t} exp\left[308.58\left(\frac{1}{56.02} - \frac{1}{T - 45.87}\right)\right]$ where: t = tissue type r = PFT-specific coefficient C_t = carbon content of tissue t $cton_t$ = C-N mass ratio of tissue t T = ambient temperature	$R_g = 0.25(GPP - R_m)$	(Smith et al., 2001, 2014)
JULES-ES	$R_{p_m} = 0.12 R_{d_c}\left(\beta + \frac{N_r + N_s}{N_l}\right)$ where: R_{d_c} = dark respiration β is a soil moisture stress factor N_i for $i = l, s, r$ are the nitrogen contents of leaves, stem and root respectively	$R_{pg} = r_g(GPP - R_{pm})$ where: $r_g = 0.25$	(Clark et al., 2011)
ISAM	$R_{m_i} = k_i \frac{C_i}{CN_i} g(T)$ where: i = leaf, stem, root C_i = carbon content of component i k_i = maintenance coefficient at 20 °C for component i CN_i = C:N ratio of component i T = Temperature	$R_g = max\{0, r_g(GPP - R_m)\}$ where: $r_g = 0.25$	(Song et al., 2013)

Table 5.1: A summary of how respiration is represented in four TRENDY models.

Chapter 6

Conclusions

This thesis has focused on the role of non-structural carbohydrates (NSC) in model predictions of plant carbon fluxes at an ecosystem, regional and global scale.

6.1 Overview

In chapter 1 our current empirical understanding of NSC within plants was investigated. The role of NSC in supporting plant respiration and growth, when photosynthetic carbon assimilation is limited, was presented and discussed. In particular the importance of NSC during periods of environmental stress was highlighted. Key uncertainties associated with how NSC dynamics are involved in plant responses to drought, in particular within mortality processes were examined. We saw that despite the importance of NSC within terrestrial ecosystems, many land surface models (LSM) do not contain comprehensive descriptions of NSC storage and utilisation. While many LSMs represent some form of labile carbon reserve, that is typically required to produce accurate predictions of certain plant processes such as leaf phenology; most LSMs do not capture all the key components associated with NSC. Specifically, there are currently few LSMs that account for the dependence of both respiration and growth on NSC, which limits their ability to capture both long and short term responses to changes in both environment and carbon availability from photosynthesis.

In chapter 2, a simple model of NSC storage and utilisation, the "Substrate Utilisation by Growth and Autotrophic Respiration" model (SUGAR), designed to work within a LSM was presented. The model equations were presented and key concepts within the model were derived. Context for how SUGAR may fit within a LSM was also given by describing the relevant equations within JULES (The Joint UK Land Environment Simulator Best et al., 2011; Clark et al., 2011). The simplicity of SUGAR allowed an approach to evaluating its parameters, that does not

require detailed time-series of NSC concentrations, which are difficult to measure.

In chapter 3, SUGAR was used to simulate plant carbon expenditure (PCE) fluxes across the Amazon basin, using predicted Gross Primary Productivity (GPP) from an ensemble of LSMs and constrained with observations. The difference between models that do not represent NSC, and models that do, and the transition between them, was demonstrated by examining the sensitivity of SUGAR to NSC turnover rate, which was varied by changing the initialised NSC pool size between simulations. In simulations with realistic estimates of NSC pool size, SUGAR was able to decouple PCE from GPP over seasonal time-scales, and a transition from source-driven to sink-driven carbon dynamics was seen in the predictions of PCE. The difference in the seasonality between GPP and PCE, predicted by SUGAR, was qualitatively consistent with observations over the Amazon and highlighted the importance of comprehensive representations of NSC in large scale ecosystem models.

In chapter 4, SUGAR was tested under stressed and non-stressed conditions by simulating carbon fluxes at a tropical through-fall exclusion (TFE) experiment and corresponding control plot. Simulations of the two forests by JULES were used to drive SUGAR off-line, and predictions of respiration and growth from both models were compared to observations. SUGAR more accurately captured the response of net primary productivity (NPP) to the drought experiment compared to JULES, suggesting an important role for NSC within the forest drought response. However, the results also highlighted the need for further development of the response of photosynthesis in JULES as reducing the sensitivity of photosynthesis to soil moisture stress also allowed more accurate predictions by JULES, and was another significant contributor to the mismatch between observations and predictions.

Finally, chapter 5 investigated the impact of a simple model of NSC on predictions of respiration, NPP and net terrestrial carbon uptake at a global scale. A simplified version of SUGAR was used to simulate respiration and growth fluxes, with output data from four LSMs from the TRENDY consortium used as driving data. These simulations showed that NSC may have a significant effect on predictions of carbon fluxes at a global scale and over multi-annual time-scales. They also presented an alternative interpretation of the growth-maintenance respiration paradigm which is at the heart of most LSMs. This may provide a more mechanistic representation and understanding of respiration within LSMs.

6.2 Future work

SUGAR is a relatively simple approach to modelling NSC, that reflects the current availability of empirical data on carbohydrate dynamics in plants. Due to its parsimonious nature, it is generally easy to run and evaluate, and facilitates a basic understanding of NSC dynamics at an ecosystem scale. However, despite the paucity of data, there are significant processes associated with NSC that are known to be important for plant function that are missing from SUGAR. In addition, there are several issues and questions that arise from attempting to integrate SUGAR into a LSM, which was the original aim of this work.

6.2.1 The effect of water availability on growth

As seen throughout this thesis, an underlying assumption in many LSMs is that plant growth is driven predominantly by the rate of photosynthesis. Growth in these models is often predicted to increase in the future as photosynthesis is stimulated by increasing CO_2 concentrations, albeit with substantial spread between models in terms of the magnitude of this change (Friend et al., 2014). However, these predictions are at odds with several observations from experimental CO_2 fertilisation studies in which plant growth is largely unaffected by increased CO_2 despite enhanced photosynthesis (Woodward, 2002; Kirschbaum, 2010; Ellsworth et al., 2017). This may be due to the limitation of plant growth by external factors such as nutrient availability, temperature, and water availability (Körner, 2003), and so representing these factors is an integral part to predicting accurate growth responses of global vegetation to climate change in the future.

It is well documented that declining water availability has a direct impact on plant growth, that is not associated with a reduced carbon supply from the inhibition of photosynthesis (Muller et al., 2011; Hsiao, 1973; Boyer, 1970). Growth in plants relies on uptake of water by cells causing them to expand, and resulting in an irreversible extension of their walls (Cosgrove, 2014; Fricke, 2017). When water availability is low, cell water uptake is prevented and growth ceases. However, this process is rarely represented in large scale vegetation models. This is in part due to a lack of NSCs that allow environmental controls of sink processes, and in part because it is not clear how cell extension can be scaled to the whole plant or ecosystem level, that most global vegetation models work at. Attempts to incorporate direct water limitation on growth into models have largely used empirically derived relationships (e.g. Guillemot et al., 2017; Mencuccini et al., 2017) in place of mechanistic representations. These allow accurate predictions of plant growth at fine spatial and temporal resolutions, however may not be applicable to the global scale as they are commonly derived from relatively small

subsets of plant species and environmental conditions. Mechanistic approaches (e.g. Steppe et al., 2006; Hölttä et al., 2010) will likely prove to be more reliable for predicting future plant growth at global scales, however, commonly these models contain large amounts of parameters which are currently difficult to evaluate (Babst et al., 2018; Peters et al., 2021). Recent efforts to measure environmental limitations on plant growth (Babst et al., 2019) may allow both mechanistic and empirical approaches to be incorporated into large-scale vegetation models and efforts should be made to evaluate these approaches across the globe. This will further our understanding of water limited plant growth and allow new theory to be tested and evaluated.

6.2.2 Dynamic carbon allocation

A further limitation of SUGAR is that it currently simulates just one NSC pool, distributed uniformly across all plant organs. In addition, different molecules such as sugars and starches are not distinguished. Yet NSC concentrations are commonly found to vary significantly throughout a plant, often being highest in leaves for example, and lowest in stems (Martínez-Vilalta et al., 2016). Idealised modelling studies suggest that partitioning and transport of substrate between organs may be important for determining the dynamic allocation of carbon to different structural tissues in response to changes in environment (Thornley, 1991; Reynolds and Thornley, 1982), for example enhanced root growth when soil nutrients or water availability are low, or enhanced leaf growth when in poor light conditions (Doughty et al., 2014; Kobe et al., 2010; Girardin et al., 2016). However, many LSMs do not allow these types of dynamic adaptations to occur, with the ratios between different plant organs being determined by predefined allometric relationships (e.g. Clark et al., 2011). Even with dynamic allometry, the transport of NSC throughout a plant is not well understood and mechanistic representations are difficult to parametrise, particularly at a global level. Nonetheless, efforts should be made to develop representations of these adaptive strategies as they play an integral role in the response of forests to changes in climate (Doughty et al., 2014).

6.2.3 Sink priority

NSC utilisation in SUGAR is limited by both the availability of carbohydrate in the NSC pool and the climatic control of temperature. However, another factor that can potentially limit NSC utilisation in plants is what is known as 'sink priority' (Hartmann et al., 2018). When the source of carbon is limiting, plants appear to dynamically change the relative allocation rates of carbon to various processes,

prioritising certain sinks over others. It is unclear what mechanisms cause this hierarchy (Hartmann et al., 2018), however suggestions include the relative position of sinks within the plant (Minchin et al., 1993) and genetic changes in proteins associated with loading and unloading carbohydrates from the phloem (Lemoine et al., 2013).

Currently in SUGAR, there is no hierarchical sink priority, as maintenance respiration (R_m), growth (G), and growth respiration (R_g) are all equally effected by the decline in available carbon from the NSC pool. This may result in unrealistic predictions of plant growth and respiration, in particular over the life cycle of a forest (Hartmann et al., 2018). As trees grow from saplings to maturity, the allometric ratios between different organs can undergo significant shifts, which can greatly effect the dynamics of NSC allocation within the tree (Hartmann et al., 2018). For example, the ratio of leaf biomass to total biomass sharply declines with tree size (Poorter et al., 2012), and as a result the specific rate of GPP (i.e. the ratio of GPP to total biomass) often declines as a tree grows. The specific cost of biomass maintenance, however, does not decline so strongly (Tang et al., 2014) and this results in declining net primary productivity (NPP) and carbon use efficiency (CUE) with increasing plant age (DeLucia et al., 2007; Mencuccini et al., 2005). Since maintenance respiration and growth have the same priority in SUGAR, this shift in CUE does not occur and instead both are equally affected by the decline in specific GPP. This can result in unrealistic predictions of forest regrowth after disturbance, for example. Some form of sink hierarchy therefore needs to be implemented into SUGAR so that, as trees grow and their specific rate of GPP declines, they prioritise maintenance respiration over growth.

One simple approach to achieving sink hierarchy in SUGAR is to introduce different dependences of maintenance respiration and growth on NSC. This can be done simply by introducing distinct Michaelis-Menten parameters (K_m) for each process. The Michaelis-Menten parameter in SUGAR determines the NSC concentration at which utilisation has been reduced by a half of its maximum value. Therefore, by giving maintenance respiration a much smaller Michaelis-Menten parameter than growth, a priority for maintenance respiration is introduced. Growth is down-regulated at larger NSC concentrations and therefore much sooner in response to declining NSC (Fig. 6.1(a)). The current limit to this development is that evaluating these parameters is extremely difficult. Measuring the affinity of different processes for NSC, while controlling for environmental drivers of utilisation is currently not possible. One possible approach, however, might be to use long term carbon use efficiency and whole plant NSC data. Having different K_m parameters for R_m and G in SUGAR introduces a NSC depen-

dence into the equilibrium carbon use efficiency (CUE, Fig. 6.1(b)), which is calculated in SUGAR by assuming that over a sufficiently long period, total NSC utilisation is approximately equal to GPP, and total plant growth is approximately equal to NPP (see chapter 2.5):

$$CUE^* = \frac{G^*}{R_m^* + R_g^* + G^*}$$ (6.1)

Using the equations for R_m, R_g and G, and cancelling terms gives:

$$CUE^* = \frac{G_0}{R_{m_0}\dfrac{W_{NSC}^* + K_{mG}}{W_{NSC}^* + K_{mR}} + \dfrac{G_0}{Y_g}}$$ (6.2)

where K_{mR} and K_{mG} are the distinct Michaelis-Menten parameters for maintenance respiration and growth respectively.

It may be possible therefore, to fit these parameters with long-term NSC and CUE data over the lifetime of a tree or forest. Such data is rare as the lifetime of forests is typically much longer than the average field experiment. However, long-term data like this would be invaluable in the understanding of NSC allocation and sink priority and would aid in further development of models, including SUGAR. The long-term evolution of NSC dynamics as trees grow from saplings to trees may unlock some of the key questions associated with our understanding of carbon allocation in plants (Hartmann et al., 2018).
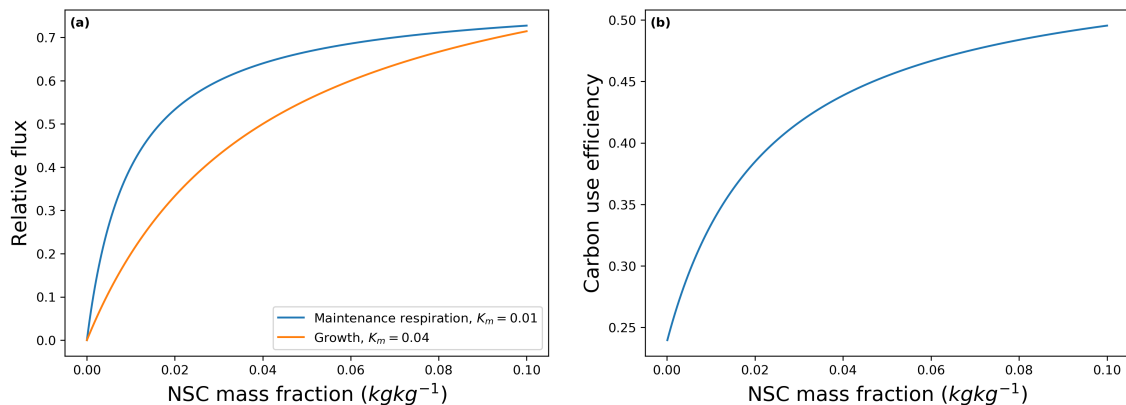
Figure 6.1: (a) The relationships between maintenance respiration (R) and growth (G), with non-structural carbohydrate (NSC) availability with distinct Michaelis-Menten parameters (K_m). Growth declines at larger concentrations of NSC relative to maintenance respiration and hence has a lower priority. (b) Equilibrium carbon use efficiency (G/(G+R)) against NSC availability.

6.2.4 Litter-fall and disturbance

An issue that arises when coupling SUGAR to a LSM is how the NSC pool interacts with litter-fall and disturbance processes. It is intuitive that during disturbance events such as fire, herbivory or wind induced litter-fall, (i.e. biomass loss that plants have no prior 'knowledge' of) all forms of biomass may be lost. That is, if for example a leaf is blown from a tree, or eaten by an animal, the whole leaf and its contents must be lost, including the NSC stored within it. This therefore changes the rate equation for NSC in SUGAR as there must now be a loss from disturbance. However, there are some litter-fall events that are not induced directly by external factors. Deciduous trees, for example, drop their leaves in response to changes in environment such as declining temperatures or water availability, however the actual process of leaf senescence is induced and controlled internally by the tree itself. There is some evidence that nutrients may be partially reabsorbed before leaves are dropped (Aerts, 1996; Killingbeck, 1996), and it may therefore be possible for plants to also partially reabsorb NSC into their stems, and drop only structural compounds in litter-fall. There is little data on the NSC concentrations within leaves before and after senescence and so this process is not well quantified. The re-absorption of NSC must necessarily work against concentration gradients and so may be a relatively small flux. Mathematically it is simplest to assume that no NSC can be re-absorbed before leaf senescence and so in future work when coupling SUGAR to a LSM, this will be assumed. However, this process may still have a large effect on whole plant NSC dynamics in deciduous species and work should be done to attempt to quantify it.

Assuming that there is no NSC re-absorption before leaf senescence, the equations in SUGAR change as follows: In SUGAR the mass fraction of NSC (W_{NSC}) is uniform throughout an ecosystem, as different plant organs are not distinguished. If the rate of total biomass (C_v) loss from litter-fall and disturbance is given by Λ, then the rate of NSC loss through these processes must be given by $W_{NSC}\Lambda$. The equation for the rate of change of NSC then becomes:

$$\frac{dC_{NSC}}{dt} = \Pi_G - R_m - R_g - G - W_{NSC}\Lambda \qquad (6.3)$$

where Π_G is Gross Primary Productivity (GPP), R_m is maintenance respiration, R_g is growth respiration, and G is structural plant growth.

The rate of change of total plant carbon biomass is given by:

$$\frac{dC_v}{dt} = \Pi_N - \Lambda \qquad (6.4)$$

where Π_N is Net Primary Productivity (NPP).

The rate of change of W_{NSC} is, therefore, given by:

$$\frac{dW_{NSC}}{dt} = \frac{(1 - W_{NSC})}{C_v}(\Pi_G - R_m - R_g) - \frac{G}{C_v} \tag{6.5}$$

To evaluate the parameters in SUGAR (ϕ and α; equations 2.37 & 2.38) we can again consider SUGAR under steady state such that the rate of change of W_{NSC} is zeros. Assuming that over a period τ_{obs}, W_{NSC} can be considered constant, then averaging over that period gives:

$$0 = \frac{1}{\tau_{obs}}\int_{\tau_{obs}}\left(\frac{dW_{NSC}}{dt} = \frac{(1 - W_{NSC})}{C_v}(\Pi_G - R_m - R_g) - \frac{G}{C_v}\right)dt \tag{6.6}$$

Using the definition of α (equation (2.38)) and substituting the definition of U (equation (2.37)) gives:

$$0 = \frac{1}{\tau_{obs}}\int_{\tau_{obs}}\left((1 - W_{NSC})\frac{\Pi_G}{C_v} - (1 - W_{NSC}(1 - \alpha))\phi F_Q(T)\frac{W_{NSC}}{W_{NSC} + K_m}\right)dt \tag{6.7}$$

Assuming that variations in the NSC pool are small relative to its total size, this can be approximated as:

$$0 = (1 - f_{NSC})\left(\frac{\Pi_G}{C_v}\right)^* - (1 - f_{NSC}(1 - \alpha))\phi F_Q^*(T)\frac{f_{NSC}}{f_{NSC} + K_m} \tag{6.8}$$

Rearranging for ϕ gives:

$$\phi = \frac{1 + a_{K_m}}{F_Q^*(T)}\left(\frac{\Pi_G}{C_v}\right)^*\frac{1 - f_{NSC}}{1 - f_{NSC}(1 - \alpha)} \tag{6.9}$$

Similarly for α, writing the rate of change of W_{NSC} in terms of NPP:

$$\frac{dW_{NSC}}{dt} = \frac{(1 - W_{NSC})}{C_v}\Pi_N - \frac{G}{C_v} \tag{6.10}$$

Averaging over the observation period, the average NPP can be aprroximated in terms of the equilibrium structural carbon growth rate (G^*) and equilibrium NSC mass fraction (f_{NSC}):

$$\Pi_N^* = \frac{G^*}{1 - f_{NSC}} \tag{6.11}$$

Similarly using equation (6.5), an expression for steady state GPP can be found in terms of equilibrium growth and respiration:

$$\Pi_G^* = R_m^* + R_g^* + \frac{G^*}{1 - f_{NSC}} \tag{6.12}$$

Equations (6.11) and (6.12) can then be used to relate steady-state carbon use efficiency to equilibrium growth and respiration:

$$CUE^* = \frac{G^*}{(R_m^* + R_g^*)(1 - f_{NSC}) + G^*} \tag{6.13}$$

Substituting equations (2.31), (2.34) and (2.33), and rearranging yields:

$$CUE^* = \frac{G_0}{R_{m_0}(1 - f_{NSC}) + \dfrac{1 - Y_g}{Y_g}(1 - f_{NSC})G_0 + G_0} \tag{6.14}$$

Rearranging gives:

$$\frac{R_{m_0}}{G_0} = \frac{1}{1 - f_{NSC}} \left[\frac{1}{CUE^*} - \frac{1 - Y_g}{Y_g}(1 - f_{NSC}) - 1 \right] \tag{6.15}$$

Finally using $\phi = R_{m_0} + \dfrac{G_0}{Y_g}$ and $G_0 = \alpha\phi$, yields:

$$\frac{R_{m_0}}{G_0} = \frac{1}{\alpha} - \frac{1}{Y_g} \tag{6.16}$$

Which allows the following expression to be written for α in terms of steady state carbon use efficiency:

$$\alpha = \left[\frac{1}{1 - f_{NSC}} \left(\frac{1}{CUE^*} - \frac{1 - Y_g}{Y_g}(1 - f_{NSC}) - 1 \right) + \frac{1}{Y_g} \right]^{-1} \tag{6.17}$$

6.2.5 Carbon starvation

Many LSMs including JULES do not explicitly represent mortality. Instead, vegetation carbon is lost through background litter-fall and disturbance rates, and mortality is implicitly represented when the forest carbon balance is negative, i.e. NPP is less than background litter-fall + disturbance. In addition this may be accelerated if respiration exceeds photosynthesis and NPP becomes negative. Structural biomass is respired, reducing plant biomass and emulating mortality. In SUGAR, however, structural carbon cannot be respired and so NPP can only become negative while there is still NSC to support respiration. When NSC is depleted, it down regulates respiration, restoring positive NPP levels. This essentially removes the implicit representation of mortality that occurs when respiration

exceeds GPP. An explicit representation of plant mortality is therefore required such that when the NSC pool is depleted, if photosynthesis is remains inhibited and respiration is down regulated, then biomass can be lost from the ecosystem.

6.2.6 End-product Inhibition

In SUGAR there is currently no upper bound on the mass fraction of NSC, and in theory if the specific rate of GPP increases sufficiently, the NSC mass fraction could become unrealistically large. In reality, large NSC mass fractions do not occur as excessive build up of substrate within leaves can actually inhibit photosynthesis, a process termed 'end-product inhibition' (Stitt, 1991). End-product inhibition is not well understood however, future work might look at improving this understanding and developing a representation that can be added to SUGAR and JULES to prevent unrealistically large NSC mass fractions.

6.2.7 Stomatal optimisation

SOX (Eller et al., 2018, 2020) is a stomatal optimisation model designed to improve the representation of stomatal responses to water availability. The model is based upon stomatal optimality theory which suggests that stomatal regulation must maximise carbon gain from photosynthesis against evaporative water loss, both associated with increasing stomatal conductance (Wolf et al., 2016). SOX assumes that the optimal stomatal conductance maximises the product of photosynthetic rate and the relative change in hydraulic conductance associated with stomatal opening. In chapter 1 of this thesis we saw that plant water and plant carbon status are inextricably linked, and there may be several applications of SUGAR that may relate to SOX:

- The first is associated with xylem repair. Once xylem is damaged in SOX, and hydraulic conductance is lost, it can be recovered instantaneously once the water stress is eased and normal photosynthesis is resumed. In reality xylem repair must depend on resource availability (Sevanto et al., 2014) and a possible area for future research is therefore the role that NSC availability in SUGAR may have in determining xylem recovery in SOX.

- Second is associated with the optimisation within SOX. Stomatal optimality theory maximises carbon gain by photosynthesis as it is assumed that greater carbon assimilation results in increased plant growth. However, throughout this thesis we have seen that plant growth does not always depend on photosynthesis, and environmental conditions may limit growth independently of carbon assimilation. NSCs are central to this and it may be necessary to take into account the NSC availability in this optimisation.

One hypothesis might be that with significant stores of NSC, plants do not need to risk opening their stomata, as they can maintain respiration and growth using their NSC reserves. Alternatively it may be that with significant NSC, any damage to xylem can be easily repaired due to high resource availability. Plants may therefore be able to risk opening their stomata further to further maximise carbon assimilation. It is not clear what role NSC might have in this optimisation but the simplicity of SUGAR may allow these hypotheses to be tested.

Bibliography

Adams, H. D., Germino, M. J., Breshears, D. D., Barron-Gafford, G. A., Guardiola-Claramonte, M., Zou, C. B., and Huxman, T. E. (2013). Nonstructural leaf carbohydrate dynamics of pinus edulis during drought-induced tree mortality reveal role for carbon metabolism in mortality mechanism. *New Phytologist*, 197(4):1142–1151.

Adams, H. D., Zeppel, M. J. B., Anderegg, W. R. L., Hartmann, H., Landhäusser, S. M., Tissue, D. T., Huxman, T. E., Hudson, P. J., Franz, T. E., Allen, C. D., Anderegg, L. D. L., Barron-Gafford, G. A., Beerling, D. J., Breshears, D. D., Brodribb, T. J., Bugmann, H., Cobb, R. C., Collins, A. D., Dickman, L. T., Duan, H., Ewers, B. E., Galiano, L., Galvez, D. A., Garcia-Forner, N., Gaylord, M. L., Germino, M. J., Gessler, A., Hacke, U. G., Hakamada, R., Hector, A., Jenkins, M. W., Kane, J. M., Kolb, T. E., Law, D. J., Lewis, J. D., Limousin, J.-M., Love, D. M., Macalady, A. K., Martínez-Vilalta, J., Mencuccini, M., Mitchell, P. J., Muss, J. D., O'Brien, M. J., O'Grady, A. P., Pangle, R. E., Pinkard, E. A., Piper, F. I., Plaut, J. A., Pockman, W. T., Quirk, J., Reinhardt, K., Ripullone, F., Ryan, M. G., Sala, A., Sevanto, S., Sperry, J. S., Vargas, R., Vennetier, M., Way, D. A., Xu, C., Yepez, E. A., and McDowell, N. G. (2017). A multi-species synthesis of physiological mechanisms in drought-induced tree mortality. *Nature Ecology & Evolution*, 1(9):1285–1291.

Aerts, R. (1996). Nutrient resorption from senescing leaves of perennials: Are there general patterns? *Journal of Ecology*, 84(4):597–608.

Ahlström, A., Raupach, M. R., Schurgers, G., Smith, B., Arneth, A., Jung, M., Reichstein, M., Canadell, J. G., Friedlingstein, P., Jain, A. K., Kato, E., Poulter, B., Sitch, S., Stocker, B. D., Viovy, N., Wang, Y. P., Wiltshire, A., Zaehle, S., and Zeng, N. (2015). The dominant role of semi-arid ecosystems in the trend and variability of the land co2 sink. *Science*, 348(6237):895–899.

Amthor, J. S. (1995). Terrestrial higher-plant response to increasing atmospheric [co2] in relation to the global carbon cycle. *Global Change Biology*, 1(4):243–274.

Amthor, J. S. (2000). The mccree–de wit–penning de vries–thornley respiration paradigms: 30 years later. *Annals of Botany*, 86(1):1–20.

Anderegg, W. R. and Anderegg, L. D. (2013). Hydraulic and carbohydrate changes in experimental drought-induced mortality of saplings in two conifer species. *Tree Physiology*, 33(3):252–260.

Anderegg, W. R. L., Plavcová, L., Anderegg, L. D. L., Hacke, U. G., Berry, J. A., and Field, C. B. (2013). Drought's legacy: multiyear hydraulic deterioration underlies widespread aspen forest die-off and portends increased future risk. *Global Change Biology*, 19(4):1188–1196.

Anderegg, W. R. L., Schwalm, C., Biondi, F., Camarero, J. J., Koch, G., Litvak, M., Ogle, K., Shaw, J. D., Shevliakova, E., Williams, A. P., Wolf, A., Ziaco, E., and Pacala, S. (2015). Pervasive drought legacies in forest ecosystems and their implications for carbon cycle models. *Science*, 349(6247):528–532.

Anderegg, W. R. L., Trugman, A. T., Badgley, G., Konings, A. G., and Shaw, J. (2020). Divergent forest sensitivity to repeated extreme droughts. *Nature Climate Change*, 10(12):1091–1095.

Araújo, T. M., Higuchi, N., and Andrade de Carvalho Júnior, J. a. (1999). Comparison of formulae for biomass content determination in a tropical rain forest site in the state of pará, brazil. *Forest Ecology and Management*, 117(1):43 – 52.

Arora, V. K., Boer, G. J., Friedlingstein, P., Eby, M., Jones, C. D., Christian, J. R., Bonan, G., Bopp, L., Brovkin, V., Cadule, P., Hajima, T., Ilyina, T., Lindsay, K., Tjiputra, J. F., and Wu, T. (2013). Carbon–concentration and carbon–climate feedbacks in cmip5 earth system models. *Journal of Climate*, 26(15):5289–5314.

Asaadi, A., Arora, V. K., Melton, J. R., and Bartlett, P. (2018). An improved parameterization of leaf area index (lai) seasonality in the canadian land surface scheme (class) and canadian terrestrial ecosystem model (ctem) modelling framework. *Biogeosciences*, 15(22):6885–6907.

Atkin, O. K., Scheurwater, I., and Pons, T. L. (2006). High thermal acclimation potential of both photosynthesis and respiration in two lowland plantago species in contrast to an alpine congeneric. *Global Change Biology*, 12(3):500–515.

Atkin, O. K., Scheurwater, I., and Pons, T. L. (2007). Respiration as a percentage of daily photosynthesis in whole plants is homeostatic at moderate, but not high, growth temperatures. *New Phytologist*, 174(2):367–380.

Atkin, O. K. and Tjoelker, M. G. (2003). Thermal acclimation and the dynamic response of plant respiration to temperature. *Trends in Plant Science*, 8(7):343–351.

Avitabile, V., Herold, M., Heuvelink, G. B. M., Lewis, S. L., Phillips, O. L., Asner, G. P., Armston, J., Ashton, P. S., Banin, L., Bayol, N., Berry, N. J., Boeckx, P., de Jong, B. H. J., DeVries, B., Girardin, C. A. J., Kearsley, E., Lindsell, J. A., Lopez-Gonzalez, G., Lucas, R., Malhi, Y., Morel, A., Mitchard, E. T. A., Nagy, L., Qie, L., Quinones, M. J., Ryan, C. M., Ferry, S. J. W., Sunderland, T., Laurin, G. V., Gatti, R. C., Valentini, R., Verbeeck, H., Wijaya, A., and Willcock, S. (2016). An integrated pan-tropical biomass map using multiple reference datasets. *Global Change Biology*, 22(4):1406–1420.

Babst, F., Bodesheim, P., Charney, N., Friend, A. D., Girardin, M. P., Klesse, S., Moore, D. J., Seftigen, K., Björklund, J., Bouriaud, O., Dawson, A., DeRose, R. J., Dietze, M. C., Eckes, A. H., Enquist, B., Frank, D. C., Mahecha, M. D., Poulter, B., Record, S., Trouet, V., Turton, R. H., Zhang, Z., and Evans, M. E. (2018). When tree rings go global: Challenges and opportunities for retro- and prospective insight. *Quaternary Science Reviews*, 197:1–20.

Babst, F., Bouriaud, O., Poulter, B., Trouet, V., P. Girardin, M., and C. Frank, D. (2019). Twentieth century redistribution in climatic drivers of global tree growth. *Science Advances*, 5(1):eaat4313.

Baker, I. T., Prihodko, L., Denning, A. S., Goulden, M., Miller, S., and da Rocha, H. R. (2008). Seasonal drought stress in the amazon: Reconciling models and observations. *Journal of Geophysical Research: Biogeosciences*, 113(G1).

Baker, T. R., Phillips, O. L., Malhi, Y., Almeida, S., Arroyo, L., Di Fiore, A., Erwin, T., Killeen, T. J., Laurance, S. G., Laurance, W. F., Lewis, S. L., Lloyd, J., Monteagudo, A., Neill, D. A., Patiño, S., Pitman, N. C. A., M. Silva, J. N., and Vásquez Martínez, R. (2004). Variation in wood density determines spatial patterns inamazonian forest biomass. *Global Change Biology*, 10(5):545–562.

Balducci, L., Deslauriers, A., Giovannelli, A., Rossi, S., and Rathgeber, C. B. (2013). Effects of temperature and water deficit on cambial activity and woody ring features in Picea mariana saplings. *Tree Physiology*, 33(10):1006–1017.

Bastos, A., Friedlingstein, P., Sitch, S., Chen, C., Mialon, A., Wigneron, J.-P., Arora, V. K., Briggs, P. R., Canadell, J. G., Ciais, P., Chevallier, F., Cheng, L., Delire, C., Haverd, V., Jain, A. K., Joos, F., Kato, E., Lienert, S., Lombardozzi, D., Melton, J. R., Myneni, R., Nabel, J. E. M. S., Pongratz, J., Poulter, B., Rödenbeck, C., Séférian, R., Tian, H., van Eck, C., Viovy, N., Vuichard, N., Walker, A. P., Wiltshire, A., Yang, J., Zaehle, S., Zeng, N., and Zhu, D. (2018).

Impact of the 2015/2016 el niño on the terrestrial carbon cycle constrained by bottom-up and top-down approaches. *Philosophical Transactions of the Royal Society B: Biological Sciences*, 373(1760):20170304.

Bastos, A., O'Sullivan, M., Ciais, P., Makowski, D., Sitch, S., Friedlingstein, P., Chevallier, F., Rödenbeck, C., Pongratz, J., Luijkx, I. T., Patra, P. K., Peylin, P., Canadell, J. G., Lauerwald, R., Li, W., Smith, N. E., Peters, W., Goll, D. S., Jain, A., Kato, E., Lienert, S., Lombardozzi, D. L., Haverd, V., Nabel, J. E. M. S., Poulter, B., Tian, H., Walker, A. P., and Zaehle, S. (2020). Sources of uncertainty in regional and global terrestrial co2 exchange estimates. *Global Biogeochemical Cycles*, 34(2):e2019GB006393. e2019GB006393 10.1029/2019GB006393.

Berry, J. and Bjorkman, O. (1980). Photosynthetic response and adaptation to temperature in higher plants. *Annual Review of Plant Physiology*, 31(1):491–543.

Best, M. J., Pryor, M., Clark, D. B., Rooney, G. G., Essery, R. L. H., Ménard, C. B., Edwards, J. M., Hendry, M. A., Porson, A., Gedney, N., Mercado, L. M., Sitch, S., Blyth, E., Boucher, O., Cox, P. M., Grimmond, C. S. B., and Harding, R. J. (2011). The joint uk land environment simulator (jules), model description - part 1: Energy and water fluxes. *Geoscientific Model Development*, 4(3):677–699.

Boyer, J. S. (1970). Leaf enlargement and metabolic rates in corn, soybean, and sunflower at various leaf water potentials. *Plant Physiology*, 46(2):233–235.

Brienen, R. J. W., Phillips, O. L., Feldpausch, T. R., Gloor, E., Baker, T. R., Lloyd, J., Lopez-Gonzalez, G., Monteagudo-Mendoza, A., Malhi, Y., Lewis, S. L., Vásquez Martinez, R., Alexiades, M., Álvarez Dávila, E., Alvarez-Loayza, P., Andrade, A., Aragão, L. E. O. C., Araujo-Murakami, A., Arets, E. J. M. M., Arroyo, L., Aymard C., G. A., Bánki, O. S., Baraloto, C., Barroso, J., Bonal, D., Boot, R. G. A., Camargo, J. L. C., Castilho, C. V., Chama, V., Chao, K. J., Chave, J., Comiskey, J. A., Cornejo Valverde, F., da Costa, L., de Oliveira, E. A., Di Fiore, A., Erwin, T. L., Fauset, S., Forsthofer, M., Galbraith, D. R., Grahame, E. S., Groot, N., Hérault, B., Higuchi, N., Honorio Coronado, E. N., Keeling, H., Killeen, T. J., Laurance, W. F., Laurance, S., Licona, J., Magnussen, W. E., Marimon, B. S., Marimon-Junior, B. H., Mendoza, C., Neill, D. A., Nogueira, E. M., Núñez, P., Pallqui Camacho, N. C., Parada, A., Pardo-Molina, G., Peacock, J., Peña-Claros, M., Pickavance, G. C., Pitman, N. C. A., Poorter, L., Prieto, A., Quesada, C. A., Ramírez, F., Ramírez-Angulo, H., Restrepo, Z., Roopsind, A., Rudas, A., Salomão, R. P., Schwarz, M., Silva, N., Silva-Espejo, J. E., Silveira, M., Stropp, J., Talbot, J., ter Steege, H., Teran-Aguilar, J., Terborgh, J., Thomas-Caesar, R., Toledo, M., Torello-Raventos, M., Umetsu, R. K., van der Heijden, G. M. F., van der Hout, P., Guimarães Vieira, I. C., Vieira, S. A., Vilanova, E.,

Vos, V. A., and Zagt, R. J. (2015). Long-term decline of the amazon carbon sink. *Nature*, 519(7543):344–348.

Brown, S. (1997). Estimating biomass and biomass change of tropical forests: A primer. *FAO Forestry Paper*, 134.

Cannell, M. G. R. and Thornley, J. H. M. (2000). Modelling the components of plant respiration: Some guiding principles. *Annals of Botany*, 85(1):45–54.

Cao, M. and Woodward, F. I. (1998). Dynamic responses of terrestrial ecosystem carbon cycling to global climate change. *Nature*, 393(6682):249–252.

Carvalhais, N., Forkel, M., Khomik, M., Bellarby, J., Jung, M., Migliavacca, M., Mu, M., Saatchi, S., Santoro, M., Thurner, M., Weber, U., Ahrens, B., Beer, C., Cescatti, A., Randerson, J. T., and Reichstein, M. (2014). Global covariation of carbon turnover times with climate in terrestrial ecosystems. *Nature*, 514:213–217.

Carvalho Jr., J. A., Higuchi, N., Araújo, T. M., and Santos, J. C. (1998). Combustion completeness in a rainforest clearing experiment in manaus, brazil. *Journal of Geophysical Research: Atmospheres*, 103(D11):13195–13199.

Chambers, J. Q., dos Santos, J., J., R. R., and Higuchi, N. (2001). Tree damage, allometric relationships, and above-ground net primary production in central amazon forest. *Forest Ecology and Management*, 152(1):73 – 84.

Chambers, J. Q., Tribuzy, E. S., Toledo, L. C., Crispim, B. F., Higuchi, N., Santos, J. d., Araújo, A. C., Kruijt, B., Nobre, A. D., and Trumbore, S. E. (2004). Respiration from a tropical forest ecosystem: partitioning of sources and low carbon use efficiency. *Ecological Applications*, 14(sp4):72–88.

Chave, J., Andalo, C., Brown, S., Cairns, M. A., Chambers, J. Q., Eamus, D., Fölster, H., Fromard, F., Higuchi, N., Kira, T., Lescure, J. P., Nelson, B. W., Ogawa, H., Puig, H., Riéra, B., and Yamakura, T. (2005). Tree allometry and improved estimation of carbon stocks and balance in tropical forests. *Oecologia*, 145(1):87–99.

Chave, J., Réjou-Méchain, M., Búrquez, A., Chidumayo, E., Colgan, M. S., Delitti, W. B., Duque, A., Eid, T., Fearnside, P. M., Goodman, R. C., Henry, M., Martínez-Yrízar, A., Mugasha, W. A., Muller-Landau, H. C., Mencuccini, M., Nelson, B. W., Ngomanda, A., Nogueira, E. M., Ortiz-Malavassi, E., Pélissier, R., Ploton, P., Ryan, C. M., Saldarriaga, J. G., and Vieilledent, G. (2014). Improved allometric models to estimate the aboveground biomass of tropical trees. *Global Change Biology*, 20(10):3177–3190.

Chaves, M. M., Pereira, J. S., Maroco, J., Rodrigues, M. L., Ricardo, C. P. P., Osório, M. L., Carvalho, I., Faria, T., and Pinheiro, C. (2002). How plants cope with water stress in the field? photosynthesis and growth. *Annals of Botany*, 89(7):907–916.

Clark, D. B., Mercado, L. M., Sitch, S., Jones, C. D., Gedney, N., Best, M. J., Pryor, M., Rooney, G. G., Essery, R. L. H., Blyth, E., Boucher, O., Harding, R. J., Huntingford, C., and Cox, P. M. (2011). The joint uk land environment simulator (jules), model description - part 2: Carbon fluxes and vegetation dynamics. *Geoscientific Model Development*, 4(3):701–722.

Collalti, A. and Prentice, I. C. (2019). Is npp proportional to gpp? waring's hypothesis 20 years on. *Tree Physiology*, 39(8):1473–1483.

Collalti, A., Tjoelker, M. G., Hoch, G., Mäkelä, A., Guidolotti, G., Heskel, M., Petit, G., Ryan, M. G., Battipaglia, G., Matteucci, G., and Prentice, I. C. (2020). Plant respiration: Controlled by photosynthesis or biomass? *Global Change Biology*, 26(3):1739–1753.

Cosgrove, D. J. (2014). *Plant Cell Growth and Elongation*. American Cancer Society.

Cox, P., Betts, R. A., Jones, C., Spall, S. A., and Totterdell, I. J. (2000). Acceleration of global warming due to carbon-cycle feedbacks in a coupled model. *Nature*, 408.

Cox, P. M., Betts, R. A., Collins, M., Harris, P. P., Huntingford, C., and Jones, C. D. (2004). Amazonian forest dieback under climate-carbon cycle projections for the 21st century. *Theoretical and Applied Climatology*, 78(1):137–156.

Cox, P. M., Pearson, D., Booth, B. B., Friedlingstein, P., Huntingford, C., Jones, C. D., and Luke, C. M. (2013). Sensitivity of tropical carbon to climate change constrained by carbon dioxide variability. *Nature*, 494.

da Costa, A. C. L., Galbraith, D., Almeida, S., Portela, B. T. T., da Costa, M., de Athaydes Silva Junior, J., Braga, A. P., de Gonçalves, P. H. L., de Oliveira, A. A., Fisher, R., Phillips, O. L., Metcalfe, D. B., Levy, P., and Meir, P. (2010). Effect of 7 yr of experimental drought on vegetation dynamics and biomass storage of an eastern amazonian rainforest. *New Phytologist*, 187(3):579–591.

da Costa, A. C. L., Metcalfe, D. B., Doughty, C. E., de Oliveira, A. A., Neto, G. F., da Costa, M. C., Silva Junior, J. d. A., Aragão, L. E., Almeida, S., Galbraith, D. R., Rowland, L. M., Meir, P., and Malhi, Y. (2014). Ecosystem respiration and net primary productivity after 8–10 years of experimental through-fall reduction in an eastern amazon forest. *Plant Ecology & Diversity*, 7(1-2):7–24.

da Costa, A. C. L., Rowland, L., Oliveira, R. S., Oliveira, A. A. R., Binks, O. J., Salmon, Y., Vasconcelos, S. S., Junior, J. A. S., Ferreira, L. V., Poyatos, R., Mencuccini, M., and Meir, P. (2018). Stand dynamics modulate water cycling and mortality risk in droughted tropical forest. *Global Change Biology*, 24(1):249–258.

Davidson, E. A., de Araújo, A. C., Artaxo, P., Balch, J. K., Brown, I. F., C. Bustamante, M. M., Coe, M. T., DeFries, R. S., Keller, M., Longo, M., Munger, J. W., Schroeder, W., Soares-Filho, B. S., Souza, C. M., and Wofsy, S. C. (2012). The amazon basin in transition. *Nature*, 481(7381):321–328.

DeLucia, E. H., Drake, J. E., Thomas, R. B., and Gonzalez-Meler, M. (2007). Forest carbon use efficiency: is respiration a constant fraction of gross primary production? *Global Change Biology*, 13(6):1157–1167.

Dewar, R. C. (1993). A root-shoot partitioning model based on carbon-nitrogen-water interactions and munch phloem flow. *Functional Ecology*, 7(3):356–368.

Dewar, R. C., Medlyn, B. E., and McMurtrie, R. E. (1998). A mechanistic analysis of light and carbon use efficiencies. *Plant, Cell & Environment*, 21(6):573–588.

Dewar, R. C., Medlyn, B. E., and Mcmurtrie, R. E. (1999). Acclimation of the respiration/photosynthesis ratio to temperature: insights from a model. *Global Change Biology*, 5(5):615–622.

Dietze, M. C., Sala, A., Carbone, M. S., Czimczik, C. I., Mantooth, J. A., Richardson, A. D., and Vargas, R. (2014). Nonstructural carbon in woody plants. *Annual Review of Plant Biology*, 65(1):667–687. PMID: 24274032.

Doughty, C. E., Malhi, Y., Araujo-Murakami, A., Metcalfe, D. B., Silva-Espejo, J. E., Arroyo, L., Heredia, J. P., Pardo-Toledo, E., Mendizabal, L. M., Rojas-Landivar, V. D., Vega-Martinez, M., Flores-Valencia, M., Sibler-Rivero, R., Moreno-Vare, L., Viscarra, L. J., Chuviru-Castro, T., Osinaga-Becerra, M., and Ledezma, R. (2014). Allocation trade-offs dominate the response of tropical forest growth to seasonal and interannual drought. *Ecology*, 95(8):2192–2201.

Doughty, C. E., Metcalfe, D. B., Girardin, C. A. J., Amezquita, F. F., Durand, L., Huaraca Huasco, W., Silva-Espejo, J. E., Araujo-Murakami, A., da Costa, M. C., da Costa, A. C. L., Rocha, W., Meir, P., Galbraith, D., and Malhi, Y. (2015a). Source and sink carbon dynamics and carbon allocation in the amazon basin. *Global Biogeochemical Cycles*, 29(5):645–655.

Doughty, C. E., Metcalfe, D. B., Girardin, C. A. J., Amézquita, F. F., Cabrera, D. G., Huasco, W. H., Silva-Espejo, J. E., Araujo-Murakami, A., da Costa, M. C., Rocha, W., Feldpausch, T. R., Mendoza, A. L. M., da Costa, A. C. L., Meir, P.,

Phillips, O. L., and Malhi, Y. (2015b). Drought impact on forest carbon dynamics and fluxes in amazonia. *Nature*, 519:78–82.

Eller, C. B., Rowland, L., Mencuccini, M., Rosas, T., Williams, K., Harper, A., Medlyn, B. E., Wagner, Y., Klein, T., Teodoro, G. S., Oliveira, R. S., Matos, I. S., Rosado, B. H. P., Fuchs, K., Wohlfahrt, G., Montagnani, L., Meir, P., Sitch, S., and Cox, P. M. (2020). Stomatal optimization based on xylem hydraulics (sox) improves land surface model simulation of vegetation responses to climate. *New Phytologist*, 226(6):1622–1637.

Eller, C. B., Rowland, L., Oliveira, R. S., Bittencourt, P. R. L., Barros, F. V., da Costa, A. C. L., Meir, P., Friend, A. D., Mencuccini, M., Sitch, S., and Cox, P. (2018). Modelling tropical forest responses to drought and el niño with a stomatal optimization model based on xylem hydraulics. *Philosophical Transactions of the Royal Society B: Biological Sciences*, 373(1760):20170315.

Elliott, S., Baker, P. J., and Borchert, R. (2006). Leaf flushing during the dry season: the paradox of asian monsoon forests. *Global Ecology and Biogeography*, 15(3):248–257.

Ellsworth, D., Anderson, I., Crous, K., Cooke, J., Drake, J., Gherlenda, A., Gimeno, T., Macdonald, C., Medlyn, B., Powell, J., Tjoelker, M., and Reich, P. (2017). Elevated co2 does not increase eucalypt forest productivity on a low-phosphorus soil. *Nature Climate Change*, 7(4):279–282.

Fatichi, S., Leuzinger, S., and Körner, C. (2014). Moving beyond photosynthesis: from carbon source to sink-driven vegetation modeling. *New Phytologist*, 201(4):1086–1095.

Fatichi, S., Pappas, C., Zscheischler, J., and Leuzinger, S. (2019). Modelling carbon sources and sinks in terrestrial vegetation. *New Phytologist*, 221(2):652–668.

Fisher, R. A., Williams, M., Da Costa, A. L., Malhi, Y., Da Costa, R. F., Almeida, S., and Meir, P. (2007). The response of an eastern amazonian rain forest to drought stress: results and modelling analyses from a throughfall exclusion experiment. *Global Change Biology*, 13(11):2361–2378.

Foley, J. A., Prentice, I. C., Ramankutty, N., Levis, S., Pollard, D., Sitch, S., and Haxeltine, A. (1996). An integrated biosphere model of land surface processes, terrestrial carbon balance, and vegetation dynamics. *Global Biogeochemical Cycles*, 10(4):603–628.

Frankenberg, C., Fisher, J. B., Worden, J., Badgley, G., Saatchi, S. S., Lee, J.-E., Toon, G. C., Butz, A., Jung, M., Kuze, A., and Yokota, T. (2011). New

global observations of the terrestrial carbon cycle from gosat: Patterns of plant fluorescence with gross primary productivity. *Geophysical Research Letters*, 38(17).

Fricke, W. (2017). *Turgor Pressure*, pages 1–6. American Cancer Society.

Friedlingstein, P., Bopp, L., Philippe, C., Jean-Louis, D., Laurent, F., Hervé, L., Patrick, M., and James, O. (2001). Positive feedback between future climate change and the carbon cycle. *Geophysical Research Letters*, 28(8):1543–1546.

Friedlingstein, P., Fung, I., Holland, E., John, J., Brasseur, G., Erickson, D., and Schimel, D. (1995). On the contribution of co2 fertilization to the missing biospheric sink. *Global Biogeochemical Cycles*, 9(4):541–556.

Friedlingstein, P., Jones, M. W., O'Sullivan, M., Andrew, R. M., Hauck, J., Peters, G. P., Peters, W., Pongratz, J., Sitch, S., Le Quéré, C., Bakker, D. C. E., Canadell, J. G., Ciais, P., Jackson, R. B., Anthoni, P., Barbero, L., Bastos, A., Bastrikov, V., Becker, M., Bopp, L., Buitenhuis, E., Chandra, N., Chevallier, F., Chini, L. P., Currie, K. I., Feely, R. A., Gehlen, M., Gilfillan, D., Gkritzalis, T., Goll, D. S., Gruber, N., Gutekunst, S., Harris, I., Haverd, V., Houghton, R. A., Hurtt, G., Ilyina, T., Jain, A. K., Joetzjer, E., Kaplan, J. O., Kato, E., Klein Goldewijk, K., Korsbakken, J. I., Landschützer, P., Lauvset, S. K., Lefèvre, N., Lenton, A., Lienert, S., Lombardozzi, D., Marland, G., McGuire, P. C., Melton, J. R., Metzl, N., Munro, D. R., Nabel, J. E. M. S., Nakaoka, S.-I., Neill, C., Omar, A. M., Ono, T., Peregon, A., Pierrot, D., Poulter, B., Rehder, G., Resplandy, L., Robertson, E., Rödenbeck, C., Séférian, R., Schwinger, J., Smith, N., Tans, P. P., Tian, H., Tilbrook, B., Tubiello, F. N., van der Werf, G. R., Wiltshire, A. J., and Zaehle, S. (2019). Global carbon budget 2019. *Earth System Science Data*, 11(4):1783–1838.

Friend, A. D., Eckes-Shephard, A. H., Fonti, P., Rademacher, T. T., Rathgeber, C. B. K., Richardson, A. D., and Turton, R. H. (2019). On the need to consider wood formation processes in global vegetation models and a suggested approach. *Annals of Forest Science*, 76(2):49.

Friend, A. D., Lucht, W., Rademacher, T. T., Keribin, R., Betts, R., Cadule, P., Ciais, P., Clark, D. B., Dankers, R., Falloon, P. D., Ito, A., Kahana, R., Kleidon, A., Lomas, M. R., Nishina, K., Ostberg, S., Pavlick, R., Peylin, P., Schaphoff, S., Vuichard, N., Warszawski, L., Wiltshire, A., and Woodward, F. I. (2014). Carbon residence time dominates uncertainty in terrestrial vegetation responses to future climate and atmospheric co2. *Proceedings of the National Academy of Sciences*, 111(9):3280–3285.

Fritts, H. C., Shashkin, A. V., Hemming, D. L., Leavitt, S. W., Wright, W. E., and Downs, G. M. (2000). Preliminary draft user manual for treering 2000.

Furze, M. E., Huggett, B. A., Aubrecht, D. M., Stolz, C. D., Carbone, M. S., and Richardson, A. D. (2019). Whole-tree nonstructural carbohydrate storage and seasonal dynamics in five temperate species. *New Phytologist*, 221(3):1466–1477.

Galiano, L., Martínez-Vilalta, J., and Lloret, F. (2011). Carbon reserves and canopy defoliation determine the recovery of scots pine 4 yr after a drought episode. *New Phytologist*, 190(3):750–759.

Gatti, L. V., Gloor, M., Miller, J. B., Doughty, C. E., Mahli, Y., Domingues, L. G., Basso, L. S., Martinewski, A., Correia, C. S. C., Borges, V. F., Freitas, S., Braz, R., Anderson, L. O., Rocha, H., Grace, J., Phillips, O. L., and Lloyd, J. (2014). Drought sensitivity of amazonian carbon balance revealed by atmospheric measurements. *Nature*, 506(76).

Gifford, R. M. (1995). Whole plant respiration and photosynthesis of wheat under increased co2 concentration and temperature: long-term vs. short-term distinctions for modelling. *Global Change Biology*, 1(6):385–396.

Gifford, R. M. (2003). Plant respiration in productivity models: conceptualisation, representation and issues for global terrestrial carbon-cycle research. *Functional Plant Biology*, 30(2):171–186.

Girardin, C. A. J., Malhi, Y., Doughty, C. E., Metcalfe, D. B., Meir, P., del Aguila-Pasquel, J., Araujo-Murakami, A., da Costa, A. C. L., Silva-Espejo, J. E., Farfán Amézquita, F., and Rowland, L. (2016). Seasonal trends of amazonian rainforest phenology, net primary productivity, and carbon allocation. *Global Biogeochemical Cycles*, 30(5):700–715.

Gloor, E., Wilson, C., Chipperfield, M. P., Chevallier, F., Buermann, W., Boesch, H., Parker, R., Somkuti, P., Gatti, L. V., Correia, C., Domingues, L. G., Peters, W., Miller, J., Deeter, M. N., and Sullivan, M. J. P. (2018). Tropical land carbon cycle responses to 2015/16 el niño as recorded by atmospheric greenhouse gas and remote sensing data. *Philosophical Transactions of the Royal Society B: Biological Sciences*, 373(1760):20170302.

Goličnik, M. (2012). On the lambert w function and its utility in biochemical kinetics. *Biochemical Engineering Journal*, 63:116–123.

Guillemot, J., Francois, C., Hmimina, G., Dufrêne, E., Martin-StPaul, N. K., Soudani, K., Marie, G., Ourcival, J.-M., and Delpierre, N. (2017). Environ-

mental control of carbon allocation matters for modelling forest growth. *New Phytologist*, 214(1):180–193.

Hansen, L. D., Church, J., Matheson, S., McCarlie, V., Thygerson, T., Criddle, R. S., and Smith, B. N. (2002). Kinetics of plant growth and metabolism. *Thermochimica Acta*, 388(1):415–425.

Harper, A. B., Cox, P. M., Friedlingstein, P., Wiltshire, A. J., Jones, C. D., Sitch, S., Mercado, L. M., Groenendijk, M., Robertson, E., Kattge, J., Bönisch, G., Atkin, O. K., Bahn, M., Cornelissen, J., Niinemets, U., Onipchenko, V., Peñuelas, J., Poorter, L., Reich, P. B., Soudzilovskaia, N. A., and Bodegom, P. V. (2016). Improved representation of plant functional types and physiology in the joint uk land environment simulator (jules v4.2) using plant trait information. *Geoscientific Model Development*, 9(7):2415–2440.

Harris, I. C. (2019). Cru jra v1.1: A forcings dataset of gridded land surface blend of climatic research unit (cru) and japanese reanalysis (jra) data; jan.1901 - dec.2017.

Hartmann, D., Klein Tank, A., Rusticucci, M., Alexander, L., Broönnimann, S., Charabi, Y., Dentener, F., Dlugokencky, E., Easterling, D., Kaplan, A., Soden, B., Thorne, P., Wild, M., and Zhai, P. (2013). *Observations: Atmosphere and Surface*, book section 2, page 159–254. Cambridge University Press, Cambridge, United Kingdom and New York, NY, USA.

Hartmann, H., Adams, H. D., Hammond, W. M., Hoch, G., Landhäusser, S. M., Wiley, E., and Zaehle, S. (2018). Identifying differences in carbohydrate dynamics of seedlings and mature trees to improve carbon allocation in models for trees and forests. *Environmental and Experimental Botany*, 152:7–18. Experiments with trees: from seedlings to ecosystems.

Hartmann, H., Bahn, M., Carbone, M., and Richardson, A. D. (2020). Plant carbon allocation in a changing world – challenges and progress: introduction to a virtual issue on carbon allocation. *New Phytologist*, 227(4):981–988.

Hartmann, H. and Trumbore, S. (2016). Understanding the roles of nonstructural carbohydrates in forest trees – from what we can measure to what we want to know. *New Phytologist*, 211(2):386–403. 2016-21190.

Haverd, V., Smith, B., Nieradzik, L., Briggs, P. R., Woodgate, W., Trudinger, C. M., Canadell, J. G., and Cuntz, M. (2018). A new version of the cable land surface model (subversion revision r4601) incorporating land use and land cover change, woody vegetation demography, and a novel optimisation-based approach to plant coordination of photosynthesis. *Geoscientific Model Development*, 11(7):2995–3026.

Hemming, D., Fritts, H., Leavitt, S., Wright, W., Long, A., and Shashkin, A. (2001). Modelling tree-ring δ13c. *Dendrochronologia*, 19:23–38.

Hewitt, A. J., Booth, B. B. B., Jones, C. D., Robertson, E. S., Wiltshire, A. J., Sansom, P. G., Stephenson, D. B., and Yip, S. (2016). Sources of uncertainty in future projections of the carbon cycle. *Journal of Climate*, 29(20):7203–7213.

Hoch, G., Richter, A., and Körner, C. (2003). Non-structural carbon compounds in temperate forest trees. *Plant, Cell & Environment*, 26(7):1067–1081.

Hsiao, T. C. (1973). Plant responses to water stress. *Annual Review of Plant Physiology*, 24(1):519–570.

Huntingford, C., Atkin, O. K., Martinez-de la Torre, A., Mercado, L. M., Heskel, M. A., Harper, A. B., Bloomfield, K. J., O'Sullivan, O. S., Reich, P. B., Wythers, K. R., Butler, E. E., Chen, M., Griffin, K. L., Meir, P., Tjoelker, M. G., Turnbull, M. H., Sitch, S., Wiltshire, A., and Malhi, Y. (2017). Implications of improved representations of plant respiration in a changing climate. *Nature Communications*, 8(1):1602.

Huntingford, C., Harris, P. P., Gedney, N., Cox, P. M., Betts, R. A., Marengo, J. A., and Gash, J. H. C. (2004). Using a gcm analogue model to investigate the potential for amazonian forest dieback. *Theoretical and Applied Climatology*, 78(1):177–185.

Huntingford, C., Lowe, J. A., Booth, B. B. B., Jones, C. D., Harris, G. R., Gohar, L. K., and Meir, P. (2009). Contributions of carbon cycle uncertainty to future climate projection spread. *Tellus B*, 61(2):355–360.

Hölttä, T., Mäkinen, H., Nöjd, P., Mäkelä, A., and Nikinmaa, E. (2010). A physiological model of softwood cambial growth. *Tree Physiology*, 30(10):1235–1252.

IPCC (2013). *Summary for Policymakers*, book section SPM, page 1–30. Cambridge University Press, Cambridge, United Kingdom and New York, NY, USA.

Jones, S., Rowland, L., Cox, P., Hemming, D., Wiltshire, A., Williams, K., Parazoo, N. C., Liu, J., da Costa, A. C. L., Meir, P., Mencuccini, M., and Harper, A. B. (2020). The impact of a simple representation of non-structural carbohydrates on the simulated response of tropical forests to drought. *Biogeosciences*, 17(13):3589–3612.

Kikuzawa, K. (1995). Leaf phenology as an optimal strategy for carbon gain in plants. *Canadian Journal of Botany*, 73(2):158–163.

Killingbeck, K. T. (1996). Nutrients in senesced leaves: Keys to the search for potential resorption and resorption proficiency. *Ecology*, 77(6):1716–1727.

Kimball, B. A., Mauney, J. R., Nakayama, F. S., and Idso, S. B. (1993). Effects of increasing atmospheric co2 on vegetation. *Vegetatio*, 104(1):65–75.

Kirschbaum, M. U. (2010). Does enhanced photosynthesis enhance growth? lessons learned from co2 enrichment studies. *Plant Physiology*, 155(1):117–124.

Kobayashi, S., Ota, Y., Harada, Y., Ebita, A., Moriya, M., Onoda, H., Onogi, K., Kamahori, H., Kobayashi, C., Endo, H., Miyaoka, K., and Takahashi, K. (2015). The jra-55 reanalysis: General specifications and basic characteristics. *Journal of the Meteorological Society of Japan. Ser. II*, 93(1):5–48.

Kobe, R. K., Iyer, M., and Walters, M. B. (2010). Optimal partitioning theory revisited: Nonstructural carbohydrates dominate root mass responses to nitrogen. *Ecology*, 91(1):166–179.

Körner, C. (2003). Carbon limitation in trees. *Journal of Ecology*, 91(1):4–17.

Krinner, G., Viovy, N., de Noblet-Ducoudré, N., Ogée, J., Polcher, J., Friedlingstein, P., Ciais, P., Sitch, S., and Prentice, I. C. (2005). A dynamic global vegetation model for studies of the coupled atmosphere-biosphere system. *Global Biogeochemical Cycles*, 19(1).

Kucharik, C. J., Foley, J. A., Delire, C., Fisher, V. A., Coe, M. T., Lenters, J. D., Young-Molling, C., Ramankutty, N., Norman, J. M., and Gower, S. T. (2000). Testing the performance of a dynamic global ecosystem model: Water balance, carbon balance, and vegetation structure. *Global Biogeochemical Cycles*, 14(3):795–825.

Körner, C. (2006). Plant co2 responses: an issue of definition, time and resource supply. *New Phytologist*, 172(3):393–411.

Körner, C. (2015). Paradigm shift in plant growth control. *Current Opinion in Plant Biology*, 25:107–114.

Landhäusser, S. M., Chow, P. S., Dickman, L. T., Furze, M. E., Kuhlman, I., Schmid, S., Wiesenbauer, J., Wild, B., Gleixner, G., Hartmann, H., Hoch, G., McDowell, N. G., Richardson, A. D., Richter, A., and Adams, H. D. (2018). Standardized protocols and procedures can precisely and accurately quantify non-structural carbohydrates. *Tree Physiology*, 38(12):1764–1778.

Lavell, A., Oppenheimer, M., Diop, C., Hess, J., Lempert, R., Li, J., Muir-Wood, R., and Myeong, S. (2012). *2012: Climate change: new dimensions in disaster risk, exposure, vulnerability, and resilience. In: Managing the Risks of Extreme Events and Disasters to Advance Climate Change Adaptation [Field, C.B., V.*

Barros, T.F. Stocker, D. Qin, D.J. Dokken, K.L. Ebi, M.D. Mastrandrea, K.J. Mach, G.-K. Plattner, S.K. Allen, M. Tignor, and P.M. Midgley (eds.)]. A Special Report of Working Groups I and II of the Intergovernmental Panel on Climate Change (IPCC). Cambridge University Press, Cambridge, UK, and New York, NY, USA.

Lawrence, D., Fisher, R., Koven, C., Oleson, K., Swenson, S., Vertenstein, M., Andre, B., Bonan, G., Ghimire, B., Kennedy, D., Kluzek, E., Knox, R., Lawrence, P., Li, F., Li, H., Lombardozzi, D., Lu, Y., Peket, J., Riley, W., and Xu, C. (2018). Clm5.0 technical description. Technical report.

Le Quéré, C., Moriarty, R., Andrew, R. M., Canadell, J. G., Sitch, S., Korsbakken, J. I., Friedlingstein, P., Peters, G. P., Andres, R. J., Boden, T. A., Houghton, R. A., House, J. I., Keeling, R. F., Tans, P., Arneth, A., Bakker, D. C. E., Barbero, L., Bopp, L., Chang, J., Chevallier, F., Chini, L. P., Ciais, P., Fader, M., Feely, R. A., Gkritzalis, T., Harris, I., Hauck, J., Ilyina, T., Jain, A. K., Kato, E., Kitidis, V., Klein Goldewijk, K., Koven, C., Landschützer, P., Lauvset, S. K., Lefèvre, N., Lenton, A., Lima, I. D., Metzl, N., Millero, F., Munro, D. R., Murata, A., Nabel, J. E. M. S., Nakaoka, S., Nojiri, Y., O'Brien, K., Olsen, A., Ono, T., Pérez, F. F., Pfeil, B., Pierrot, D., Poulter, B., Rehder, G., Rödenbeck, C., Saito, S., Schuster, U., Schwinger, J., Séférian, R., Steinhoff, T., Stocker, B. D., Sutton, A. J., Takahashi, T., Tilbrook, B., van der Laan-Luijkx, I. T., van der Werf, G. R., van Heuven, S., Vandemark, D., Viovy, N., Wiltshire, A., Zaehle, S., and Zeng, N. (2015). Global carbon budget 2015. *Earth System Science Data*, 7(2):349–396.

Lemoine, R., La Camera, S., Atanassova, R., Dédaldéchamp, F., Allario, T., Pourtau, N., Bonnemain, J.-L., Laloi, M., Coutos-Thévenot, P., Maurousset, L., Faucher, M., Girousse, C., Lemonnier, P., Parrilla, J., and Durand, M. (2013). Source-to-sink transport of sugar and regulation by environmental factors. *Frontiers in Plant Science*, 4:272.

Levis, S., Bonan, G. B., Vertenstein, M., and Oleson, K. (2004). The community land model's dynamic global vegetation model (clm-dgvm): Technical description and user's guide. Technical report, University Corporation for Atmospheric Research.

Liu, J., Bowman, K. W., Schimel, D. S., Parazoo, N. C., Jiang, Z., Lee, M., Bloom, A. A., Wunch, D., Frankenberg, C., Sun, Y., O'Dell, C. W., Gurney, K. R., Menemenlis, D., Gierach, M., Crisp, D., and Eldering, A. (2017). Contrasting carbon cycle responses of the tropical continents to the 2015–2016 el niño. *Science*, 358(6360).

Lombardozzi, D. L., Bonan, G. B., Smith, N. G., Dukes, J. S., and Fisher, R. A. (2015). Temperature acclimation of photosynthesis and respiration: A key uncertainty in the carbon cycle-climate feedback. *Geophysical Research Letters*, 42(20):8624–8631.

Lovenduski, N. S. and Bonan, G. B. (2017). Reducing uncertainty in projections of terrestrial carbon uptake. *Environmental Research Letters*, 12:4.

Luo, X., Keenan, T. F., Fisher, J. B., Jiménez-Muñoz, J.-C., Chen, J. M., Jiang, C., Ju, W., Perakalapudi, N.-V., Ryu, Y., and Tadić, J. M. (2018). The impact of the 2015/2016 el niño on global photosynthesis using satellite remote sensing. *Philosophical Transactions of the Royal Society B: Biological Sciences*, 373(1760):20170409.

Mahmud, K., Medlyn, B. E., Duursma, R. A., Campany, C., and De Kauwe, M. G. (2018). Inferring the effects of sink strength on plant carbon balance processes from experimental measurements. *Biogeosciences*, 15(13):4003–4018.

Marengo, J. A., Souza, C. M., Thonicke, K., Burton, C., Halladay, K., Betts, R. A., Alves, L. M., and Soares, W. R. (2018). Changes in climate and land use over the amazon region: Current and future variability and trends. *Frontiers in Earth Science*, 6:228.

Martínez-Vilalta, J., Poyatos, R., Aguadé, D., Retana, J., and Mencuccini, M. (2014). A new look at water transport regulation in plants. *New Phytologist*, 204(1):105–115.

Martínez-Vilalta, J., Sala, A., Asensio, D., Galiano, L., Hoch, G., Palacio, S., Piper, F. I., and Lloret, F. (2016). Dynamics of non-structural carbohydrates in terrestrial plants: a global synthesis. *Ecological Monographs*, 86(4):495–516.

McCree, K. J. (1970). An equation for the rate of respiration of white clover grown under controlled conditions. pages 221–9 pp. Wageningen, The Netherlands: Centre for Agricultural Publishing and Documentation.

McDowell, N., Pockman, W. T., Allen, C. D., Breshears, D. D., Cobb, N., Kolb, T., Plaut, J., Sperry, J., West, A., Williams, D. G., and Yepez, E. A. (2008). Mechanisms of plant survival and mortality during drought: why do some plants survive while others succumb to drought? *New Phytologist*, 178(4):719–739.

McDowell, N. G. (2011). Mechanisms linking drought, hydraulics, carbon metabolism, and vegetation mortality. *Plant Physiology*, 155(3):1051–1059.

Medvigy, D., Wofsy, S. C., Munger, J. W., Hollinger, D. Y., and Moorcroft, P. R. (2009). Mechanistic scaling of ecosystem function and dynamics in space and

time: Ecosystem demography model version 2. *Journal of Geophysical Research: Biogeosciences*, 114(G1).

Meir, P., Mencuccini, M., Binks, O., da Costa, A. L., Ferreira, L., and Rowland, L. (2018). Short-term effects of drought on tropical forest do not fully predict impacts of repeated or long-term drought: gas exchange versus growth. *Philosophical Transactions of the Royal Society B: Biological Sciences*, 373(1760):20170311.

Meir, P., Wood, T. E., Galbraith, D. R., Brando, P. M., Da Costa, A. C. L., Rowland, L., and Ferreira, L. V. (2015). Threshold responses to soil moisture deficit by trees and soil in tropical rain forests: Insights from field experiments. *BioScience*, 65(9):882–892.

Meiyappan, P., Jain, A. K., and House, J. I. (2015). Increased influence of nitrogen limitation on co2 emissions from future land use and land use change. *Global Biogeochemical Cycles*, 29(9):1524–1548.

Melton, J. R. and Arora, V. K. (2016). Competition between plant functional types in the canadian terrestrial ecosystem model (ctem v. 2.0. *Geoscientific Model Development*, 9(1):323–361.

Mencuccini, M., Manzoni, S., and Christoffersen, B. (2019). Modelling water fluxes in plants: from tissues to biosphere. *New Phytologist*, 222(3):1207–1222.

Mencuccini, M., Martínez-Vilalta, J., Vanderklein, D., Hamid, H. A., Korakaki, E., Lee, S., and Michiels, B. (2005). Size-mediated ageing reduces vigour in trees. *Ecology Letters*, 8(11):1183–1190.

Mencuccini, M., Salmon, Y., Mitchell, P., Hölttä, T., Choat, B., Meir, P., O'Grady, A., Tissue, D., Zweifel, R., Sevanto, S., and Pfautsch, S. (2017). An empirical method that separates irreversible stem radial growth from bark water content changes in trees: theory and case studies. *Plant, Cell & Environment*, 40(2):290–303.

Metcalfe, D. B., Meir, P., Aragão, L. E. O. C., Lobo-do Vale, R., Galbraith, D., Fisher, R. A., Chaves, M. M., Maroco, J. P., da Costa, A. C. L., de Almeida, S. S., Braga, A. P., Gonçalves, P. H. L., de Athaydes, J., da Costa, M., Portela, T. T. B., de Oliveira, A. A. R., Malhi, Y., and Williams, M. (2010). Shifts in plant respiration and carbon use efficiency at a large-scale drought experiment in the eastern amazon. *New Phytologist*, 187(3):608–621.

Millard, P., Sommerkorn, M., and Grelet, G.-A. (2007). Environmental change and carbon limitation in trees: a biochemical, ecophysiological and ecosystem appraisal. *New Phytologist*, 175(1):11–28.

Minchin, P. E. H., Thorpe, M. R., and Farrar, J. F. (1993). A simple mechanistic model of phloem transport which explains sink priority. *Journal of Experimental Botany*, 44(5):947–955.

Mitchell, P. J., O'Grady, A. P., Tissue, D. T., White, D. A., Ottenschlaeger, M. L., and Pinkard, E. A. (2013). Drought response strategies define the relative contributions of hydraulic dysfunction and carbohydrate depletion during tree mortality. *New Phytologist*, 197(3):862–872.

Morgan, J. M. (1984). Osmoregulation and water stress in higher plants. *Annual Review of Plant Physiology*, 35(1):299–319.

Muller, B., Pantin, F., Génard, M., Turc, O., Freixes, S., Piques, M., and Gibon, Y. (2011). Water deficits uncouple growth from photosynthesis, increase C content, and modify the relationships between C and growth in sink organs. *Journal of Experimental Botany*, 62(6):1715–1729.

Nepstad, D. C., de Carvalho, C. R., Davidson, E. A., Jipp, P. H., Lefebvre, P. A., Negreiros, G. H., da Silva, E. D., Stone, T. A., Trumbore, S. E., and Vieira, S. (1994). The role of deep roots in the hydrological and carbon cycles of amazonian forests and pastures. *Nature*, 372(6507):666–669.

Nepstad, D. C., Tohver, I. M., Ray, D., Moutinho, P., and Cardinot, G. (2007). Mortality of large trees and lianas following experimental drought in an amazon forest. *Ecology*, 88(9):2259–2269.

O'Brien, M. J., Burslem, D. F. R. P., Caduff, A., Tay, J., and Hector, A. (2015). Contrasting nonstructural carbohydrate dynamics of tropical tree seedlings under water deficit and variability. *New Phytologist*, 205(3):1083–1094.

O'Brien, M. J., Leuzinger, S., Philipson, C. D., Tay, J., and Hector, A. (2014). Drought survival of tropical tree seedlings enhanced by non-structural carbohydrate levels. *Nature Climate Change*, 4:710–714.

Oleson, K. W., Niu, G.-Y., Yang, Z.-L., Lawrence, D. M., Thornton, P. E., Lawrence, P. J., Stöckli, R., Dickinson, R. E., Bonan, G. B., Levis, S., Dai, A., and Qian, T. (2008). Improvements to the community land model and their impact on the hydrological cycle. *Journal of Geophysical Research: Biogeosciences*, 113(G1).

Palacio, S., Hoch, G., Sala, A., Körner, C., and Millard, P. (2014). Does carbon storage limit tree growth? *New Phytologist*, 201(4):1096–1100. 2013-16122.

Pan, Y., Birdsey, R. A., Fang, J., Houghton, R., Kauppi, P. E., Kurz, W. A., Phillips, O. L., Shvidenko, A., Lewis, S. L., Canadell, J. G., Ciais, P., Jackson, R. B., Pacala, S. W., McGuire, A. D., Piao, S., Rautiainen, A., Sitch, S., and Hayes, D. (2011). A large and persistent carbon sink in the world's forests. *Science*, 333(6045):988–993.

Parazoo, N. C., Bowman, K., Fisher, J. B., Frankenberg, C., Jones, D. B. A., Cescatti, A., Pérez-Priego, O., Wohlfahrt, G., and Montagnani, L. (2014). Terrestrial gross primary production inferred from satellite fluorescence and vegetation models. *Global Change Biology*, 20(10):3103–3121.

Parida, B. R. (2011). *The influence of plant nitrogen availability on the global carbon cycle and N2O emissions*. PhD thesis, University of Hamburg, Hamburg. http://hdl.handle.net/11858/00-001M-0000-0012-3EF0-D.

Peters, R. L., Steppe, K., Cuny, H. E., De Pauw, D. J., Frank, D. C., Schaub, M., Rathgeber, C. B., Cabon, A., and Fonti, P. (2021). Turgor – a limiting factor for radial growth in mature conifers along an elevational gradient. *New Phytologist*, 229(1):213–229.

Phillips, O. L., Aragão, L. E. O. C., Lewis, S. L., Fisher, J. B., Lloyd, J., López-González, G., Malhi, Y., Monteagudo, A., Peacock, J., Quesada, C. A., van der Heijden, G., Almeida, S., Amaral, I., Arroyo, L., Aymard, G., Baker, T. R., Bánki, O., Blanc, L., Bonal, D., Brando, P., Chave, J., de Oliveira, Á. C. A., Cardozo, N. D., Czimczik, C. I., Feldpausch, T. R., Freitas, M. A., Gloor, E., Higuchi, N., Jiménez, E., Lloyd, G., Meir, P., Mendoza, C., Morel, A., Neill, D. A., Nepstad, D., Patiño, S., Peñuela, M. C., Prieto, A., Ramírez, F., Schwarz, M., Silva, J., Silveira, M., Thomas, A. S., Steege, H. t., Stropp, J., Vásquez, R., Zelazowski, P., Dávila, E. A., Andelman, S., Andrade, A., Chao, K.-J., Erwin, T., Di Fiore, A., C., E. H., Keeling, H., Killeen, T. J., Laurance, W. F., Cruz, A. P., Pitman, N. C. A., Vargas, P. N., Ramírez-Angulo, H., Rudas, A., Salamão, R., Silva, N., Terborgh, J., and Torres-Lezama, A. (2009). Drought sensitivity of the amazon rainforest. *Science*, 323(5919):1344–1347.

Poorter, H., Niklas, K. J., Reich, P. B., Oleksyn, J., Poot, P., and Mommer, L. (2012). Biomass allocation to leaves, stems and roots: meta-analyses of interspecific variation and environmental control. *New Phytologist*, 193(1):30–50.

Potkay, A., Trugman, A. T., Wang, Y., Venturas, M. D., Anderegg, W. R. L., Mattos, C. R. C., and Fan, Y. (2021). Coupled whole-tree optimality and xylem hydraulics explain dynamic biomass partitioning. *New Phytologist*, n/a(n/a).

Poulter, B., Frank, D., Ciais, P., Myneni, R. B., Andela, N., Bi, J., Broquet, G., Canadell, J. G., Chevallier, F., Liu, Y. Y., Running, S. W., Sitch, S., and van der

Werf, G. R. (2014). Contribution of semi-arid ecosystems to interannual variability of the global carbon cycle. *Nature*, 509.

Powell, T. (2015). *Determining drought sensitivity of the Amazon forest: does plant hydraulics matter?* PhD thesis.

Powell, T. L., Galbraith, D. R., Christoffersen, B. O., Harper, A., Imbuzeiro, H. M. A., Rowland, L., Almeida, S., Brando, P. M., Costa, A. C. L., Costa, M. H., Levine, N. M., Malhi, Y., Saleska, S. R., Sotta, E., Williams, M., Meir, P., and Moorcroft, P. R. (2013). Confronting model predictions of carbon fluxes with measurements of amazon forests subjected to experimental drought. *New Phytologist*, 200(2):350–365.

Quentin, A. G., Pinkard, E. A., Ryan, M. G., Tissue, D. T., Baggett, L. S., Adams, H. D., Maillard, P., Marchand, J., Landhäusser, S. M., Lacointe, A., Gibon, Y., Anderegg, W. R., Asao, S., Atkin, O. K., Bonhomme, M., Claye, C., Chow, P. S., Clément-Vidal, A., Davies, N. W., Dickman, L. T., Dumbur, R., Ellsworth, D. S., Falk, K., Galiano, L., Grünzweig, J. M., Hartmann, H., Hoch, G., Hood, S., Jones, J. E., Koike, T., Kuhlmann, I., Lloret, F., Maestro, M., Mansfield, S. D., Martínez-Vilalta, J., Maucourt, M., McDowell, N. G., Moing, A., Muller, B., Nebauer, S. G., Niinemets, U., Palacio, S., Piper, F., Raveh, E., Richter, A., Rolland, G., Rosas, T., Saint Joanis, B., Sala, A., Smith, R. A., Sterck, F., Stinziano, J. R., Tobias, M., Unda, F., Watanabe, M., Way, D. A., Weerasinghe, L. K., Wild, B., Wiley, E., and Woodruff, D. R. (2015). Non-structural carbohydrates in woody plants compared among laboratories. *Tree Physiology*, 35(11):1146–1165.

Rastetter, E. B., Ryan, M. G., Shaver, G. R., Melillo, J. M., Nadelhoffer, K. J., Hobbie, J. E., and Aber, J. D. (1991). A general biogeochemical model describing the responses of the c and n cycles in terrestrial ecosystems to changes in co2, climate, and n deposition1. *Tree Physiology*, 9(1-2):101–126.

Reichstein, M., Bahn, M., Ciais, P., Frank, D., Mahecha, M. D., Seneviratne, S. I., Zscheischler, J., Beer, C., Buchmann, N., Frank, D. C., Papale, D., Rammig, A., Smith, P., Thonicke, K., van der Velde, M., Vicca, S., Walz, A., and Wattenbach, M. (2013). Climate extremes and the carbon cycle. *Nature*, 500(7462):287–295.

Restrepo-Coupe, N., Levine, N. M., Christoffersen, Bradley, O., Albert, L. P., Wu, J., Costa, M. H., Galbraith, D., Imbuzeiro, H., Martins, G., Araujo, A. C., Malhi, Y. S., Zeng, X., Moorcroft, P., and Saleska, S. R. (2016). Do dynamic global vegetation models capture the seasonality of carbon fluxes in the amazon basin? a data-model intercomparison. *Global Change Biology*, 23(1):191–208.

Reynolds, J. F. and Thornley, J. H. M. (1982). A shoot:root partitioning model. *Annals of Botany*, 49(5):585–597.

Rogers, A., Medlyn, B. E., Dukes, J. S., Bonan, G., von Caemmerer, S., Dietze, M. C., Kattge, J., Leakey, A. D. B., Mercado, L. M., Niinemets, U., Prentice, I. C., Serbin, S. P., Sitch, S., Way, D. A., and Zaehle, S. (2017). A roadmap for improving the representation of photosynthesis in earth system models. *New Phytologist*, 213(1):22–42.

Rowland, L., da Costa, A. C. L., Galbraith, D. R., Oliveira, R. S., Binks, O. J., Oliveira, A. A. R., Pullen, A. M., Doughty, C. E., Metcalfe, D. B., Vasconcelos, S. S., Ferreira, L. V., Malhi, Y., Grace, J., Mencuccini, M., and Meir, P. (2015). Death from drought in tropical forests is triggered by hydraulics not carbon starvation. *Nature*, 528.

Rowland, L., da Costa, A. C. L., Oliveira, A. A. R., Almeida, S. S., Ferreira, L. V., Malhi, Y., Metcalfe, D. B., Mencuccini, M., Grace, J., and Meir, P. (2018). Shock and stabilisation following long-term drought in tropical forest from 15 years of litterfall dynamics. *Journal of Ecology*, 106(4):1673–1682.

Rowland, L., da Costa, A. C. L., Oliveira, R. S., Bittencourt, P. R. L., Giles, A. L., Coughlin, I., de Britto Costa, P., Bartholomew, D., Domingues, T. F., Miatto, R. C., Ferreira, L. V., Vasconcelos, S. S., Junior, J. A. S., Oliveira, A. A. R., Mencuccini, M., and Meir, P. (2021). The response of carbon assimilation and storage to long-term drought in tropical trees is dependent on light availability. *Functional Ecology*, 35(1):43–53.

Roxburgh, S. H., Berry, S. L., Buckly, T. N., Barnes, B., and Roderick, M. L. (2005). What is npp? inconsistent accounting of respiratory fluxes in the definition of net primary production. *Functional Ecology*, 19(3):378–382.

Ryan, M. G. (1991). Effects of climate change on plant respiration. *Ecological Applications*, 1(2):157–167.

Ryan, M. G. and Asao, S. (2014). Phloem transport in trees. *Tree Physiology*, 34(1):1–4.

Saatchi, S. S., Houghton, R. A., Dos Santos Alvalá, R. C., Soares, J. V., and Yu, Y. (2007). Distribution of aboveground live biomass in the amazon basin. *Global Change Biology*, 13(4):816–837.

Sala, A. and Mencuccini, M. (2014). Plump trees win under drought. *Nature Climate Change*, 4:666–667.

Sala, A., Piper, F., and Hoch, G. (2010). Physiological mechanisms of drought-induced tree mortality are far from being resolved. *New Phytologist*, 186(2):274–281.

Salomón, R. L., De Roo, L., Oleksyn, J., De Pauw, D. J. W., and Steppe, K. (2019). Trespire – a biophysical tree stem respiration model. *New Phytologist*, n/a(n/a).

Saxe, H., Cannell, M. G. R., Johnsen, Ø., Ryan, M. G., and Vourlitis, G. (2001). Tree and forest functioning in response to global warming. *New Phytologist*, 149(3):369–399.

Schwalm, C. R., Williams, C. A., Schaefer, K., Baldocchi, D., Black, T. A., Goldstein, A. H., Law, B. E., Oechel, W. C., Paw U, K. T., and Scott, R. L. (2012). Reduction in carbon uptake during turn of the century drought in western north america. *Nature Geoscience*, 5(8):551–556.

Sellar, A. A., Jones, C. G., Mulcahy, J. P., Tang, Y., Yool, A., Wiltshire, A., O'Connor, F. M., Stringer, M., Hill, R., Palmieri, J., Woodward, S., de Mora, L., Kuhlbrodt, T., Rumbold, S. T., Kelley, D. I., Ellis, R., Johnson, C. E., Walton, J., Abraham, N. L., Andrews, M. B., Andrews, T., Archibald, A. T., Berthou, S., Burke, E., Blockley, E., Carslaw, K., Dalvi, M., Edwards, J., Folberth, G. A., Gedney, N., Griffiths, P. T., Harper, A. B., Hendry, M. A., Hewitt, A. J., Johnson, B., Jones, A., Jones, C. D., Keeble, J., Liddicoat, S., Morgenstern, O., Parker, R. J., Predoi, V., Robertson, E., Siahaan, A., Smith, R. S., Swaminathan, R., Woodhouse, M. T., Zeng, G., and Zerroukat, M. (2019). Ukesm1: Description and evaluation of the u.k. earth system model. *Journal of Advances in Modeling Earth Systems*, 11(12):4513–4558.

Sellers, P., Randall, D., Collatz, G., Berry, J., Field, C., Dazlich, D., Zhang, C., Collelo, G., and Bounoua, L. (1996). A revised land surface parameterization (sib2) for atmospheric gcms. part i: Model formulation. *Journal of Climate*, 9(4):676 – 705.

Sevanto, S., McDowell, N. G., Dickman, L. T., Pangle, R., and Pockman, W. T. (2014). How do trees die? a test of the hydraulic failure and carbon starvation hypotheses. *Plant, Cell & Environment*, 37(1):153–161.

Signori-Müller, C., Oliveira, R. S., Barros, F. d. V., Tavares, J. V., Gilpin, M., Diniz, F. C., Zevallos, M. J. M., Yupayccana, C. A. S., Acosta, M., Bacca, J., Chino, R. S. C., Cuellar, G. M. A., Cumapa, E. R. M., Martinez, F., Mullisaca, F. M. P., Nina, A., Sanchez, J. M. B., da Silva, L. F., Tello, L., Tintaya, J. S., Ugarteche, M. T. M., Baker, T. R., Bittencourt, P. R. L., Borma, L. S., Brum, M., Castro, W., Coronado, E. N. H., Cosio, E. G., Feldpausch, T. R., Fonseca, L. d. M.,

Gloor, E., Llampazo, G. F., Malhi, Y., Mendoza, A. M., Moscoso, V. C., Araujo-Murakami, A., Phillips, O. L., Salinas, N., Silveira, M., Talbot, J., Vasquez, R., Mencuccini, M., and Galbraith, D. (2021). Non-structural carbohydrates mediate seasonal water stress across amazon forests. *Nature Communications*, 12(1):2310.

Sitch, S., Friedlingstein, P., Gruber, N., Jones, S. D., Murray-Tortarolo, G., Ahlström, A., Doney, S. C., Graven, H., Heinze, C., Huntingford, C., Levis, S., Levy, P. E., Lomas, M., Poulter, B., Viovy, N., Zaehle, S., Zeng, N., Arneth, A., Bonan, G., Bopp, L., Canadell, J. G., Chevallier, F., Ciais, P., Ellis, R., Gloor, M., Peylin, P., Piao, S. L., Le Quéré, C., Smith, B., Zhu, Z., and Myneni, R. (2015). Recent trends and drivers of regional sources and sinks of carbon dioxide. *Biogeosciences*, 12(3):653–679.

Sitch, S., Huntingford, C., Gedney, N., Levy, P. E., Lomas, M., Piao, S. L., Betts, R., Ciais, P., Cox, P., Friedlingstein, P., Jones, C. D., Prentice, I. C., and Woodward, F. I. (2008). Evaluation of the terrestrial carbon cycle, future plant geography and climate-carbon cycle feedbacks using five dynamic global vegetation models (dgvms). *Global Change Biology*, 14(9):2015–2039.

Smith, B., Prentice, I. C., and Sykes, M. T. (2001). Representation of vegetation dynamics in the modelling of terrestrial ecosystems: comparing two contrasting approaches within european climate space. *Global Ecology and Biogeography*, 10(6):621–637.

Smith, B., Wårlind, D., Arneth, A., Hickler, T., Leadley, P., Siltberg, J., and Zaehle, S. (2014). Implications of incorporating n cycling and n limitations on primary production in an individual-based dynamic vegetation model. *Biogeosciences*, 11(7):2027–2054.

Song, Y., Jain, A. K., and McIsaac, G. F. (2013). Implementation of dynamic crop growth processes into a land surface model: evaluation of energy, water and carbon fluxes under corn and soybean rotation. *Biogeosciences*, 10(12):8039–8066.

Sperry, J. S. and Love, D. M. (2015). What plant hydraulics can tell us about responses to climate-change droughts. *New Phytologist*, 207(1):14–27.

Sperry, J. S., Venturas, M. D., Anderegg, W. R. L., Mencuccini, M., Mackay, D. S., Wang, Y., and Love, D. M. (2017). Predicting stomatal responses to the environment from the optimization of photosynthetic gain and hydraulic cost. *Plant, Cell & Environment*, 40(6):816–830.

Steppe, K., De Pauw, D. J. W., Lemeur, R., and Vanrolleghem, P. A. (2006). A mathematical model linking tree sap flow dynamics to daily stem diameter fluctuations and radial stem growth. *Tree Physiology*, 26(3):257–273.

Stitt, M. (1991). Rising co2 levels and their potential significance for carbon flow in photosynthetic cells. *Plant, Cell & Environment*, 14(8):741–762.

Stocker, T., Qin, D., Plattner, G.-K., Alexander, L., Allen, S., Bindoff, N., Bréon, F.-M., Church, J., Cubasch, U., Emori, S., Forster, P., Friedlingstein, P., Gillett, N., Gregory, J., Hartmann, D., Jansen, E., Kirtman, B., Knutti, R., Krishna Kumar, K., Lemke, P., Marotzke, J., Masson-Delmotte, V., Meehl, G., Mokhov, I., Piao, S., Ramaswamy, V., Randall, D., Rhein, M., Rojas, M., Sabine, C., Shindell, D., Talley, L., Vaughan, D., and Xie, S.-P. (2013). *Technical Summary*, book section TS, page 33–115. Cambridge University Press, Cambridge, United Kingdom and New York, NY, USA.

Tang, J., Luyssaert, S., Richardson, A. D., Kutsch, W., and Janssens, I. A. (2014). Steeper declines in forest photosynthesis than respiration explain age-driven decreases in forest growth. *Proceedings of the National Academy of Sciences*, 111(24):8856–8860.

Thornley, J. and Cannell, M. (2000). Modelling the components of plant respiration: Representation and realism. *Annals of Botany*, 85(1):55 – 67.

Thornley, J. H. M. (1970). Respiration, growth and maintenance in plants. *Nature*, 227:304–305.

Thornley, J. H. M. (1971). Energy, respiration, and growth in plants. *Annals of Botany*, 35(4):721–728.

Thornley, J. H. M. (1991). A transport-resistance model of forest growth and partitioning. *Annals of Botany*, 68(3):211–226.

Thornley, J. H. M. (1997). Modelling allocation with transport/conversion processes. *Silva Fennica*, 31(3):341–355.

Thornley, J. H. M. (2011). Plant growth and respiration re-visited: maintenance respiration defined -it is an emergent property of, not a separate process within, the system - and why the respiration : photosynthesis ratio is conservative. *Annals of Botany*, 108(7):1365–1380.

Thornley, J. H. M. and Johnson, I. R. (1990). *Plant and Crop Modelling. A Mathematical Approach to Plant and Crop Physiology*. The Blackburn Press.

Trugman, A. T., Detto, M., Bartlett, M. K., Medvigy, D., Anderegg, W. R. L., Schwalm, C., Schaffer, B., and Pacala, S. W. (2018). Tree carbon allocation explains forest drought-kill and recovery patterns. *Ecology Letters*, 21(10):1552–1560.

Tyree, M. T. and Sperry, J. S. (1989). Vulnerability of xylem to cavitation and embolism. *Annual Review of Plant Physiology and Plant Molecular Biology*, 40(1):19–36.

UN Food and Agriculture Organization Rome (2015). Global forest resources assessment.

Wagner, F., Rossi, V., Stahl, C., Bonal, D., and Hérault, B. (2012). Water availability is the main climate driver of neotropical tree growth. *PloS one*, 7(4):e34074–e34074.

Wagner, F. H., Hérault, B., Bonal, D., Stahl, C., Anderson, L. O., Baker, T. R., Becker, G. S., Beeckman, H., Boanerges Souza, D., Botosso, P. C., Bowman, D. M. J. S., Bräuning, A., Brede, B., Brown, F. I., Camarero, J. J., Camargo, P. B., Cardoso, F. C. G., Carvalho, F. A., Castro, W., Chagas, R. K., Chave, J., Chidumayo, E. N., Clark, D. A., Costa, F. R. C., Couralet, C., da Silva Mauricio, P. H., Dalitz, H., de Castro, V. R., de Freitas Milani, J. E., de Oliveira, E. C., de Souza Arruda, L., Devineau, J.-L., Drew, D. M., Dünisch, O., Durigan, G., Elifuraha, E., Fedele, M., Ferreira Fedele, L., Figueiredo Filho, A., Finger, C. A. G., Franco, A. C., Freitas Júnior, J. L., Galvão, F., Gebrekirstos, A., Gliniars, R., Graça, P. M. L. D. A., Griffiths, A. D., Grogan, J., Guan, K., Homeier, J., Kanieski, M. R., Kho, L. K., Koenig, J., Kohler, S. V., Krepkowski, J., Lemos-Filho, J. P., Lieberman, D., Lieberman, M. E., Lisi, C. S., Longhi Santos, T., López Ayala, J. L., Maeda, E. E., Malhi, Y., Maria, V. R. B., Marques, M. C. M., Marques, R., Maza Chamba, H., Mbwambo, L., Melgaço, K. L. L., Mendivelso, H. A., Murphy, B. P., O'Brien, J. J., Oberbauer, S. F., Okada, N., Pélissier, R., Prior, L. D., Roig, F. A., Ross, M., Rossatto, D. R., Rossi, V., Rowland, L., Rutishauser, E., Santana, H., Schulze, M., Selhorst, D., Silva, W. R., Silveira, M., Spannl, S., Swaine, M. D., Toledo, J. J., Toledo, M. M., Toledo, M., Toma, T., Tomazello Filho, M., Valdez Hernández, J. I., Verbesselt, J., Vieira, S. A., Vincent, G., Volkmer de Castilho, C., Volland, F., Worbes, M., Zanon, M. L. B., and Aragão, L. E. O. C. (2016). Climate seasonality limits leaf carbon assimilation and wood productivity in tropical forests. *Biogeosciences*, 13(8):2537–2562.

Wagner, F. H., Hérault, B., Rossi, V., Hilker, T., Maeda, E. E., Sanchez, A., Lyapustin, A. I., Galvão, L. S., Wang, Y., and Aragão, L. E. O. C. (2017). Climate drivers of the amazon forest greening. *PLOS ONE*, 12(7):1–15.

Waring, R. H., Landsberg, J. J., and Williams, M. (1998). Net primary production of forests: a constant fraction of gross primary production? *Tree Physiology*, 18(2):129–134.

Wiley, E. and Helliker, B. (2012). A re-evaluation of carbon storage in trees lends greater support for carbon limitation to growth. *New Phytologist*, 195(2):285–289.

Williams, K. E., Harper, A. B., Huntingford, C., Mercado, L. M., Mathison, C. T., Falloon, P. D., Cox, P. M., and Kim, J. (2018). Revisiting the first islscp field experiment to evaluate water stress in julesv5.0. *Geoscientific Model Development Discussions*, pages 1–47.

Wiltshire, A. J., Burke, E. J., Chadburn, S. E., Jones, C. D., Cox, P. M., Davies-Barnard, T., Friedlingstein, P., Harper, A. B., Liddicoat, S., Sitch, S., and Zaehle, S. (2021). Jules-cn: a coupled terrestrial carbon–nitrogen scheme (jules vn5.1). *Geoscientific Model Development*, 14(4):2161–2186.

Wolf, A., Anderegg, W. R. L., and Pacala, S. W. (2016). Optimal stomatal behavior with competition for water and risk of hydraulic impairment. *Proceedings of the National Academy of Sciences*, 113(46):E7222.

Woodward, F. I. (2002). Potential impacts of global elevated co2 concentrations on plants. *Current Opinion in Plant Biology*, 5(3):207–211.

Wu, J., Albert, L. P., Lopes, A. P., Restrepo-Coupe, N., Hayek, M., Wiedemann, K. T., Guan, K., Stark, S. C., Christoffersen, B., Prohaska, N., Tavares, J. V., Marostica, S., Kobayashi, H., Ferreira, M. L., Campos, K. S., da Silva, R., Brando, P. M., Dye, D. G., Huxman, T. E., Huete, A. R., Nelson, B. W., and Saleska, S. R. (2016). Leaf development and demography explain photosynthetic seasonality in amazon evergreen forests. *Science*, 351(6276):972–976.

Würth, M. K. R., Peláez-Riedl, S., Wright, S. J., and Körner, C. (2005). Non-structural carbohydrate pools in a tropical forest. *Oecologia*, 143(1):11–24.